

This article was downloaded by:

On: 21 January 2011

Access details: *Access Details: Free Access*

Publisher *Taylor & Francis*

Informa Ltd Registered in England and Wales Registered Number: 1072954 Registered office: Mortimer House, 37-41 Mortimer Street, London W1T 3JH, UK



International Reviews in Physical Chemistry

Publication details, including instructions for authors and subscription information:

<http://www.informaworld.com/smpp/title~content=t713724383>

Preparation, characterisation and structure of Ti and Al ultrathin oxide films on metals

Qi-Hui Wu^a; Alessandro Fortunelli^b; Gaetano Granozzi^c

^a Department of Physics, La Trobe University, Bundoora 3086, VIC, Australia ^b Molecular Modeling Laboratory, IPCF-CNR, I-56124 Pisa, Italy ^c Dipartimento di Scienze Chimiche, Università di Padova, Consorzio INSTM and Unità di Ricerca INFN-CNR, 35131 Padova, Italy

To cite this Article Wu, Qi-Hui, Fortunelli, Alessandro and Granozzi, Gaetano(2009) 'Preparation, characterisation and structure of Ti and Al ultrathin oxide films on metals', *International Reviews in Physical Chemistry*, 28: 4, 517 — 576

To link to this Article: DOI: 10.1080/01442350903172453

URL: <http://dx.doi.org/10.1080/01442350903172453>

PLEASE SCROLL DOWN FOR ARTICLE

Full terms and conditions of use: <http://www.informaworld.com/terms-and-conditions-of-access.pdf>

This article may be used for research, teaching and private study purposes. Any substantial or systematic reproduction, re-distribution, re-selling, loan or sub-licensing, systematic supply or distribution in any form to anyone is expressly forbidden.

The publisher does not give any warranty express or implied or make any representation that the contents will be complete or accurate or up to date. The accuracy of any instructions, formulae and drug doses should be independently verified with primary sources. The publisher shall not be liable for any loss, actions, claims, proceedings, demand or costs or damages whatsoever or howsoever caused arising directly or indirectly in connection with or arising out of the use of this material.

Preparation, characterisation and structure of Ti and Al ultrathin oxide films on metals

Qi-Hui Wu^{a*}, Alessandro Fortunelli^{b*} and Gaetano Granozzi^{c*}

^aDepartment of Physics, La Trobe University, Bundoora 3086, VIC, Australia; ^bMolecular Modeling Laboratory, IPCF-CNR, via Giuseppe Moruzzi 1, I-56124 Pisa, Italy; ^cDipartimento di Scienze Chimiche, Università di Padova, Consorzio INSTM and Unità di Ricerca INFN-CNR, 35131 Padova, Italy

(Received 19 May 2009; final version received 7 July 2009)

The growth of ultrathin oxide films on metal substrates offers a solution to many of the experimental difficulties inherent to the studies of surfaces of bulk oxides and provides new interesting materials with unprecedented structures and properties. In this article we review the preparation and characterisation of ultrathin titanium oxide (TiO_x) and aluminium oxide (AlO_x) films grown on metal and metal alloy surfaces, emphasising those results that highlight new concepts and insights into metal oxide surface physics and chemistry. Different methods of preparation and characterisation are discussed and the resulting chemical compositions and surface structures are described by taking into account the results provided by computational approaches, and putting emphasis in outlining the structural novelty of interface-stabilised versus bulk-like phases and on the importance of kinetic effects in orienting the growth.

Keywords: ultrathin oxide films; oxide nanostructures; nanopatterned templates; growth and synthesis; metal supports

| | Contents | PAGE |
|--------|--------------------------------|------|
| 1. | Introduction | 519 |
| 2. | Methodologies | 520 |
| 2.1. | Preparative strategies | 521 |
| 2.1.1. | Surface oxidation | 522 |
| 2.1.2. | Film deposition | 523 |
| 2.1.3. | Post-deposition treatments | 524 |
| 2.2. | Theoretical tools | 524 |
| 3. | Titanium oxide ultrathin films | 526 |
| 3.1. | Bulk TiO_x phases | 527 |
| 3.1.1. | TiO | 527 |
| 3.1.2. | Ti_2O_3 | 527 |

*Corresponding authors. Email: Q.Wu@latrobe.edu.au; fortunelli@ipcf.cnr.it; gaetano.granozzi@unipd.it

| | |
|--|-----|
| 3.1.3. TiO ₂ | 528 |
| 3.2. Surface oxidation of Ti metal and alloys | 528 |
| 3.2.1. Oxidation of Ti metal | 528 |
| 3.2.1.1. Polycrystalline Ti (poly-Ti) | 528 |
| 3.2.1.2. Single crystal Ti (single-Ti) | 530 |
| 3.2.2. Oxidation of Ti alloys | 530 |
| 3.2.2.1. Polycrystalline alloys | 530 |
| 3.2.2.2. Single crystal alloys and surface alloys | 531 |
| 3.3. Ultrathin TiO _x films on other metal surfaces | 533 |
| 3.3.1. Mo | 533 |
| 3.3.1.1. Mo(100) | 534 |
| 3.3.1.2. Mo(110) | 534 |
| 3.3.1.3. Mo(112) | 534 |
| 3.3.2. Ni(110) | 535 |
| 3.3.3. Cu(100) | 538 |
| 3.3.4. Pt | 538 |
| 3.3.4.1. Pt(100) | 239 |
| 3.3.4.2. Pt(111) | 540 |
| 3.3.4.3. Pt(110) | 547 |
| 3.3.5. Ru(0001) | 547 |
| 3.3.6. Au(111) | 548 |
| 3.3.7. W(100) | 549 |
| 4. Aluminium oxide ultrathin films | 550 |
| 4.1. Bulk aluminum oxides (Al ₂ O ₃) | 550 |
| 4.1.1. α-Al ₂ O ₃ | 550 |
| 4.1.2. κ-Al ₂ O ₃ | 552 |
| 4.1.3. γ-Al ₂ O ₃ and θ-Al ₂ O ₃ | 552 |
| 4.2. Surface oxidation of Al metal | 553 |
| 4.3. Surface oxidation of M _x Al alloys (M = Ni, Fe, Cu) | 553 |
| 4.3.1. NiAl | 553 |
| 4.3.1.1. NiAl(110) | 554 |
| 4.3.1.2. NiAl(100) | 556 |
| 4.3.1.3. NiAl(111) | 557 |
| 4.3.2. Ni ₃ Al | 558 |
| 4.3.2.1. Ni ₃ Al(111) | 559 |
| 4.3.2.2. Ni ₃ Al(110) | 559 |
| 4.3.2.3. Ni ₃ Al(100) | 561 |
| 4.3.3. FeAl | 561 |
| 4.3.4. CuAl | 562 |
| 4.4. Ultrathin alumina films on other metal surfaces | 563 |
| 5. Conclusions and perspectives | 564 |
| Glossary | 566 |
| Acknowledgements | 567 |
| References | 567 |

1. Introduction

Transition metal oxides (TMOs) represent strategic materials for advanced devices in many innovative technologies: they are largely used as catalysts and photocatalysts [1,2], chemical sensors [3,4], corrosion inhibitors [5,6], components in microelectronics (for their dielectric properties) [7,8], opto-electronics (as transparent conductors) and magnetic devices [9]. Since most of their relevant properties are related to their surfaces, in the past two decades many efforts have been devoted to better characterise the structure and reactivity of TMOs surfaces and interfaces [10–14].

Despite many studies in the field of surface science (SS) of oxides, there are still some open questions at a fundamental level, such as the relationships between surface atomic structure, electronic properties and chemical reactivity and the role played by defects. Answering such questions and setting well-grounded structure/property relationships requires rigorous studies where the effective ultra-high-vacuum (UHV) surface-sensitive probes provided by modern SS are applied to well-characterised systems (i.e. model systems) [15,16]. The level of understanding provided by such a methodology is currently under test in order to demonstrate that it is capable to provide information on the real systems, overcoming the so-called *pressure and material gaps* [17,18].

However, when using SS probes employing charged particles (i.e. electrons and ions), the insulating properties of many bulk oxides often generate charging problems which makes it difficult, or even impossible, to apply many SS techniques to the study of oxide bulk surfaces. In recent years, attention has then progressively shifted to oxide model systems in the form of *ultrathin* (UT) epitaxial films grown on single-crystal metal surfaces [12,19–27]. In the following, by the term UT we mean films characterised by thickness in the range up to a few monolayers (MLs), i.e. thickness $\leq 1\text{--}2$ nm. As a matter of fact, if the substrate has good conduction properties (e.g. a metal), the reduced thickness of the oxide UT film allows the probe-particles to tunnel towards the substrate. This route leads to ordered oxide surfaces suitable to be studied by means of scanning tunnelling microscopy (STM), photoemission and electron excitation techniques [12,19,20]. To underline the freedom in oxide stoichiometry, the notation MO_x is adopted to indicate UT films of the M metal.

While the results to date have demonstrated that films with thickness of the order of several MLs are adequate to simulate bulk-terminated oxide surfaces, more and more examples are reported of UT films with radically new structures, stoichiometries and properties [22]. Actually, UT oxide films represent a potentially new class of materials where innovative properties with respect to bulk phases are produced, associated with the interaction with the substrate (metal proximity effects) and/or the confinement of atomic-scale structures in at least one dimension [28–30]. For example, in order to optimise the interaction with the substrate, the film can adjust its structure, producing a strain which is maintained until a critical thickness is reached, over which it recovers its thermodynamically stable bulk structure. Indeed, most of the recent focus on UT films is related to the possibility of stabilising phases and structures which are not obtainable in bulk form due to thermodynamic and/or kinetic constraints.

Carefully playing with the preparation procedures, tailor-made UT oxide films with specific stoichiometries and defect arrangements can be obtained which provide a suitable playground with a two-fold flavour: on the one hand, to test ideas and concepts on the properties (chemical reactivity, magnetism, etc.) of oxides surfaces, and on the other hand,

to produce unprecedented structures with still unexplored properties. A number of excellent review articles have appeared in the literature in the field of UT oxide films: they have been mainly focused on the epitaxial growth procedures of oxide UT films [20,31] or on their relevance in catalysis [23–25,32,33]. However, apart from specific reports on VO_x UT films on Pd and Rh supports [22,34], not too much emphasis has been put so far in underlying the wide structural diversity intrinsic to interface-stabilised phases in the extremely low coverage regime of UT films.

In this work we review the literature data on titania and alumina UT oxide films on metals and metal alloy surfaces, focusing on the preparation and characterisation strategies and putting particular emphasis on the interface-stabilised phases and on the structural models so far developed for them. The choice of the two systems herein considered is suggested by several factors:

- (a) They represent two prototypical oxides: alumina is a non-reducible oxide, much used as a support in catalysis [35], whereas titania is a reducible oxide where the metal can switch among several oxidation states, and is hence a strategic material for several advanced applications [36].
- (b) Titania and alumina bulk surfaces have been investigated in great detail [37,38], so that there is a good reference with respect to which the novelty of the UT films can be assessed.
- (c) Titania and alumina UT films have been deeply investigated by computational tools and several model structures have been proposed, thus allowing one an attempt to draw some building principles of general relevance.

This review will be organised as follows: in Section 2 we discuss some methodologies of relevance for the preparation, characterisation and theoretical treatment of MO_x UT films. In Sections 3 and 4 we review the literature data of titania and alumina UT films, respectively, on different metallic substrates, introducing first in each section a brief discussion on the relative bulk phases. In Section 5 we draw some general conclusions and give an outlook for future developments and applications.

2. Methodologies

In this section we summarise the main methodologies currently adopted to prepare UT oxide films and to characterise (both experimentally and theoretically) their chemical and structural properties. A lot of different SS experimental techniques have been applied to study the chemical composition, thickness, electronic and crystal structures of UT oxides films including, for example, X-ray photoelectron spectroscopy (XPS), ultraviolet photoelectron spectroscopy (UPS), Auger electron spectroscopy (AES), electron energy loss spectroscopy (EELS) and high resolution EELS (HREELS), thermal desorption spectroscopy (TDS), Fourier transform-reflectance-absorption infrared spectroscopy (FT-RAIRS), scanning tunnelling microscopy (STM), scanning tunnelling spectroscopy (STS), transmission electron microscopy (TEM), low energy ion scattering (LEIS), medium energy ion scattering (MEIS), X-ray diffraction (XRD), ion-scattering spectroscopy (ISS), X-ray photoemission diffraction (XPD) [39] and electron diffraction techniques including low energy electron diffraction (LEED), low energy electron microscopy (LEEM) [40] and reflection high energy electron diffraction (RHEED). Many of these are common tools in

modern SS and we assume that the reader can easily have access to their principles in standard SS textbooks. For those of them having a less general use, we have indicated some specific reference to pertinent review articles.

We will now focus on the preparative general methods and on the theoretical framework which is currently adopted to provide reliable structural models and simulation of spectroscopic data to be compared with the experimental ones.

2.1. Preparative strategies

The preparation of UT epitaxial films requires growth procedures under strictly controlled conditions, usually in UHV, in order to ensure the necessary kinetic conditions of growth (low rates to favour epitaxy) of materials of adequate purity. Given the extreme sensitivity of the resulting layers to the actual growth conditions on both kinetic and thermodynamic grounds, a crucial step is the establishment of clear and reproducible procedures. As a first step, this entails investigating the nature of the nucleation sites at the substrate surface in the very early stages of growth, i.e. in the sub-ML thickness range. Once the sites that determine the overlayer-substrate registry at the atomic scale have been established, one is left with the challenge of driving the stoichiometry and structure of the UT film via an appropriate control of the growth parameters. These are usually the substrate temperature, the growth rate, the nature of the oxidising agent, its partial pressure, the actual deposition protocol (stepwise and alternated with annealing cycles or continuous), the temperature and duration of the post-deposition heat treatments, the controlled doping by means of ion implantation or chemical reactions, etc. Actually, a subtle interplay between kinetic and thermodynamic factors may lead to rather distinct (structurally or chemically) films. Recently, the presence of strong kinetic effects have been outlined in a study where the growth and the transformations between different UT films have been followed *in situ* and in real time by using LEEM and micro-LEED (μ -LEED) [41].

All the techniques developed to prepare UT oxide films imply a stage where an oxidation process of the parent metal M is done under strictly controlled conditions. In Reference [20] a detailed discussion of the possible oxidising gases has been reported: molecular oxygen is the standard procedure, but more strongly oxidising agents like atomic oxygen (AO) or nitrogen oxides, like NO_2 (which works by dissociating to $\text{NO}+\text{O}$ on the substrate) can be used. In order to optimise the growth of stoichiometric UT films, it is needed that the metal oxidation occurs at a rate much higher than that of UT film growth. Under this condition, the growth of understoichiometric (reduced) MO_x phases or even metallic clusters, possible in the case of metals exhibiting multiple oxidation states, is strongly inhibited. So the choice of strong oxidation agents such as AO is not indicated if the goal is preparing MO_x interface-stabilised phases.

Another strategic point is the choice of the metallic substrate on which to grow the UT oxide film. If the goal is the preparation of stoichiometric and low-defective UT oxide films, the substrate choice is dictated by the standard epitaxy rules, i.e. the smallest mismatch between the substrate and the overgrowing film. When the lattice mismatch is larger than a few per cents, perfect epitaxial growth becomes impossible so that sometimes a stoichiometric film grows in a micro-crystalline form, with a lot of additional interfaces and grain boundaries where the control of the morphology at microscopic level is low. On the other hand, if the goal is preparing interface-stabilised nanostructures on

a substrate some mismatch is quite beneficial to nucleate surface-stabilised 2D islands which can also in favourable cases completely wet the substrate.

2.1.1. Surface oxidation

One possibility to prepare UT MO_x oxide films is by directly oxidising the substrate formed by the parent metal M single crystal (Figure 1). This procedure is similar to the one adopted in microelectronics to grow SiO_2 on Si single crystals by direct exposure of the Si wafer to O_2 . The actual conditions needed to prepare a crystalline UT film are dictated by the thermodynamics and kinetics of the oxidation process and by the kinetics of the ordering of the oxide network. However, such a method lacks flexibility if compared with the deposition of the film on a different substrate (Section 2.1.2). Actually, the direct oxidation of the metal single crystal often presents problems connected to the lattice mismatch between the metal and its oxide (this is the same reason why amorphous SiO_2 is grown on Si wafers) and only in selected cases the direct oxidation of the metal substrate leads to films of good quality.

A way to make the method more flexible is to put an oxidising agent in contact with the surface of an intermetallic alloy $\text{M}_x\text{M}'_y$ crystal (or even a surface alloy) where one of the two components (M , the most reactive metal) is preferentially oxidised [31]. The inert component M' can be either a noble metal or even a reactive metal with a distinctly lower aptitude to be oxidised. The advantage is that the mismatch problem can be partially

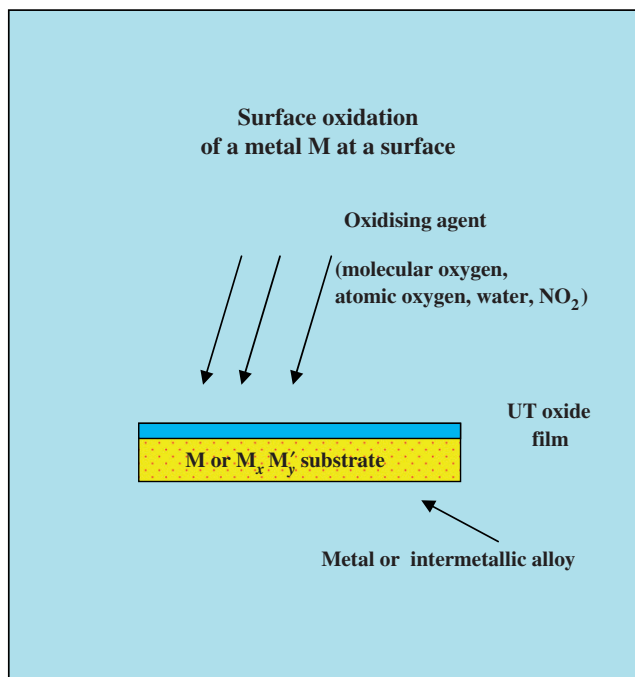


Figure 1. [Colour online] Schematic drawing of the surface oxidation (SO) method for growing UT oxide films (MO_x) on metal (M) or intermetallic ($\text{M}_x\text{M}'_y$) alloy substrates.

released by a tailored choice of the alloy itself: the effect can be simple engineering of interatomic distances, but more subtle changes in the redox properties of M due to the intermetallic bond cannot be excluded. This method has been largely employed to grow AlO_x and TiO_x UT films on different intermetallic alloys (Sections 3.2.2 and 4.3).

2.1.2. Film deposition

The most widely used and flexible method to prepare UT oxide MO_x films is to directly grow the film on a metallic single crystal substrate of different chemical nature (M') under UHV conditions. The metal M is oxidised either (a) directly during deposition in a reactive oxygen atmosphere (reactive deposition, RD), or (b) after the deposition, by means of an annealing treatment in an oxidising atmosphere (post-oxidation, PO), see Figure 2. The two methods will not necessarily provide the same results because they imply different nucleation and growth steps. In the literature one can find reports where the two different procedures are compared [42,43], but the most widely used and effective procedure is the RD one. The PO procedure is preferred when the the M' substrate is easily oxidised.

Usually, the metal M is evaporated (e.g. using a Knudsen cell) and deposited onto a clean and ordered M' substrate whose long range ordering and purity have been previously checked by LEED and a surface chemical probe. An important issue is calibration of the deposited metal dose and of the film thickness. Typically, the former is determined using a quartz microbalance and/or by angle-resolved XPS experiments [44], while the latter is expressed in ML equivalents (MLE) which is calculated assuming a specific interlayer distance between adjacent planes in the film. The assumption of such interlayer distance can then bias the MLE actual value. Considering that the measurement of the metal dose is subjected to large experimental errors, transferability of data coming from different laboratories is often a critical point.

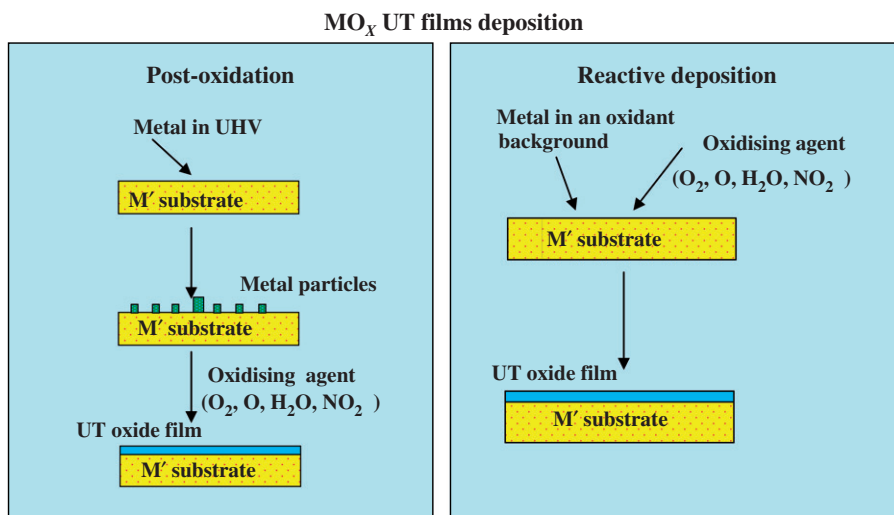


Figure 2. [Colour online] Schematic drawing of the methods usually adopted for growing UT oxide films (MO_x) on a metal (M') substrate.

2.1.3. *Post-deposition treatments*

If investigating the structure of the UT film is the actual issue, routinely the first step in the characterisation of the deposited film consists in examining the possible changes in the LEED pattern with respect to the substrate. However, prior to this very often the film is subjected to some post-deposition treatment which has the main objective of improving its structural order. Such post-deposition treatments can also get a strategic preparative valency. Actually, playing with several experimental parameters, such as the pressure conditions (typically UHV or oxygen background), temperature, heating rate and overall time, can provide many opportunities to come up with rather different structures and stoichiometries of the final UT MO_x film. A further post-deposition treatment might consist in exposing the film to reactive gases other than oxygen to induce chemical transformations (e.g. reduction using hydrogen).

2.2. *Theoretical tools*

Theoretical and computational tools have become an essential component in the investigation of UT metal-supported oxide phases, as in many other fields of science and technology. This is understandable in view of the fact that these phases often present unusual or even unprecedented structures, and that – despite recent progresses – the same basic physics of the UT-oxide/metal-support interaction has not been completely clarified [45].

Given the size and the complexity of the unit cells that are typically encountered, among first-principles approaches density-functional (DF) methods [46] currently represent the best compromise between accuracy and computational effort. The choice of the specific approximation to the exchange-correlation (xc-) functional is however non-trivial: either functionals based on the generalised gradient approximation (GGA) [47] or hybrid functionals [48] are usually employed, the former sometimes augmented by a Hubbard U-term in the so-called GGA+U approaches [49–52]. The problem with these interfacial systems is however that the xc-functional that best describes the oxide component is often not well suited for the metallic one, and vice versa, while very little is known about the validation of the xc-functional for the description of the oxide/metal *interaction*. Hybrid xc-functionals, that contain an Hartree–Fock exchange component, for example, are often able to better describe the energetics of bulk oxides with respect to GGA xc-functionals, but their Hartree–Fock exchange component itself gives problems in the description of metallic systems [53]. A possible solution that has been explored in the literature is to reduce the weight of the Hartree–Fock exchange and use it as an empirical parameter to match experimental data [54]. More advanced xc-functionals are probably needed to overcome these issues. A somewhat related problem is connected with the common presence of metallic elements in low oxidation states within the oxide layer. Especially for TMOs one can therefore wonder what is the degree of electron localisation in these species, and which xc-functional is able to correctly grasp the physics involved. On the one hand, in fact, hybrid and GGA+U methods have been shown to provide more accurate predictions of reduced states of transition metals in bulk oxides than local or semilocal approaches (see, e.g. [55,56] for titania). On the other hand, it should also be considered that these highly-reduced species – especially in the case of UT polar films – are in contact with the metal support, and their electronic structure can be strongly influenced by and

merge into that of the support (metallisation of the oxide layer as a depolarisation mechanism [25]). Again, to date there is no conclusive evidence to clearly favour one approach, and further validation studies are strongly needed. It should be noted that, when dealing with *polar* UT phases within the usual supercell approximation, i.e. phases that present a net dipole moment perpendicular to the surface, it is advisable to include a dipole correction into the Hamiltonian [57], as it effectively cancels spurious interactions due to the periodic boundary conditions in planar *polar* slabs [58].

Once the correct theoretical methods has been selected, it can be profitably employed in the machinery of structure prediction, which is the first step of any in-depth investigation and the basis of structure-property relationships. Starting from experimental information (typically, STM images with atomistic resolution whenever they are available, but also data coming from spectroscopic and chemical measurements), trial structures can be devised and put to computational test first by local energy minimisations using one of the many codes available (see for example [59]), to check that they correspond to local stationary points in the energy hypersurface, and then by first-principles molecular dynamics via, e.g. short runs of Car-Parrinello simulations [60], to check that they are true local minima and that there is no other lower-lying configuration in their immediate neighbourhood. Modern computational protocols and facilities nowadays allow one to improve upon this well-established scheme of biased or inspired guesses [34], by considering systematic searches within a first-principle framework. Density-functional global optimisation (DF-GO) methods have been already applied to gas-phase silicon [61], metal [62], metal oxide [63] and also supported metal [64] clusters, and there is, in principle, no difficulty (except possibly computational cost) in employing them to explore novel metal-supported UT oxide phases. Indeed, the first such example has already appeared in the literature, in which not only the structural but also the stoichiometry degrees of freedom have been explored by a GO algorithm [65], and many others are to be expected in a near future.

Naturally, the availability of computationally less demanding approaches could reduce the CPU requirements by orders of magnitude. Continuing with the analogy with metal clusters, for example, empirical potential have been derived in the literature that provide a reasonably accurate description of the metal-metal (see, e.g. [66]) and metal-oxide (see, e.g. [67]) bonding, even though improvements are still needed (see, e.g. [68]), and have thus been employed in GO simulations involving hundreds of atoms for both suspended and supported metal particles (1000 atoms is the current limit [69]). It can be noted in this connection that the limitations of the empirical potentials can in principle be overcome (at least in part) by using combined first-principles/empirical-potential approaches coupled with structural recognition algorithms [70]. The implementation of such a programme to UT oxide films has so far been hindered by difficulties in deriving accurate empirical potentials for oxide systems [71–79], especially considering that there are still some open problems concerned with the basic physics of UT systems and how to reliably model it. The potentiality of the approach has nevertheless been exemplified in a recent work by studying what is probably the most complex phenomenon in this field: the growth process of an UT oxide layer [80].

Matching experimental and simulated STM images (or STS spectra) is naturally the first goal in the process of structural characterisation. STM images are usually simulated theoretically via the Tersoff–Hamann approach [81], that links the experimentally

observed contrast to the modulation of the local density of states (LDOS) at the bias energy with respect to the Fermi level (E_f) at a given distance from the sample. The agreement between experimental and simulated STM contrasts in general however does not guarantee the correctness of a structural model, as different configurations can produce similar STM images. It is therefore reasonable to check the theoretical predictions against other experimentally-derived quantities. Once the structural problem is solved, the first-principles prediction of other properties (e.g. UPS, XPS and IRAS data) implies a comparable (or sometimes even smaller) computational effort, and has been profitably employed to complement STM characterisation (see, e.g. [24]).

A further step forward, once a given phase has been structurally clarified, is to consider not just a single structural model but several possible ones, each one with its own range of stability, and thus a complete phase diagram as a function of external parameters such as temperature (T) or oxygen pressure (P_{O_2}). This is the so-called *first-principles* or *ab initio* thermodynamics [82]. In this approach, the information coming from the DF calculations is used as an input for a thermodynamic analysis by evaluating the Gibbs free energy, G, of the slab as a function of T and P_{O_2} :

$$G(T, P_{O_2}) = E_{tot} + PV + F_{vib}$$

where E_{tot} is directly obtained from DF total energy calculations, the second term is the classical PV contribution, and F_{vib} accounts for the vibrational contribution to the Helmholtz free energy and can in principle also be calculated within the DF approach or from experimental data of phonon spectra. By expressing the chemical potential of the various species involved in the equilibrium as a function of the external parameters (with possible interdependencies and constraints due to the presence of bulk reservoirs), and using $G(T, P_{O_2})$ from the above formula, the phase diagram of the system can be routinely calculated. A word of caution is however needed to say because of the possible limitations of current DF approaches, as the energy ordering of the different structures can in some cases be incorrectly predicted (see, e.g. [83]). As a final step, the kinetics of growth should be simulated, since it is known – as remarked in the previous subsection – that some of these phases are only kinetically stable [41,84]. Some information in this respect can be derived from a thermodynamic analysis, as done e.g. [85].

3. Titanium oxide ultrathin films

Titania (TiO_2) is one of the most prominent materials for applications in technologically important areas such as photo-assisted oxidation [86], heterogeneous catalysis (used both as active catalysts as well as supports for metal catalysts) [87,88], gas sensors [89], wastewater remediation [90], optical devices (optical filters and optical waveguides) [91,92], antireflective coatings [93] and photovoltaic devices [94]. Since most of such peculiar properties are surface dependent, a detailed description of the surface properties of titania [37] is crucial to exploit the full potential of these systems in innovative devices. Moreover, a rapidly expanding subset of studies is focusing on the innovative properties that can be introduced when nano-dimensional titania phases are considered [36], e.g. nanosheets, nanotubes, nanorods and nanoclusters.

Because Ti can be present in several different oxidation states, most common being Ti^{2+} , Ti^{3+} and Ti^{4+} , many different oxides (TiO_x) are observed in nature, ranging from

fully oxidised ($x=2$) to reduced ones ($1 < x < 2$) [95]. The basic building block of all these oxides is a Ti centred octahedron whose connectivity with adjacent octahedra is highly variable. The most common bulk phases are TiO, Ti₂O₃ and TiO₂, which have been intensively studied, while other phases like Ti₃O₅, Ti₄O₇, Ti₅O₉, Ti₆O₁₁ and Ti₈O₁₅ [96,97] also exist. In addition to phases that have a well-defined stoichiometry, there is a strong tendency to form non-stoichiometric phases, i.e. phases presenting a variable stoichiometry where x can vary in a limited range while maintaining the same basic structure. Another peculiarity of reduced titania phases is the formation of the so-called Magnéli phases, formed through the formation of crystallographic shear planes [98]. However, relatively few studies have been carried out on the investigation of their structural and electronic properties due to the difficulty of their preparation. Recently, a report has been published where the surface properties of reduced TiO_{*x*} phases and the corresponding peculiar electronic and structural properties have been discussed [99]. As in all oxides, the structure and dynamics of defects play a relevant role to tailor the properties of titania and such aspects have been recently reviewed [100,101].

All these aspects (nano-dimensionality, reduced stoichiometry and defects) can be addressed by studying titania in the form of UT films. This motivates the intense activity that has been focused on the fabrication and characterisation of TiO_{*x*} films with a large range of x values. In the following we will first briefly consider the main peculiarities of the reference bulk phases and then review the work done on UT TiO_{*x*} films, produced either by surface oxidation (SO) of metallic Ti surfaces or by deposition of TiO_{*x*} films on a different metal surface.

3.1. Bulk TiO_{*x*} phases

3.1.1. TiO

TiO (titanium monoxide) presents a defective rock-salt structure which can contain a high concentration of randomly distributed vacancies in both the Ti and O sublattices, so that it can be prepared in a broad range of chemical composition depending on temperature and annealing conditions [102]. It represents a high-temperature phase in the titanium–oxygen phase diagram, which exists in equilibrium over a wide temperature interval from 1523 to 2033 K and over a wide composition range from TiO_{0.51} to TiO_{1.27} [103–106]. At temperatures below 1523 K it undergoes atomic and vacancy ordering, but the disordered state can be preserved via quenching from high temperatures [107]. Structural vacancies are an important part of the crystal structure of TiO and play an essential role for the magnetic [108], electrical and thermal properties [109].

3.1.2. Ti₂O₃

Ti₂O₃ (titanium sesquioxide) is attracting growing attention [110,111] as a consequence of its peculiar electronic properties. At room temperature (RT), Ti₂O₃ is isomorphous with the corundum (α -Al₂O₃) structure, i.e. metal and oxide ions are 6- and 4-fold coordinated, respectively. However, the hexagonal c/a ratio in Ti₂O₃ is anomalously low compared with that found in other corundum-like oxides. In addition, Ti₂O₃ undergoes a gradual transition to a metallic state in the temperature range 400–550 K, which is accompanied by an increase in the c/a ratio [112,113]. The electronic structure of bulk Ti₂O₃ oxide

(where the Ti^{+3} atoms have a d^1 electronic configuration) [114,115] and its surface [116] has been recently studied and compared with that of other corundum-like oxides.

3.1.3. TiO_2

TiO_2 surfaces can be considered as the most important model systems in the SS of TMOs, and are by far the most extensively studied oxide surface: the reader can find plenty of information in the most recent review articles [37,38].

Bulk TiO_2 (titanium dioxide) crystallises into three main phases, rutile, anatase and brookite. However, only rutile and anatase have played a significant role in the applications so far. Upon heating, interconversion between these phases can be observed which strongly depends on the actual crystallite sizes [36,117]: rutile is the most stable polymorph at the macroscale and ambient pressures and temperatures [118], while anatase and brookite become energetically preferred at small particle sizes because of their intrinsic lower surface energy [119–121].

However, if one considers TiO_2 in the form of UT films, other possible structural reference phases can in principle enter into the game. In particular, it has been demonstrated that colloidal solutions of TiO_2 nanosheets can be obtained by a top-down method (i.e. by delamination of layered bulk titanates [122]): they have a *lepidocrocite-like* [123] structure, and they have been characterised by XRD [124], TEM [125] and X-ray absorption fine structure (XAFS) [126] methods. In principle, also the $\text{TiO}_2(\text{B})$ polymorph could represent a possible candidate for the structure of UT fully oxidised films. Such an uncommon bulk phase is recently obtaining much attention because of a possible enhancement of the titania photocatalytic activity [127]. $\text{TiO}_2(\text{B})$ has been observed for the first time in 1980 [128] and recently characterised by TEM as a lamellae-like phase growing on anatase crystals [127].

3.2. Surface oxidation of Ti metal and alloys

The easiest way to produce TiO_x UT films is via SO of substrates exposing Ti atoms. This is an easy process because of the well-known tendency of Ti to bind to oxygen (see for example the use of Ti evaporation in vacuum technology). At variance with other metals [20], molecular oxygen is sufficiently reactive to accomplish total oxidation of Ti.

3.2.1. Oxidation of Ti metal

3.2.1.1. *Polycrystalline Ti (poly-Ti)*. The earliest UT TiO_x films were prepared by SO of a poly-Ti surface. The early stages of the growth were extensively studied in a wide range of O_2 partial pressures and substrate temperatures using various SS techniques, such as AES [129,130], XPS [130,131], mirror electron microscopy (MEM) [129] and direct recoils spectrometry (DRS) [130]. Azoulay *et al.* [130] studied the initial oxidation stages of poly-Ti at RT with O_2 exposure of 0–1000 L (L = Langmuir, i.e. exposure to 1 s at 10^{-6} torr) utilising DRS, AES and XPS for samples prepared in different ways: the role of the sample history was evidenced. Mixtures of different oxidation states of Ti (0, +2, +3, +4) are present during the whole course of oxygen exposure. Qualitatively, increasing amounts of the higher valence states are displayed for higher oxygen exposures.

Oxidation of pure titanium was investigated at RT under different oxygen pressures (10^{-8} – 10^{-6} torr). The kinetics of oxidation for each pressure was determined [131]. Measured film thicknesses were larger at higher pressures. Deconvolution of XPS spectra showed that TiO was the major oxide present and TiO₂ the minor component. Formation of Ti₂O₃ and Ti₃O₅ was also observed.

In a subsequent article [132], reactions of a well-characterised polycrystalline titanium surface with oxygen and water at 150–850 K were studied in UHV by XPS, TDS and FT-RAIRS. At 150 K, O₂ oxidises Ti⁰ to Ti²⁺, Ti³⁺ and Ti⁴⁺, but Ti exposure to H₂O at this temperature produces only Ti²⁺ species. At temperatures above 300 K, further oxidation of Ti by H₂O was observed. Maximum oxidation by both oxygen and water is achieved at 550–600 K. At a temperature of 650 K, Ti is gradually oxidised from Ti⁰ to Ti⁴⁺ with increasing exposure of O₂ (in Figure 3) [132]. Upon heating the oxidised titanium above 850 K, the oxide layer is completely reduced to Ti⁰. Depth profiling of an oxidised

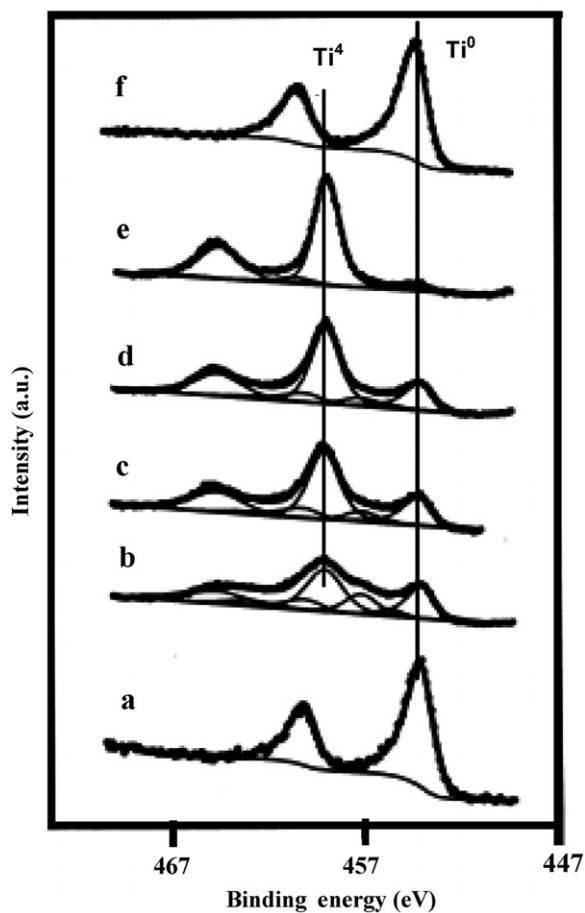


Figure 3. Ti 2p XPS spectra of (a) a clean Ti sample at 650 K, and after exposures to O₂ of (b) 6 L, (c) 12 L, (d) 18 L, (e) 24 L and (f) finally heating to 850 K in vacuum. From Reference [132].

Ti surface also showed that some reduced Ti species (Ti^{3+} and Ti^{2+}) are localised close to the oxide-metal interface.

The effect of temperature in low O_2 partial pressure (3×10^{-9} to 5×10^{-8} torr) was further studied [133,134]. The results demonstrated that at temperatures below 498 K only TiO_2 is detected whereas at higher temperatures there is evidence for the presence of Ti_2O_3 . This is due to the desorption of O_2 at low O_2 pressures and subsequent partial decomposition of TiO_2 at higher temperatures.

3.2.1.2. *Single crystal Ti (single-Ti)*. In the group of Madey [135,136] the SO of Ti(0001) has been studied using EELS, AES, electron stimulated desorption (ESD), UPS, and photo-stimulated desorption (PSD). The oxidation occurs at temperature as low as 90 K, and, according to PSD and ESD results, a fraction of the surface oxide behaves as expected for fully oxidised TiO_2 . Two distinct oxygen species were found: one sub-surface oxygen located below the Ti(0001) surface plane, giving rise to the lower work function, and the second assigned to surface oxygen of the TiO_x film. Unfortunately they did not provide any details on the surface oxide composition and surface reaction mechanism.

More recently Takakuwa *et al.* [137,138] investigated the initial oxidation kinetics on the Ti(0001) surface at 700 K by real-time AES combined with RHEED and high resolution XPS using synchrotron radiation. The results showed that: (1) O_2 adsorption obeys a zero-order reaction scheme before and after saturation; (2) in the initial stages of oxide growth, Ti_2O and TiO are the major species which induce a surface roughening; and (3) the roughened morphology is recovered by oxidation of Ti_2O and TiO into Ti_2O_3 , Ti_3O_5 and TiO_2 when higher dosing is carried out. Their results are similar to those reported on poly-Ti surface [130].

From the above reported results, we can conclude that the composition of TiO_x films greatly depends on the O_2 pressure and substrate temperature during oxidation: fully oxidised TiO_2 can be more easily obtained by oxidation of Ti surface at low temperature under high O_2 partial pressure, because TiO_2 is not stable at high temperature in vacuum. In these studies, structural details of the films have not been proposed.

3.2.2. Oxidation of Ti alloys

3.2.2.1. *Polycrystalline alloys*. The RT adsorption of oxygen on NiTi and FeTi was studied by AES [139]. Oxygen interacts preferentially with titanium at RT, leading to the formation of an overlayer of TiO_2 at low O_2 exposures ($\sim 2 \text{ L}$) for both NiTi and FeTi. Higher oxygen exposure induces a larger Ti segregation for NiTi in comparison to FeTi alloys and a thicker oxide is grown on the former. Heating an oxide-covered NiTi sample to 800 K leads to the complete dissolution of the oxide into the bulk.

The UPS and AES have been applied to study the oxidation of a polycrystalline Ni_3Ti sample [140]. At low temperature (150 K) oxygen adsorption leads to oxygen bonding to both Ni and Ti, so that Ni and Ti oxides form simultaneously. Upon heating to high temperature ($>700 \text{ K}$), Ni oxide is reduced to metallic Ni, and the resulting surface is thus covered with TiO_x . Dosing oxygen on clean Ni_3Ti at higher temperature ($>300 \text{ K}$) enhances the Ti-oxygen interaction leaving the Ni constituent unaffected.

3.2.2.2. *Single crystal alloys and surface alloys.* Most of the work done in this field is related to surfaces of PtTi alloys or surface alloys, whose structure and properties have been reviewed by Bardi [141]. In general, noble metals alloyed with the transition metals of the left side of the periodic table produce compounds with highly negative enthalpy of formation which very often form ordered intermetallic compounds. This class of materials gives rise to a wealth of surface phenomena, among which we can cite the formation of ordered 2D ('two-dimensional') phases, often referred as surface alloys. While the surface of bulk alloys are easily obtained by cleaving bulk alloy crystals, surface alloys are usually obtained by evaporating the minority component on a single crystal of the majority one or by segregation phenomena in bulk alloys.

The bulk Pt₃Ti alloy has a face centred cubic (fcc) structure where Ti atoms are at the cube corners and Pt atoms at the face centres. The (111) planes in the bulk have ABC... stacking sequence with a mixed composition of three Pt atoms and one Ti atom per unit cell in each plane (see Figure 4). The valence-band (VB) photoemission spectrum of Pt₃Ti cannot be obtained as a simple superposition or averaging of the VB spectra of the two metallic Pt [142] and Ti [143] elements, demonstrating that a strong hybridisation occurs in Pt₃Ti between the Pt 5d and Ti 3d states [144]. Alloying produces a distinct electronic structure with a deep minimum in the DOS at the E_f. This is correlated with the high heat of formation upon alloying [145]. Due to the inherent difficulties in preparing Pt₃Ti single crystals, the SO of the surfaces obtained by cleaving was studied by a limited number of groups. However, Pt₃Ti surface alloys can be easily prepared by deposition of one ML of Ti on the Pt(111) surface and successive short annealing in UHV at 773 K, resulting in the appearance of a (2 × 2) LEED pattern which has been interpreted as the signature of an ordered Pt₃Ti(111) surface alloy [146].

First, Bardi and Ross studied the SO of Pt₃Ti(111) and Pt₃Ti(100) surfaces as a function of O₂ pressure and substrate temperature by AES, and LEED [147]. For an O₂ pressure ranging between 10⁻⁸ and 10⁻⁶ torr and a substrate temperature between 600 and 1000 K, the AES and LEED measurements demonstrated the formation of a single-layer oxide phase, with TiO stoichiometry: the Ti atoms probably form a compact plane at the

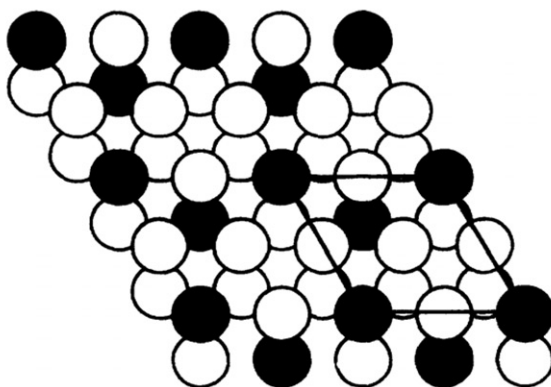


Figure 4. Top view of a Pt₃Ti(111) surface showing two atomic planes. The 2 × 2 superstructure is outlined and the Ti atoms are hatched.

interface with the substrate surface and the O atoms are situated on top of this Ti layer. The growth of a TiO ML results in the depletion of Ti from the underlying subsurface region. At a sufficiently higher temperature (1000–1200 K) and O₂ pressure (1×10^{-6} – 5×10^{-5} torr), SO leads to the growth of a multilayer phase, identified as TiO_{1.2}. This phase is derived from the TiO lattice by removing some Ti atoms to form an ordered-vacancy lattice. Oxidising in extreme conditions (atmospheric pressure, 1273 K) produces the formation of a thick film of TiO₂ (rutile), the most thermodynamically favoured bulk titanium oxide. Later results reported by Paul *et al.* [148] confirmed segregation of Ti at the surface of Pt₃Ti(111) at elevated temperatures (>650 K), but were interpreted as the formation of TiO₂ with some Ti³⁺ defects. Further data have been reported by Chen *et al.* [149] who have also investigated the SO of Pt₃Ti(111) single crystal surface as a function of the sample temperature by XPS and STM in relatively high O₂ pressure. They found evidence for oxygen-induced surface segregation of Ti to form TiO_x on the Pt₃Ti(111) surface, and clearly revealed two different oxidation processes: the oxide formed below 700 K (O₂ = 50 L) is prevalently TiO₂, compared with the Ti₂O₃ oxide formed at higher temperature (Figure 5). TiO₂ grows in the form of islands on the substrate surface while Ti₂O₃ wets the substrate surface and forms a flat and homogeneous oxide layer. This is in good agreement with the wetting behaviour of the TiO_x/Pt(111) UT films discussed in Section 3.3.4.2. The STM images showed that the TiO₂ oxide nucleates preferentially at defects, whereas the Ti₂O₃ oxide grows from step edges. Moreover, the authors demonstrated that the TiO₂ oxide can be reduced by adsorption of CO, while Ti₂O₃ oxide is irreducible under the same conditions. The formation of two different oxides on Pt₃Ti(111) is of relevance for the preparation of titania-supported catalysts.

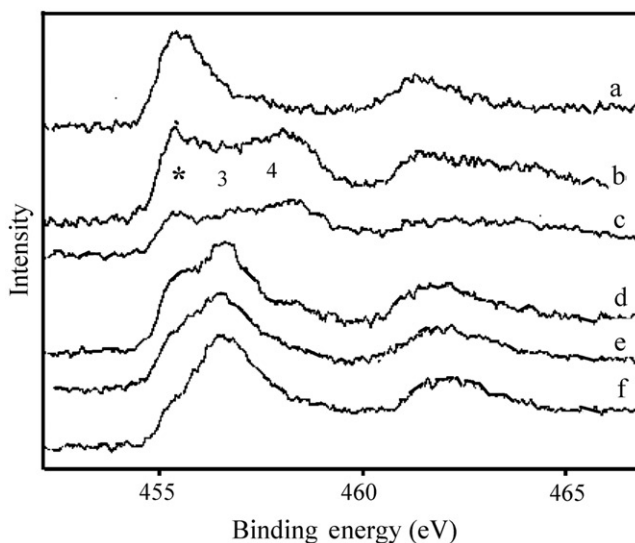


Figure 5. XPS spectra at grazing emission for clean Pt₃Ti(111) and Pt₃Ti(111) oxidised in O₂ (50 L) at different temperatures: (a) clean surface; (b) oxidation at 375°C; (c) oxidation at 400°C; (d) oxidation at 450°C; (e) oxidation at 650°C; (f) oxidation at 800°C. *corresponds to the metallic Ti* peak, 3 to Ti³⁺ and 4 to Ti⁴⁺. From Reference [149].

TiO₂ must be considered an active part in any catalytic reaction under reducing atmosphere. In comparison, Ti₂O₃ can be characterised as an inactive support for the active component. As the two oxides have different wetting behaviours with respect to a metallic phase, the dispersion and the electronic structure of titania-supported catalysts will be affected.

Matsumoto *et al.* [150] have studied the formation of TiO_x films by SO using ozone (O₃) on a Pt₃Ti surface alloy [146] at 300 K and subsequent annealing at 1000 K. Smooth thin films with a (3 × 5) structure were observed at 1 ML, and they propose that such structure is due to one layer of a Ti₂O₃ film similar to the (1 × 2) strands formed on reduced TiO₂(110) surfaces [37].

The SO of the single crystal stepped Pt₃Ti(510) surface at oxygen pressures below 10⁻⁵ torr and a temperature of 770 K was also studied [151]. The Pt₃Ti(510) surface consists of (100) terraces separated by double atomic steps. The exposure of the clean surface to oxygen at pressures in the range 10⁻⁷–10⁻⁵ torr leads to the growth of a TiO oxide layer which covers completely the substrate surface with a thickness of a few atomic layers. The TiO film has long range order and exhibits complex LEED patterns. The STM measurements indicated that the ordered array of steps is kept in the early stages of the oxide film growth, whereas a change of the step morphology and step orientation is observed during the oxidation process.

Very recently Hsieh *et al.* [152] have reported a real-time STM imaging study of the oxidation of the (2 × 2) Pt₃Ti(111) surface alloy (see Figure 4) at 300 K by continuously scanning with STM while either O₂ or NO₂ was introduced into the chamber. O₂ exposures did not cause any evident structural changes even if oxygen was detected on the surface by using AES. In contrast, NO₂ exposures caused definite changes in the surface morphology at 300 K. However, annealing both surfaces to 950 K resulted in the formation of an ordered TiO_x overlayer as characterised by both LEED and STM. The differences observed when the NO₂ gas was used as oxidising agent were interpreted as the consequence of the stronger oxidative power of the NO₂ gas. The structure of the TiO_x films obtained in this study has been related with those obtained for the films deposited by RD on the Pt(111) substrate (see Section 3.3.4.2).

The structure and composition of the TiO_x phases obtained by low-pressure oxidation at ~800 K of the Ni₉₄Ti₆(110) surface were investigated by XPS, LEIS, XPD and LEED [153]. Oxide layers consisting mainly of TiO₂ were grown on the alloy surface and their structure investigated by using XPD. The TiO₂ phase formed in the very early stages of oxidation has a quasi-hexagonal unit cell and its structure has no equivalent in any of the stable phases of TiO₂. The authors proposed a structure consisting of a layer of titanium atoms embedded between two atomic planes of oxygen atoms.

3.3. Ultrathin TiO_x films on other metal surfaces

3.3.1. Mo

Such a substrate has been intensively investigated in the group of Goodman and the complete work has been recently reviewed [23]. Three different Mo surfaces were used and the structure of the resulting TiO_x UT films was found to be rather dependent on the actual substrate surface.

3.3.1.1. *Mo(100)*. TiO_x films of varying thickness (<10.0 nm) were prepared on the $\text{Mo}(100)$ surface by evaporation of Ti in oxygen (5×10^{-7} torr) between 500 and 700 K [154]. The structure of TiO_x films depends on both coverage and annealing temperature. Owing to the excellent lattice match between $\text{Mo}(100)$ and $\text{TiO}_2(001)$ faces (4.45 versus 4.59 Å), the unannealed film showed a fully oxidised stoichiometry, a rutile structure and was well ordered along the [010] and [001] directions of the $\text{Mo}(100)$ substrate. Because of the presence of low coordination Ti cations (fourfold coordinated), the $\text{TiO}_2(001)$ surface is thermodynamically unstable and tends to facet or reconstruct. A $(2\sqrt{2} \times \sqrt{2})R45^\circ$ LEED pattern of reconstructed $\text{TiO}_2(001)$ surface was observed after annealing to 900–1200 K in UHV. The annealed films are partially reduced and exhibit Ti^{3+} and Ti^{2+} states.

3.3.1.2. *Mo(110)*. Ordered TiO_x films were prepared on a $\text{Mo}(110)$ substrate in two ways [155]. The first method consists of RD of Ti in 2×10^{-7} torr O_2 onto $\text{Mo}(110)$ at 600–700 K followed by annealing to 800 K in $\sim 10^{-7}$ torr O_2 . The second method consists of initially dosing <1 ML Ti onto the substrate, subsequently evaporating Ti in 2×10^{-7} torr at 600–700 K and then annealing to 800 K in $\sim 10^{-7}$ torr O_2 . LEED and XPS indicated that the films prepared with first method showed a (1×1) rectangular $\text{TiO}_2(100)$ structure, whereas the films prepared with the second way showed a (1×1) hexagonal $\text{Ti}_2\text{O}_3(0001)$ structure. Subsequently, they changed the growing conditions by exploring deposition of Ti in an O_2 ambient (5×10^{-7} torr) at 600 K, followed by annealing to higher temperatures (900–1200 K) in 5×10^{-7} torr O_2 [156]. XPS showed that TiO_x films annealed at 900 K were partially reduced, exhibiting small amount of Ti^{4+} , Ti^{3+} and Ti^{2+} species, whereas films annealed to 1200 K were fully oxidised and exhibited only Ti^{4+} . This result is however inconsistent with the data reported for films obtained by SO of a poly-Ti sample which have shown that the film is completely reduced to Ti^0 at high temperatures [132]. STM measurements revealed that the film grows at 900 K in a layer-by-layer way and that flat rutile $\text{TiO}_2(110)$ terraces with three different orientations are exposed (Figure 6). A further annealing of the films to 1200 K leads to a three-dimensional structure and a rough surface.

3.3.1.3. *Mo(112)*. A well-ordered 1 ML thick (8×2) - TiO_x film was grown on the $\text{Mo}(112)$ surface [157–159]. The preparation was rather complex: the authors first prepared well-ordered UT silica film by repeating: (1) evaporation of less than 1 ML of Si onto the $\text{Mo}(112)$ surface at RT; and then (2) oxidation at 800 K in a 1×10^{-7} torr O_2 for 5 min, followed by an increase in the substrate temperature to 1200 K for an additional 5 min, until a constant Si/Mo AES ratio was achieved. Then Ti (1–1.5 ML) was deposited onto this well-ordered UT SiO_2 film following oxidation at 850 K in 5×10^{-8} torr O_2 . After that, the sample was oxidised at 800 K in 5×10^{-8} torr O_2 for 10 min. The sample was then annealed at 1200 K in 5×10^{-8} torr O_2 for 10 min and subsequently annealed at 1400 K in 1×10^{-8} torr for additional 5 min to completely remove the SiO_2 film. Finally, an ordered (8×2) - TiO_x film was formed on the $\text{Mo}(112)$ surface. The structural model is shown in Figure 7, where Ti atoms decorate every eight Mo atoms in the $\text{Mo}(112)$ troughs and are bound to the surface via Ti–O–Mo bonds and to each other via Ti–O–Ti linkages. The same group also directly grew UT TiO_x films on $\text{Mo}(112)$ by stepwise deposition of

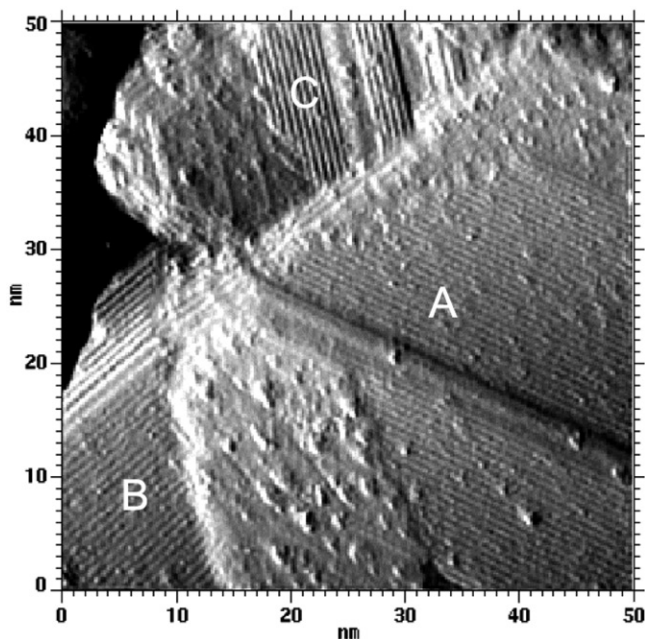


Figure 6. STM image ($V=2.0$ V, $I=2.0$ nA) of a titania film grown on Mo(110): Three different domains (labelled as A, B and C) of rutile (110)-(1 × 1) structure with a spacing of ~ 0.65 nm between the Ti-[001] rows. From Reference [156].

Ti onto the substrate surface followed by oxidation at 850 K [160]. Different TiO_x structural phases were obtained. XPS showed that the Ti 2p core level position shifts from lower to higher binding energy (BE) with an increase in the Ti coverage from sub- to multilayer. The Ti 2p peak of a TiO_x film with more than a ML coverage can be resolved into two peaks, one at 458.1 eV corresponding to the first layer, where Ti ions bind to the substrate Mo atoms through Ti–O–Mo linkages, and a second feature at 458.8 eV corresponding to multilayer TiO_2 where the Ti ions are connected via Ti–O–Ti linkages. Based on these assignments, the single Ti 2p_{3/2} peak at 455.75 eV observed for the (8 × 2)- TiO_x monolayer film was assigned to Ti^{3+} , consistent with the results obtained with HREELS.

Very recently, Zhang *et al.* [161] have reported a theoretical DF-based study where $\text{TiO}_x/\text{Mo}(112)$ UT films were analysed. They found that at the experimental pressure and temperature conditions used to grow the films a structure with a stoichiometry of TiO_3 is preferred. This conclusion is based on the thermodynamic analysis of the film stability as a function of the oxygen partial pressure and is corroborated by the comparison of computed and measured properties such as STM images, vibrational modes and core level BEs.

3.3.2. Ni(110)

TiO_x films grown on the Ni(110) surface were mainly investigated by the group of Thornton [162–165] using STM, LEED, HREELS, AES and synchrotron radiation. The oxide overlayers were prepared by PO of Ti film in 1×10^{-7} mbar O_2 at temperatures from

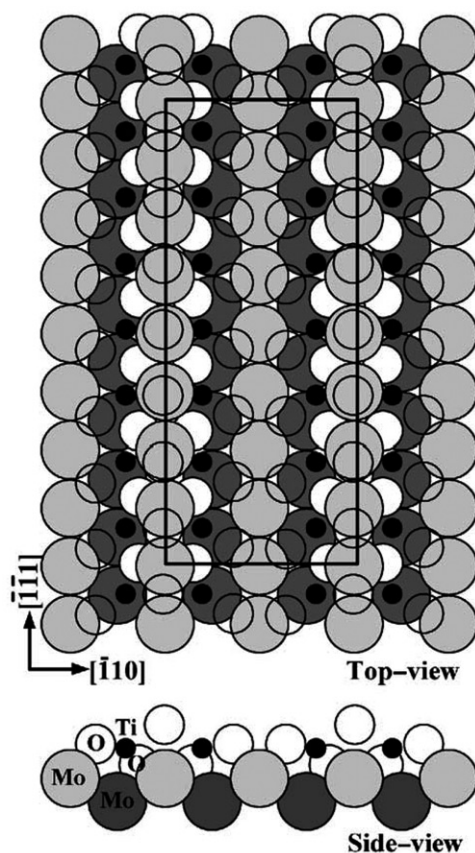


Figure 7. Top view of a possible structural model for the (8×2) - TiO_x film on Mo(112). From Reference [158].

800 to 900 K. In a series of several papers rather different interpretations of the experimental results were reported because, as explained by the authors, an inaccurate determination of the unit cells was caused by STM drifting. In the following we refer to the latest experimental interpretation [165]. A table summarising the TiO_x phases is shown in Figure 8. At low Ti coverages (< 1 MLE), a quasi-hexagonal phase was found similar to the one previously observed by Atrei *et al.* [153] on the $\text{Ni}_{94}\text{Ti}_6(110)$ alloy, i.e. a layer of titanium sandwiched between oxygen layers. At a coverage close to 1 MLE, a fully oxidised wetting layer was obtained which had been previously assigned to a $\text{TiO}(001)$ structure. Subsequently, such interpretation has been reconsidered [165] and the new model is very similar to the *lepidocrocite-like* nanosheet (albeit rotated by 90° with respect to the substrate) previously observed on the (1×2) -Pt(110) substrate [166] (see Section 3.3.4.3). For higher Ti coverage (in the range of about 1–6 MLE), under the same preparation conditions, it has been shown that 3D rods of rutile $\text{TiO}_2(110)$ grow on the wetting layer. The same authors [165] have studied the reactivity of such films with water using synchrotron-radiation-based surface tools such as soft X-ray photoelectron

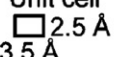
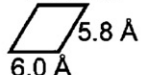
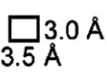
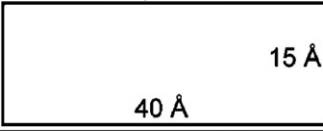
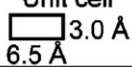
| | | |
|--|---------|--|
| | | Substrate: Ni(110) Unit cell  |
| Ti coverage (MLE) Oxidised to saturation by 10^{-7} mbar O_2 Annealed to 900 K | < 1 MLE | TiO ₂ quasi hexagonal overlayer Unit cell  |
| | ~ 1 MLE | TiO ₂ wetting overlayer Unit cell  Supercell  |
| | > 1 MLE | TiO ₂ (110) overlayer on wetting layer Unit cell  |

Figure 8. A table summarising the TiO₂ phases prepared on Ni(110) at different coverages expressed in MLE. From Reference [165].

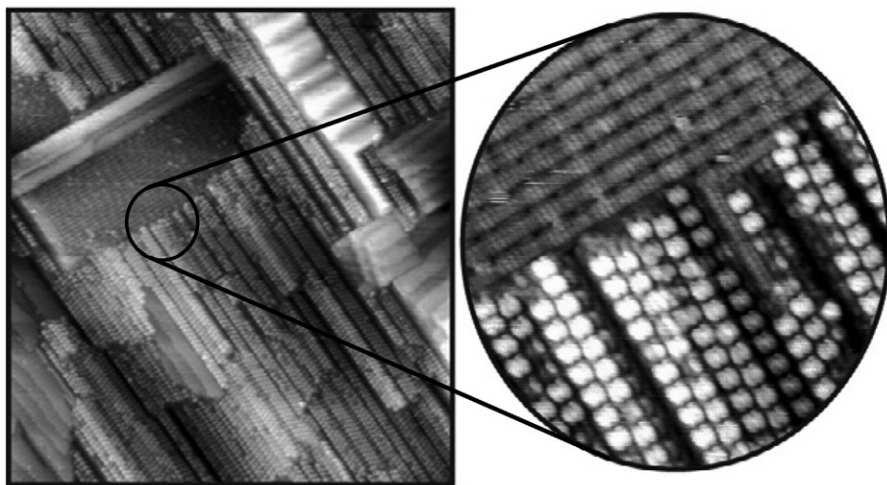


Figure 9. (a) $1000 \text{ \AA} \times 1000 \text{ \AA}$ STM image ($V = 1.2 \text{ V}$, $I = 0.9 \text{ nA}$) of a film grown by post-oxidation of 0.5 ML Ti on planar Ni(110). Both rectangular and hexagonal terminations of the TiO₂ film are observed. (b) Part of the image in (a) showing the titanium oxide nanodot structure coexisting with the rectangular NiO(001) structure. From Reference [164].

spectroscopy (SXPS) and X-ray absorption near-edge structure (XANES). They also reported the formation of an ordered array of TiO₂ nanodots (Figure 9) by a PO of 0.5 ML of Ti on Ni(110) [164] which may have applications in display technology [167] and solar cells [168]. Finally, very recently the same authors have reported the formation of reduced

TiO_x UT films by further annealing 2–4 MLE thick rutile TiO₂(110) islands at 1110 K for 15 min in a pressure of 1×10^7 mbar O₂ [169]. The resulting structures were discussed on the basis of the presence of crystallographic shear planes.

3.3.3. Cu(100)

Maeda *et al.* [170] have investigated the growth, structure and chemical state of UT TiO_x films on Cu(100). These oxide films were prepared by evaporating Ti at RT on a Cu(100) substrate where oxygen was chemisorbed at oxygen pressure 1×10^4 Pa, followed by a PO in 10^{-5} Pa O₂ at 623 K. The film has been proposed to consist of oxygen–titanium–oxygen trilayers with the stoichiometry of TiO₂. The LEED pattern obtained up to 1 ML is a hexagonal mesh, with two domains rotated by 90° with respect to each other with a lattice constant equal to 0.29 nm, but the author were unable to relate it to other known titania structures. However, the authors did not realise that a similar structure had already been proposed by Atrei *et al.* [153] in their study on the SO of the Ni₉₄Ti₆(110) alloy. The results also indicated that such structure is not stable above 1 ML.

Passeggi Jr *et al.* [171] also compared the TiO_x films obtained by PO of a Ti thin film and Ti/O₂ RD processes on Cu(100). The equilibrium oxide stoichiometry seemed to depend on the substrate temperature, the interface effects and the way oxygen is incorporated. The only way to obtain a fully oxidised film with a sharp interface with the substrate was through the RD process.

Recently, [172,173] TiO_x films were deposited on the Cu(100) surface previously saturated with oxygen, presenting a $(\sqrt{2} \times 2\sqrt{2})R45^\circ$ LEED pattern with a Cu missing-row reconstruction. The TiO_x films were prepared by evaporation of Ti at 573 K in an O₂ atmosphere ($P_{O_2} = 10^{-6}$ mbar). TiO_x films with different kinds of long-range order were obtained, depending on the oxide coverage and on the preparation procedure. An oxide phase with a centred rectangular unit cell ($3.61 \times 11.54 \text{ \AA}^2$) was observed in the very first stages of the Ti deposition. It consists of flat islands of uniform thickness. The growth of this phase is characterised by strong interaction between the oxide islands and the substrate. The STM results showed that the oxide film does not grow over the substrate surface but it is embedded within the outermost layer of the substrate. This particular growth could be explained by the missing row reconstruction induced by the saturation of the Cu surface with chemisorbed oxygen. It was impossible to prepare a complete layer of this centred rectangular phase, because prior to the completion of this layer, a quasi-hexagonal phase started to grow. The transition between these two phases was continuous and there was a quite large range of coverage where these two oxide phases coexist. At higher coverage (>1 ML), the substrate surface is completely covered by the oxide and the LEED pattern shows a regular hexagonal unit cell with composition TiO₂, explained as a O–Ti–O trilayer of close-packed atomic planes. This structure is fully consistent with the model previously proposed by Maeda *et al.* [170], and similar to the structure that was already suggested for the TiO₂ film prepared by SO of the Ni₉₄Ti₆(110) alloy [153].

3.3.4. Pt

Such a substrate has been the most intensively investigated one. There are several reasons for this choice: the first one is related to the relatively low reactivity of Pt toward oxygen, which favours a sharp substrate/oxide-film interface and a scarce substrate/oxide-film

interaction, as anticipated by the theoretical calculations by Jennison *et al.* [174] who calculated the relative energies of the Pt/O, Pt/Ti and Ti/O interfaces. Actually, more reactive substrates are expected to influence the interfacial chemistry via their participation to the oxidation process during the film growth.

In addition, the choice of the Pt substrate was originally stimulated also by the promotion properties of Pt in photocatalysis [175] and by the fact that TiO_x/Pt system is a prototypical example of the strong metal support interaction (SMSI) effect [176]. Actually, the origin of the SMSI effect was first clarified by Dulub *et al.* [177] by atomically resolved STM images: Pt islands deposited on TiO₂(110) were encapsulated by an ordered TiO_x film after UHV annealing at 1100 K with a corresponding decrease in the catalytic activity. Similar structures were subsequently observed by analysing the corresponding *inverse catalyst model*, i.e. directly growing TiO_x films on the Pt(111) substrate (the *z'* phase, see Section 3.3.4.2).

All the three low-index Pt surfaces have been investigated, but the most abundant data set has been obtained on Pt(111) by some accurate and long-term work done by the research groups of two of the authors of the present review. Most probably, the fact that it has been possible to clarify the fine details of seven different UT phases on the Pt(111) substrate is directly related to the higher surface density of Pt(111) with respect to the other low-index surfaces, which is beneficial in minimising the tendency of Ti atoms to interdiffuse into the Pt bulk and form alloys [178], which in turns tend to mess up the film growth. A comparable level of details have been obtained on VO_x UT films on similar noble metal substrates (i.e. Pd(111) and Rh(111)) [22,34].

Since the degree of understanding attained for the TiO_x/Pt(111) system by using a large set of experimental and theoretical tools is remarkable, in the following we will illustrate the major results obtained on such system in more details than for the other discussed systems.

3.3.4.1. *Pt(100)*. Matsumoto *et al.* [150] have investigated the growth of UT TiO_x films on Pt(100) by a complete set of experimental tools, i.e. LEED, XPS, AES, TPD, XPD, LEIS and STM. TiO_x films were prepared by RD of Ti in an oxygen atmosphere (6.7×10^{-5} Pa) at 300 K, followed by a subsequent annealing at higher temperatures (750–1300 K). The structure of these films strongly depended on the coverage of Ti and the annealing temperatures. Films with a (3 × 5) structure were observed after annealing of <1 ML Ti above 750 K [150]. This structure was attributed to one layer of a Ti₂O₃ film. Subsequent annealing to 700–950 K in vacuum produced disordered oxide regions and domains of a (4 × 13) structure with a square Ti–O net. This film further transformed upon annealing at 1000–1100 K into a phase exhibiting a (2√2 × 2√2)R45° structure that was attributed to a Ti₅O₈ film. When annealing ~2 ML of Ti at 850–1000 K, a (4 × 3√5)R60° structure was observed. The authors proposed that this structure is a TiO₂ tetragonal net with some O atoms in the second layer. The (4 × 3√5)R60° structure changed to a (3 × 5) structure after annealing above 960 K in vacuum due to the reduction of Ti ions. All the above reported structural assignments were made on an empirical basis, without any support from theoretical results and also the assigned stoichiometries were only tentative.

The same authors have also studied the structural and chemical changes occurring at the (3 × 5)-Ti₂O₃ film during oxidation with O₃ (ozone), NO₂ (nitrogen dioxide) and NO (nitric oxide) at 600 K, and reduction with CO and HCOOH (formic acid) [179].

3.3.4.2. *Pt(111)*. The $\text{TiO}_x/\text{Pt}(111)$ system was first studied by Boffa *et al.* [180] in 1995, when they reported on the preparation and characterisation (by XPS, LEED, STM and LEIS) of UT TiO_x films up to 5 ML range. They described their wetting behaviour and the tendency of interdiffusion of Ti into the substrate after different annealing treatments. A total of two ordered nanostructures were at that time described. First they described the presence, for a large coverage range, of a stoichiometric TiO_2 phase with a hexagonal ($\sqrt{43} \times \sqrt{43}$) $R7.6^\circ$ superstructure which corresponds to a unit cell of $18.2 \times 18.2 \text{ \AA}^2$. However, subsequent work by Sedona *et al.* [181] has demonstrated that this phase is actually a reduced phase (labelled as *w*, see below) whose structure has been solved [84] (see below). By annealing at high temperature (923–1123 K) in UHV, a second phase was observed. In this case the XPS spectrum showed two distinct components for the Ti $2p_{3/2}$ peak: one at 458 eV, identical to that reported in the previous phase and assigned to Ti^{4+} ions, and another at 456.2 eV which was assigned to Ti^{3+} ions. The authors proposed for this phase, a stoichiometry close to Ti_4O_7 . After the annealing the authors individuated from the LEED a commensurate structure with a size of $13.9 \times 18.2 \text{ \AA}^2$, noted as $[\begin{smallmatrix} 5 & 0 \\ 1 & 7 \end{smallmatrix}]$. Unfortunately, the quality of the STM images was not sufficient to derive any atomic model for the corresponding film. Only a simplified structural model of the TiO_2 layer, derived from the (111) surface of rutile with significantly expanded O–O spacing, was proposed. For the Ti_4O_7 phase, a close relationship with the (110) surface of rutile and an ordered array of O defects was suggested [180].

To rationalise the behaviour of such $\text{TiO}_x/\text{Pt}(111)$ system, an extensive work has been done in the SS group of the University of Padova. With respect to the two phases reported by Boffa *et al.* [180], a more complex situation with plenty of different phases has been described: after a long and patient search [182], optimised experimental conditions have been found, which revealed as effective recipes for preparing seven different almost pure (as judged by LEED and spot STM images) UT phases of TiO_x ($1.2 \leq x \leq 2$) on $\text{Pt}(111)$ [181]. All the resulting phases have been characterised by different surface science techniques, i.e. photoemission from core and valence levels (including synchrotron radiation studies) [181,183], LEED [181,184], XPD [181], STM [181,184], and models have been obtained by DF calculations (see Section 2.2 for the adopted theoretical framework) so that reliable stoichiometries were derived [84,185–187].

The preparation procedures for obtaining the $\text{TiO}_x/\text{Pt}(111)$ films implied two main steps: (i) the deposition of a precursor film at RT by RD with a well-defined Ti dose in an O_2 pressure of 10^{-5} Pa, (ii) a post-deposition thermal treatments at different temperatures and O_2 pressures ($5 \times 10^{-4} \leq P_{\text{O}_2} \leq 10^{-8}$ Pa). In particular, in order to get optimised conditions for each phase, the Ti coverage (expressed in MLE), the post-deposition annealing temperature and oxygen pressure were carefully analysed. Figure 10 summarises such optimised conditions as well as the structural parameters deduced from the LEED patterns (Figure 11) and STM images (Figure 12) of the different long-range TiO_x phases, which correspond to different stoichiometries and defects distribution [84,181,183,184]. The combined LEED and high resolution STM data have shown that each phase corresponds to large domains with either hexagonal or rectangular unit cell. The hexagonal structures can either be arranged in a so-called *wagon-wheel-like* [184] or in a *kagome-like* (a Japanese word meaning bamboo basket) lattice [84] (where hexagons are sharing their vertices). Some of the rectangular structures are characterised by a peculiar *zigzag-like* appearance [185,186].

| | | | | | |
|--|------------------------|---|--|--|---|
| Annealing O ₂ pressure (Pa) | 5 × 10 ⁻⁴ | | rect-TiO₂ $\begin{bmatrix} 1.16 & 0.18 \\ 0.58 & 1.56 \end{bmatrix}$ Incommensurate rectangular 3.8 Å x 3.2 Å | | rect'-TiO₂ $\begin{bmatrix} 1.37 & 0.0 \\ 1.95 & 2.55 \end{bmatrix}$ Incommensurate centred rectangular 3.7 Å x 12.2 Å |
| | 10 ⁻⁵ | k-TiO_{1.5} $\begin{bmatrix} 2.15 & 0.0 \\ 0.0 & 2.15 \end{bmatrix}$ Incommensurate hexagonal 6 Å x 6 Å | z-TiO_{1.33} $\begin{bmatrix} 2.5 & 0 \\ 1.8 & 3.6 \end{bmatrix}$ Incommensurate rectangular 6.8 Å x 8.6 Å | w-TiO_{1.2} $\begin{bmatrix} 7 & 1 \\ -1 & 6 \end{bmatrix}$ Commensurate hexagonal 18.2 Å x 18.2 Å $(\sqrt{43} \times \sqrt{43})R7.6^\circ$ | |
| | 10 ⁻⁸ (UHV) | | z'-TiO_{1.2} $\begin{bmatrix} 6 & 0 \\ 3 & 6 \end{bmatrix}$ Commensurate rectangular 16.6 Å x 14.4 Å $(6 \times \sqrt{3})-rect$ | w'-TiO_x $\begin{bmatrix} 8 & 3 \\ -3 & 5 \end{bmatrix}$ Commensurate hexagonal 19.4 Å x 19.4 Å $(7 \times 7)R21.8^\circ$ | |
| | | 0.4 | 0.8 | 1.2 | ≥2 |
| Equivalent monolayer (MLE) | | | | | |

Figure 10. Summary of the TiO_x phases on Pt(111) prepared in different conditions (i.e. O₂ pressure, in Pa, and Ti dose, in MLE): *k* = kagomé; *z* = zigzag-like; *w* = wagon-wheel-like; *rect* = rectangular. Superstructures in matrix notation are related to the hexagonal mesh of Pt(111) with $d = 2.77 \text{ \AA}$ and $\alpha = 120^\circ$. The corresponding unit cells are also reported. The actual stoichiometries reported were obtained from the corresponding models derived by DF calculations. Based on data from References. [84,181,183].

The set of TiO_x phases can be divided into two groups depending on the oxidation state of Ti, whose occurrence is basically driven by the oxygen partial pressure during the post-deposition annealing. For $P_{O_2} < 10^{-5} \text{ Pa}$, the *w*, *w'*, *z* and *z'* reduced phases are obtained (Figure 10), characterised by a Ti 2p BE at 456.4 eV. They are all wetting Ti–O bilayers where the Ti layer is at the interface with the Pt substrate and the O layer is the topmost layer (as proven by XPD data [181]). As a whole, the different structures of the reduced phases can be interpreted as the final products of a self-assembling process where the Ti atoms tend to organise in pseudo-epitaxial regions on Pt(111), while the O atoms in the topmost layer (more abundant due to stoichiometry constraints) solve the *packing* problem by creating pseudo-epitaxial regions that exhibit dislocation lines (dark *troughs*) or regions where Ti vacancies (defects or *picoholes*) can be formed, as clearly seen in the corresponding STM images (Figure 12) [84]. According to DF simulations of the STM images within the Tersoff–Hamann approach (see Section 2.2), the *zigzag-like habitus* of the *z* and *z'* phases is to be connected to true electronic effects related to the presence of differently coordinated Ti atoms: the brighter spots correspond to four-coordinated Ti ions (Ti₄), whereas the darker ones to three-coordinated Ti ions (Ti₃) (see in Figure 13 the case of the *z*-TiO_{1.33} phase [185]).

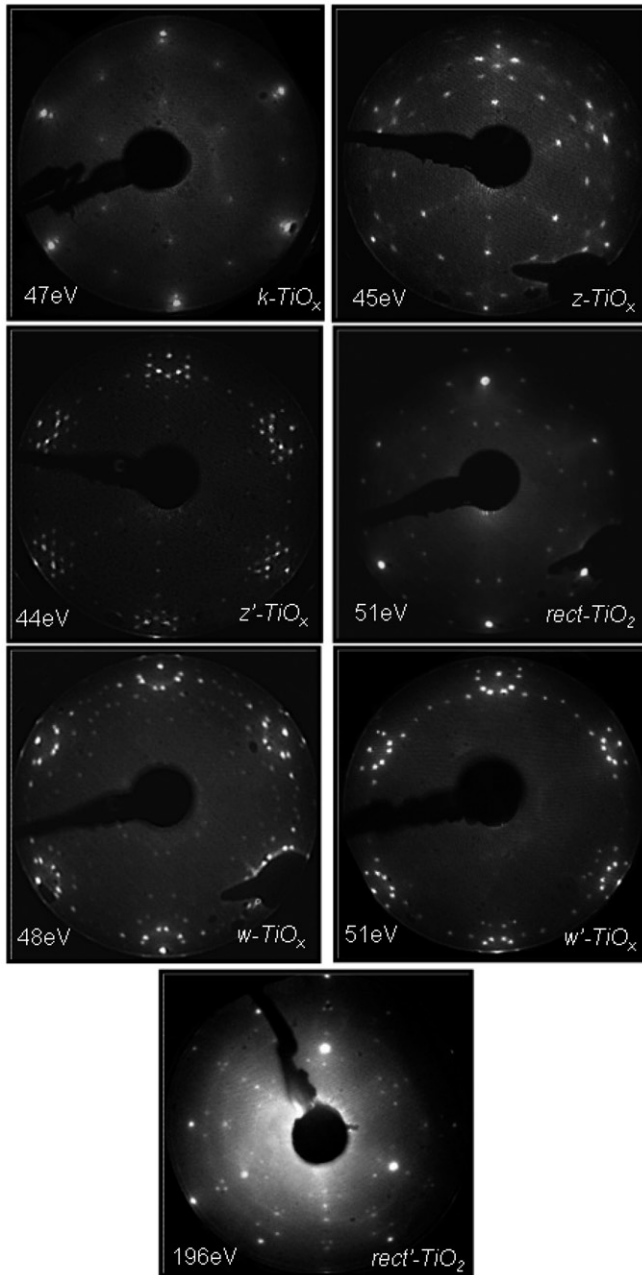


Figure 11. Summary of the LEED patterns of the observed TiO_x long-range ordered phases grown on Pt(111). The pertinent primary beam energies are reported in each panel. Based on data from References [181,183].

| | | | | | | |
|--|------------------------|----------------------------|-------------------------------|-----|--------------------------------|--|
| Annealing O ₂ pressure (Pa) | 5 × 10 ⁻⁴ | | <i>rect</i> -TiO ₂ | | <i>rect'</i> -TiO ₂ | |
| | 10 ⁻⁵ | <i>k</i> -TiO _x | <i>z</i> -TiO _x | | <i>w</i> -TiO _x | |
| | | | <i>z'</i> -TiO _x | | <i>w'</i> -TiO _x | |
| | 10 ⁻⁸ (UHV) | | <i>z'</i> -TiO _x | | <i>w'</i> -TiO _x | |
| | | 0.4 | 0.8 | 1.2 | ≥ 2 | |
| Equivalent monolayer (MLE) | | | | | | |

Figure 12. High-resolution STM images: *k*-TiO_x phase (30 Å × 30 Å, $V = -0.4$ V, $I = 1.06$ nA), *z*-TiO_x phase (60 Å × 60 Å, $V = 0.1$ V, $I = 1.5$ nA), *z'*-TiO_x phase (90 Å × 90 Å, $V = 0.8$ V, $I = 1.5$ nA), *rect*-TiO₂ phase (90 Å × 90 Å, $V = 0.8$ V, $I = 1.5$ nA), *w*-TiO_x phase (75 Å × 75 Å, $V = 1.3$ V, $I = 1.9$ nA), *w'*-TiO_x phase (126 Å × 126 Å, $V = 0.2$ V, $I = 1.0$ nA). Based on data from References [181,184].

An interesting study has been carried out on another *zigzag-like* phase, i.e. the one labelled as *z'*, easily prepared by annealing the *z* phase at ca. 673 K in UHV [185,186]. Depending on the post-annealing time in UHV, the evolution of surface defects (*troughs* and *picoholes*) has been followed by atomically resolved STM images and it represents an example on how a SS rigorous approach on model systems can provide valuable insights on the role and evolution of defects in oxides. A detailed description of the evolution of each defect as a consequence of heating has been obtained at the DF level (Figure 14) [186]. A similar, but not identical, *z'* phase has been found to grow on Pt and Pd islands deposited on TiO₂(110) single crystals and heated in UHV at high temperature [177,188]: as a consequence of the SMSI effect the metal islands are encapsulated after a UHV annealing by a very thin TiO_x layer where a *zigzag-like* motif is observed. However, it is to be noted that the preparative conditions are slightly different in the two cases. Based on the results of DF calculation, Jennison *et al.* [174] proposed an atomic model consisting of a polar self-limited double layer which is rather complex and contains some questionable points. In addition, recently Bowker raised the question whether this *z'-like* layer is an intermetallic-like alloy or a complete TiO_x bilayer [189]. However, the excellent

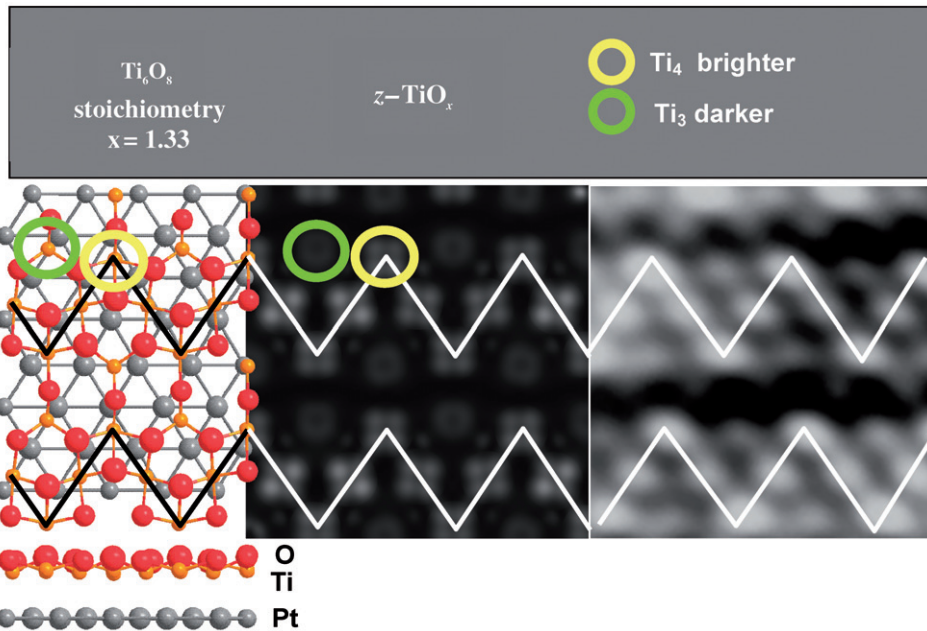


Figure 13. DF-derived model (left) for the *zigzag-like* $z\text{-TiO}_{1.33}/\text{Pt}(111)$ system. Ti atoms in orange, O atoms in red and Pt atoms in grey. The experimental (right) and Tersoff–Hamann simulated STM images are compared. The different Ti coordinations (Ti_4 and Ti_3) are outlined with circles of different colours. Based on data in Reference [185].

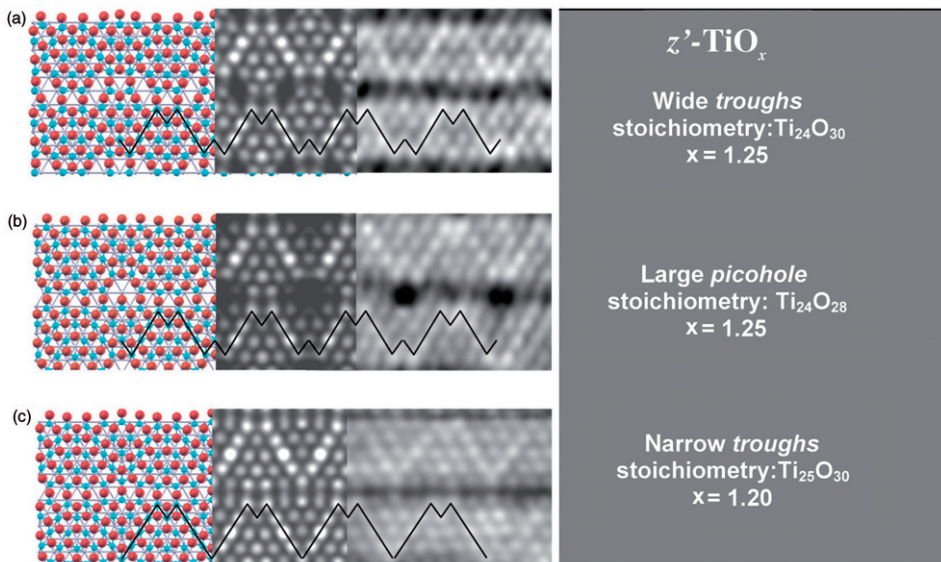


Figure 14. DF-derived model (left) for the *zigzag-like* $z'\text{-TiO}_x/\text{Pt}(111)$ system. Ti atoms in light blue, O atoms in red. The experimental (right) and Tersoff–Hamann simulated STM images for the different defects observed during the UHV annealing are compared. Based on data of Reference [186].

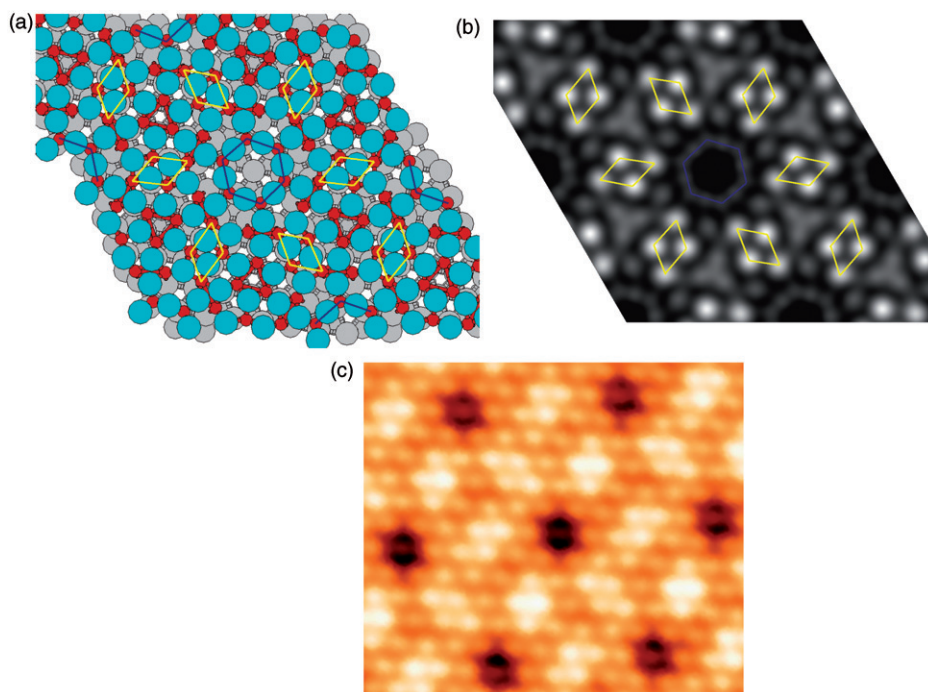


Figure 15. *Wagon-wheel-like* w - $\text{TiO}_x/\text{Pt}(111)$ phase: (a) DF-derived structural model: yellow segments link the Ti_4 atoms; blue segments link the six Ti_3 atoms at the border of the central cavity; (b) simulated constant-current STM image at +1.0 V; (c) experimental constant-current STM image at +1.0 V. In (a), Pt atoms are depicted in grey, Ti in red and O in light blue. From Reference [84].

agreement between the recent DF model and experiments [186] gives some support to the latter hypothesis, at least in the case of the TiO_x/Pt system.

An interpretation similar to the one invoked for the z phase (i.e. the different coordination of Ti atoms) has also been proposed to explain the *wagon-wheel* contrast of the w phase (Figure 15) [84]. However, despite the good agreement between experimental and simulated STM images, there are still open questions concerning this w phase. The main issue is that in this case, at variance with the z' case, the theoretical Ti coverage (0.7 MLE) does not match the experimentally derived one ($0.8 < x < 1.2$ MLE, see Figure 10). One is therefore forced to hypothesise that some of the deposited Ti atoms do not stay in the TiO_x film, but intermix with the support, possibly producing some sort of Pt/Ti sub-surface and/or surface alloy, similar to what it has been suggested in the literature for the encapsulating *pin-wheel* phase obtained after UHV heating of the $\text{Pd}/\text{TiO}_2(110)$ system [188]. In addition, the structure depicted in Figure 15 is a stable local minimum, but other stable structures with the same stoichiometry are also predicted at a DF level, such as a *pin-wheel* phase showing a *habitus* similar to the one found for the $\text{TiO}_x/\text{Pd}(111)/\text{TiO}_2(110)$ system [188]. Hence it seems that the actually observed phase is the result of a subtle balance between different factors, like the nature of the substrate, the preparative (kinetic) conditions, so that the mentioned debate on the

nature of the observed phase (i.e. intermetallic-like alloy versus a complete TiO_x bilayer) is still an open question and further investigations are needed to solve it.

For $P_{\text{O}_2} > 10^{-5}$ Pa, the *rect* and *rect'* phases were obtained corresponding to a fully oxidised Ti with a BE at 458.6 eV, which have, at variance with the reduced films, an O–Pt interface. Interestingly, as a consequence of the scarce Pt–O interaction [174], such *rect* and *rect'* oxidised phases are observed with identical cell parameters both on the Pt(111) [187] and (1×2) -Pt(110) substrates (see Section 3.3.4.3, [166,190]), and tend to dewet from the substrate and grow as flat islands. A similar *rect*- VO_2 phase was already observed on Pd(111) [191]. The *rect* phase is actually confined to a thickness corresponding to four atomic layers, while the *rect'* one can be up to several layers thick and is actually obtained when higher Ti doses are used (>1.2 MLE). The really important point is that, because of the scarce interaction between the fully oxidised film and the Pt substrate (as also demonstrated by specific DF calculations [187]), the substrate acts as a mere *arena* where the films assemble and the actual final phases can be representative of titania confined at the nanoscale, which potentially are different from the bulk-like phases. Actually, the structure of the *rect* nanophase has been unequivocally associated with a self-limited *lepidocrocite-like* nanosheet, in complete agreement with DF calculations and XPD experiments [166,190] (see Section 3.3.4.3). Preliminary data on the *rect'* phase favour the assignment of its structure to the layered $\text{TiO}_2(\text{B})$ phase [192].

Larger Ti deposits (>2 MLE) produced nanoparticles (NPs) of fully oxidised titania on top of a reduced wetting ML, whose structure is actually depending on the preparation procedure [193]. These NPs are 3D, randomly distributed but exhibit a preferential azimuthal orientation with respect to the Pt(111) substrate, probably because of the templating effect of the wetting ML. When the deposition is carried out by successive steps, followed by a thermal treatment of the sample at 920 K in O_2 (1.33×10^{-5} Pa), the fully oxidised titania NPs grow on top of the *w* phase. The deposition procedure is similar to the one adopted by Boffa *et al.* [180] and this might explain the discrepancy between their interpretation of the $(\sqrt{43} \times \sqrt{43})\text{R}7.6^\circ$ phase and the one subsequently reported: according to the first study this phase would be fully oxidised and would exist in a large coverage range between 1 and 5 MLs, whereas the subsequent interpretation, supported by XPD and theory [84,181], associates it to the reduced *w* phase, i.e. a 1 ML-thick phase exhibiting the *wagon-wheel-like* structure. Most probably, Boffa *et al.* wrongly associated the LEED of the wetting ML with the XPS data of the fully oxidised NPs deposited on top of it.

After studying the geometric structures of these TiO_x phases on Pt(111), an electronic structure investigation of the same phases by means of high-resolution Ti 2p and O 1s core level and by VB UPS using synchrotron radiation has been reported [183]. The VB data were collected with photons of 200 eV energy, corresponding to the minimum cross section for the Pt 5d levels so that the contribution of the substrate is effectively quenched and the structure of the film evidenced. The VB-UPS results demonstrated that the electronic structure of the reduced films is quite similar to that previously reported for the oxidation of metal Ti, and fairly consistent with the presence of a Ti–Pt interface, in agreement with previously reported XPD data [181]. The analysis of the region near E_f has also suggested that mixing of Ti–Pt states play a major role in determining the electronic structure of the reduced films.

Very recently, Agnoli *et al.* [41] have reported a study where the combined use of LEEM and μ -LEED allowed the *in-situ* monitoring of dynamical processes at the $\text{TiO}_x/\text{Pt}(111)$ interface. The transformations between different phases were investigated and a general outcome of this study was that the kinetic factors have a relevant role in the preparation of such UT films and must be taken into account in order to explain the observed transformations. In particular, heat-induced mass transport of Ti atoms in and out of the substrate bulk is to be hypothesised to clarify some observed coverage dependent phenomena.

Finally, we mention that the catalytic properties of UT $\text{TiO}_x/\text{Pt}(111)$ films themselves have started to be explored [194,195].

3.3.4.3. *Pt(110)*. The fully oxidised titania phases prepared on the Pt(111) substrate were also prepared under similar conditions on the (1×2) -Pt(110) substrate. Such surface orientation (two-fold symmetry) was chosen in order to induce single-domain growth of the overgrowing film. This is further favoured by the (1×2) missing-row reconstruction of Pt(110) with its highly anisotropic corrugation: the surface is atomically smooth along the [110] close-packed direction, while it shows alternating ridges and *troughs* along the reconstructed [001] azimuth.

Actually, *lepidocrocite-like* single-domain nanosheets (i.e. the *rect*- TiO_2 phase already seen on Pt(111)) were obtained with a (14×4) coincidence superstructure and their structure, electronic properties and morphology have been discussed in great details on the basis of LEED, photoemission (both core and VB), XPD, STM and DF calculations [166,190]. The excellent agreement between simulated and experimental XPD patterns gave the ultimate demonstration of the structure of the investigated nanosheet (Figure 16). According to the DF calculations, the formation of the *lepidocrocite-like* nanosheet can be thought as originating from a (100) oriented anatase bilayer which spontaneously restructure by a uniaxial relative sliding of one single layer with respect to the other by half a unit cell. The process is self driven by the spatial confinement, whereas a minor role is played by the interaction with the substrate. Figure 17 shows a comparison between the experimental high resolution STM image of the (14×4) -*rect* phase and the corresponding Tersoff–Hamann simulation carried out on the *lepidocrocite-like* nanosheet.

3.3.5. *Ru(0001)*

The structure, chemical composition and thermal stability of TiO_x films with thickness of up to 3 ML grown on a Ru(0001) substrate were investigated by STM, XPS and AES [196]. The films were prepared by evaporation of Ti in 1×10^{-7} mbar O_2 onto Ru(0001) at 640 K, followed by annealing in 1×10^{-7} mbar O_2 or in UHV at temperatures between 700 and 1000 K. Depending on the Ti coverage and post-annealing conditions, several different structures of Ti oxide were found. The authors describe the formation of triangular ML islands, whose density depends on whether post-annealing is done under O_2 pressure or in UHV. At ML coverage the system is not fully oxidised. Flash annealing to 1000 K in oxygen leads to the formation of a fully oxidised film exhibiting an imperfect Moiré pattern, associated with a hexagonal overlayer with a lattice constant of 0.3 nm, whose structure is fully consistent with the model previously proposed by Maeda *et al.* [170] on top of Cu(100) and by Bardi *et al.* for the SO of the $\text{Ni}_{94}\text{Ti}_6(110)$ alloy [153].

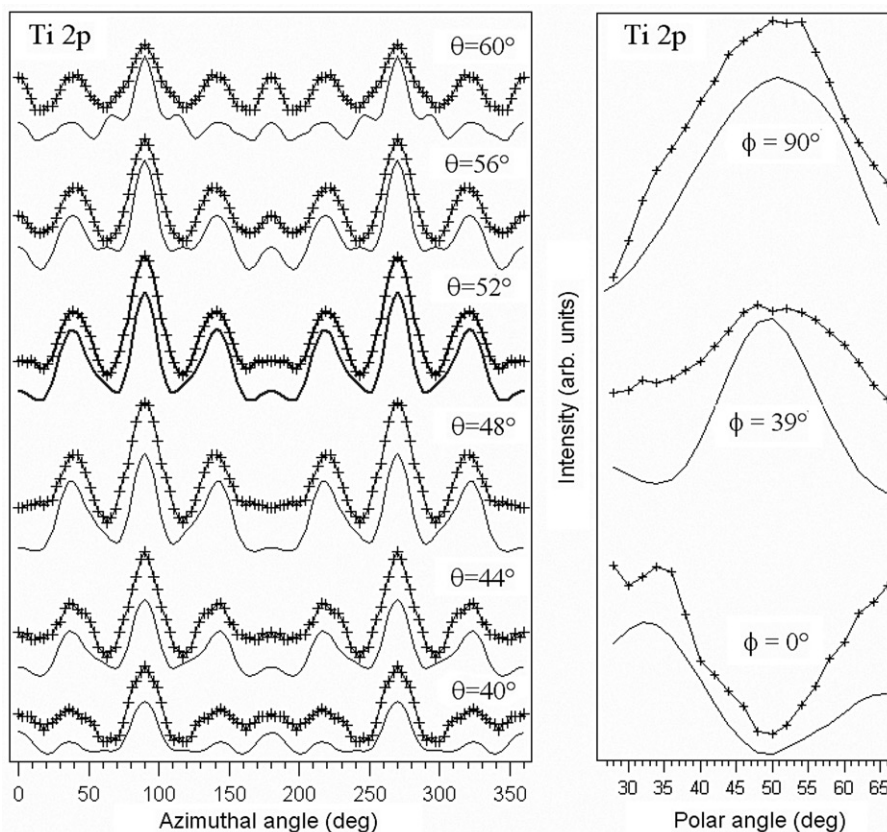


Figure 16. Comparison between selected azimuthal and polar simulated (full lines) and experimental (marked lines) XPD scans for Ti 2p emission from a single *lepidocrocite-like* nanosheet on (1×2) -Pt(110). From Reference [190].

3.3.6. *Au(111)*

The Au(111) surface has also been considered as a substrate for the growth of titania UT films [197–199]. A peculiar preparation technique was adopted in Reference [199]: the reactive-layer-assisted deposition, in which a physisorbed multilayer of one reactant is first deposited on a substrate and the second reactant (metal) is then physical-vapour deposited onto this layer. The metal atoms react with the loosely bound molecular multilayer at relatively low temperatures. Raising the substrate temperature then causes any unreacted, adsorbed molecule to desorb from the substrate surface, and the final product compound is left on the surface in the form of an ensemble of NPs, rather than UT films. In the case of TiO_x on a 10 ML thick layer of H_2O adsorbed on Au(111) the system was characterised via XPS and STM measurements, showing that it consists of titania NPs of 0.5–1 nm in size self-organised in complex patterns on the surface [199]. Well-separated TiO_x islands were instead prepared via physical vapour deposition of Ti on the bare Au(111) surface and successive PO conducted at 300 K with a final annealing at

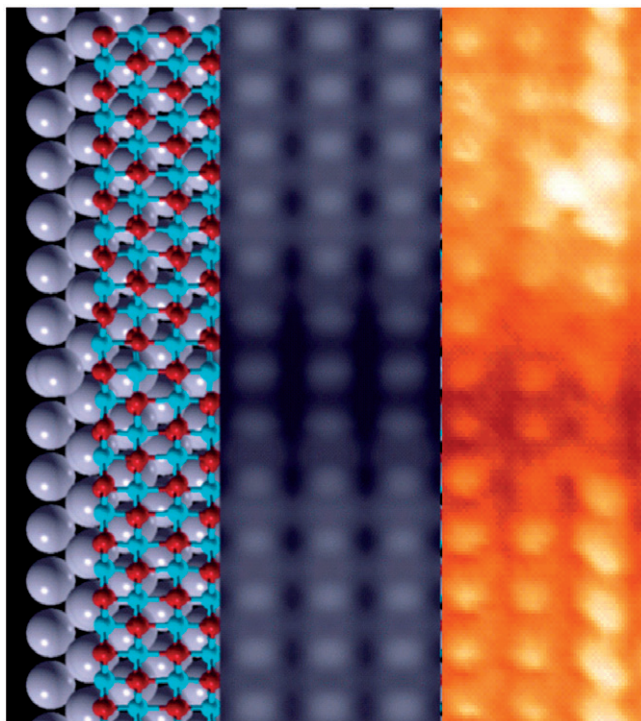


Figure 17. [Colour online] Left panel: top view of the 14×1 slab DF model of the *lepidocrocite-like* titania nanosheet. Central panel: Tersoff-Hamann simulation of the STM image. Right panel: experimental STM image ($V = +1$ V). From Reference [190].

temperatures ranging from 600 to 900 K [200]. Ti was shown to nucleate at the elbow sites of the herringbone reconstruction of the substrate, the oxidation state of Ti was found to depend on the annealing temperature, with TiO_2 stoichiometry obtained at the higher values, and partially reduced phases produced at lower T. Moreover, UT TiO_2 films have been prepared on Au(111)/mica substrates by either electron beam evaporation from TiO_2 -containing graphite crucible or dip coating in titanium tetrasopropoxide solutions [201]. It was reported that fully oxidised TiO_2 films can be deposited at $P_{\text{O}_2} > 4 \times 10^{-5}$ mbar which tend to cluster into 3D NPs. In the case of a 10 nm thick TiO_2 film, the Au surface is completely covered by TiO_2 . For dip coating, the precursor concentration in the solutions strongly influences the TiO_2 films surface morphology. At higher concentration (>0.01 M) small and highly porous island are formed; at lower concentrations a thin continuous film is obtained. In addition, UT TiO_2 films were also synthesised by evaporation of Ti on the Au NPs covered Si(111) surface in O_2 atmosphere ($P_{\text{O}_2} = 5 \times 10^{-8}$ mbar) [202]. The results showed that the TiO_2 films prefer to grow on the spots among the Au NPs with both (111) and (110) orientations.

3.3.7. $W(100)$

Epitaxial TiO_x films of thickness ranging from 0.3 to 7 nm were grown on the W(100) surface [203–205]. The thicker films were shown to exhibit an epitaxial growth and to be

terminated with a TiO₂(110) surface. As the film thickness decreased, however, the formation of interface-stabilised, non-stoichiometric phases was demonstrated via LEED and XPS. Unfortunately, no STM images were given for the thinnest films, so that no structural model was proposed. Their electronic properties have been studied by photoemission and vibrational spectroscopies [205]. When the films are below 7 ML, they appear non-stoichiometric due to the charge transfer from the W substrate and thus cause band bending and pushed VB onset of TiO₂ films to higher BE. The work function of the W substrate increases by 1.3 eV when covered by 0.3 ML of TiO₂. The thicker TiO₂ films (>7 ML) display stoichiometric TiO₂ properties and show the VB onset 2.85 eV below the E_f. The vibrational spectroscopy indicated three phonon bands at 368, 438 and 829 cm⁻¹ (at 273 K) for these TiO₂ films and their intensity scales linearly with film thickness and shift slightly to lower frequencies with temperature.

4. Aluminium oxide ultrathin films

Al₂O₃ is a material that has a great number of technological applications: as a catalyst or catalyst support, as a cutting-tool or protective material and as tunnelling barrier in electronic-device fabrication. It is a good insulator with a band gap of 9.5 eV [206] and cannot be made conducting by doping. The common chemical composition of aluminum oxide is Al₂O₃ (also named as alumina or sapphire), which exhibits several different bulk phases. Besides the stable phase α -Al₂O₃, alumina can also exist in a number of metastable polymorphs [207–209] such as, β -, γ -, η -, ν -, κ - and θ -alumina [210]. The structures of the metastable aluminas can be divided into two distinct categories based on either an fcc or hexagonal close packed (hcp) arrangement of the anions. The first step towards an understanding of the different physical properties of the diverse polymorphs is the inspection of their atomic structures.

In the following we first briefly summarise the main peculiarities of the reference bulk phases and then review the work done on UT alumina films, produced either by SO or by deposition on a different metal surface. Most of the work done on the growth of alumina UT films has been done by SO of bulk surfaces of M_xAl alloys (M = Ni, Fe, Cu) single crystals. The alumina films prepared by this method are sometimes long-range ordered and well characterised. At variance with the titania UT films, as evidenced in Section 4.3, the deposition of alumina films by Al evaporation is rather problematic. Most probably such a difference is to be traced back to the easier oxidation of Ti with respect to Al atoms.

For a better comparison of the properties of UT alumina films on different substrates, we summarise in Table 1 their chemical composition, film thickness, crystal structure and LEED pattern.

4.1. Bulk aluminum oxides (Al₂O₃)

4.1.1. α -Al₂O₃

The α -phase has been well studied both experimentally [211–214] and theoretically [210,215–219]. Depending on crystallographic definition (crystal or lattice symmetry), α -Al₂O₃ is described as trigonal or rhombohedral [211–214]. The crystal structure can be viewed as O atoms arranged in a close packed hexagonal array (stacking sequence *ABAB*...), with the Al atoms occupying two-thirds of the octahedral interstitial sites

Table 1. The chemical composition, film thickness, crystal structure and LEED pattern of the alumina films prepared at different conditions on Al single crystals and Al alloy single crystals.

| Substrate | Temperature (K) | Oxygen partial pressure (Pa) | Chemical composition | Film thickness (nm) | Crystal structure | LEED pattern |
|-------------------------|---------------------|--|--|---------------------|---|---|
| Al single crystals | <573 >573 | $>1.33 \times 10^{-4}$ $<1.33 \times 10^{-4}$ | $\text{Al}_{2-x}\text{O}_3$ $\text{Al}_2\text{O}_{3-x} \rightarrow \text{Al}_2\text{O}_3$ | <4 ~6 | Amorphous $\gamma\text{-Al}_2\text{O}_3$ | $\begin{pmatrix} 3.37 & -1 \\ 2.53 & 4 \end{pmatrix}$ |
| NiAl(110) | 1200 | $<1 \times 10^{-6}$ | $\text{Al}_{10}\text{O}_{13}$ | 0.5 | $\gamma\text{-Al}_2\text{O}_3$ | |
| NiAl(100) | 1200 | $<1 \times 10^{-6}$ | Al_2O_3 | 1.0 | $\theta\text{-Al}_2\text{O}_3$ | 2×1 two domains |
| NiAl(111) | 1000 >1100 | $<1 \times 10^{-6}$ $<1 \times 10^{-6}$ | Al_2O_3 Al_2O_3 | 0.5 0.5 | $\gamma\text{-Al}_2\text{O}_3$ $\alpha\text{-Al}_2\text{O}_3$ | Hexagonal $a = 3.04 \text{ \AA}$ Facets |
| Ni ₃ Al(111) | 1100 | $<1 \times 10^{-6}$ | Al_2O_3 | 0.5 | $\gamma\text{-Al}_2\text{O}_3$ | $\begin{pmatrix} 0.41 & 0.28 \\ -0.28 & 0.69 \end{pmatrix}$ |
| Ni ₃ Al(110) | 1100 | $>1 \times 10^{-5}$ $<1 \times 10^{-6}$ | Al_2O_3 Al_2O_3 | 0.5 0.5 | $\gamma\text{-Al}_2\text{O}_3$ $\kappa\text{-Al}_2\text{O}_3$ | $\begin{pmatrix} 0.65 & 0.27 \\ -0.27 & 0.39 \end{pmatrix}$ |
| Ni ₃ Al(100) | 800 | $<1 \times 10^{-6}$ | Al_2O_3 | 0.5 | $\gamma\text{-Al}_2\text{O}_3$ | $\begin{pmatrix} 0.76 & 0.35 \\ -0.68 & 0.48 \end{pmatrix}$ |
| FeAl(100) | 1100 980 1130 | 1×10^{-4} | Al_2O_3 Al_2O_3 Al_2O_3 | 0.5 0.5 0.6 | Al_2O_3 Al_2O_3 Al_2O_3 | $\begin{pmatrix} 0.79 & 0.21 \\ -0.575 & 0.575 \end{pmatrix}$ $c(6 \times 6)$ superstructure $c(6 \times 6)$ & $a(2 \times 1)$ superstructure |
| FeAl(110) | 800–1000 1130 | 1×10^{-4} 1×10^{-5} | Al_2O_3 Al_2O_3 | 1.0 0.6 | Amorphous | $\begin{pmatrix} 3.37 & -1 \\ 2.53 & 4 \end{pmatrix}$ |
| FeAl(111) | 980–1130 | 1×10^{-5} | Al_2O_3 | 0.6–0.8 | | $(6.4 \times 6.4)\text{R}30^\circ$ |
| CuAl(111) | 960 | 1×10^{-5} | Al_2O_3 Al_2O_3 | 0.4 | $\gamma\text{-Al}_2\text{O}_3$ | $(7/\sqrt{3} \times 7/\sqrt{3})\text{R}30^\circ$ |

present between the O layers (space group $R3c$) [212–214]. Each oxygen layer has a layer of aluminium atoms in a $(\sqrt{3} \times \sqrt{3})R30^\circ$ arrangement on each side, and these aluminium–oxygen–aluminium sandwich structures then repeat to form the crystal. The primitive lattice of the structure is rhombohedral with lattice parameters, $a_0 = 5.13 \text{ \AA}$ and $\alpha = 55^\circ 20'$ [212].

4.1.2. $\kappa\text{-Al}_2\text{O}_3$

The crystal structure of the κ -phase of Al_2O_3 belongs to the orthorhombic class and contains eight Al_2O_3 molecules per cell (space group $Pna2_1$) [220–222]. In terms of coordination polyhedra, it can be described as an ABAC . . . closed-packed stacking of O atoms, with Al atoms occupying octahedral and tetrahedral sites. The number of octahedral and tetrahedral Al atoms in a unit cell is 12 and 4, respectively [210,223–225].

4.1.3. $\gamma\text{-Al}_2\text{O}_3$ and $\theta\text{-Al}_2\text{O}_3$

Up to now, the basic structural properties of $\gamma\text{-Al}_2\text{O}_3$ have not yet been fully clarified. The prevailing understanding is that $\gamma\text{-Al}_2\text{O}_3$ is a defective spinel structure (space group $Fd\bar{3}m$) with vacancies on cation sites and two types of cation coordinations, the octahedral coordination Al–O₆ and the tetrahedral coordination Al–O₄ (in $\alpha\text{-Al}_2\text{O}_3$ there is only Al–O₆ coordination). 8/3 cation vacancies per cubic unit cell (one vacancy in every nine cation) are required to maintain the Al_2O_3 stoichiometry. There exists a long-standing controversy as to whether the vacancies should occupy the octahedral or the tetrahedral sites. An empirical pair potential has been used to model the structure of $\gamma\text{-Al}_2\text{O}_3$, followed by density of state (DOS) calculations [226]. It was tentatively concluded that the cation vacancy prefers the octahedral site. With the cation vacancies further involved, investigation on the properties of $\gamma\text{-Al}_2\text{O}_3$ becomes a formidable task.

It is known that $\theta\text{-Al}_2\text{O}_3$, a metastable precursor phase of $\alpha\text{-Al}_2\text{O}_3$, has a similar local coordination to $\gamma\text{-Al}_2\text{O}_3$ [207,227]. It was also shown that a common transformation sequence from $\gamma\text{-Al}_2\text{O}_3$ to $\alpha\text{-Al}_2\text{O}_3$ involves the $\theta\text{-Al}_2\text{O}_3$ phase [228–230]. Similar to $\alpha\text{-Al}_2\text{O}_3$, $\theta\text{-Al}_2\text{O}_3$ is an ordered phase, so its electronic and optical properties can be calculated unambiguously [210,231,232]. A good understanding of the electronic and optical properties of $\theta\text{-Al}_2\text{O}_3$ is certainly of help for the elucidation of $\gamma\text{-Al}_2\text{O}_3$ in general. The crystal structure of $\theta\text{-Al}_2\text{O}_3$ has also been investigated by SEM, X-ray and electron diffraction, HRTEM and vibrational spectroscopy by Husson and Repelin [227]. It is reported to possess a monoclinic symmetry with the space group $C2/m$. There are 5 ions per formula unit with all of the ions located at the 4i Wyckoff position. The aluminium cations occupy four octahedral and four tetrahedral interstitials of the oxygen sublattice. On the theory side, in addition to structural calculations in very good agreement with the crystallographic data, Wilson *et al.* [233] developed an interatomic potential model for simulations in Al_2O_3 . They used a shell model, a compressible ion model, as well as a compressible ion model with both dipole and quadrupole polarisability of the O²⁻ ions to calculate the energy difference between α - and $\theta\text{-Al}_2\text{O}_3$. The $\theta\text{-Al}_2\text{O}_3$ phase was found to be less stable. They also concluded that the compressible O ion is the origin for stabilising the α -structure with respect to the θ -structure.

The crystal structures and the transformation mechanisms among the η , γ and θ phases have been studied by X-ray and neutron powder diffraction by Zhou and Snyder [208].

The profile analysis of various reflection zones in the defective spinel structure shows different coherent domain sizes, which can be associated with the tetrahedral and octahedral Al sites within the O sublattice. The authors are of the opinion that the transition aluminas should be considered spinel deformed rather than tetragonal deformed. This however is not fully supported by theoretical indications [234–236] suggesting that the spinel model of γ -Al₂O₃ does not accurately reflect its structure. These indications have been used to derive a more realistic non-cubic model [237] that has also been tested in terms of mechanical and electronic properties [238], yielding results in reasonable agreement with experimental data, even though further work is still needed to fully settle the structural issues [239].

4.2. Surface oxidation of Al metal

The growth of alumina films by SO of Al(111) single crystal substrates has been investigated [240–243]. However, the resulting films are not particularly well defined and are often polycrystalline or randomly oriented [240]. This is because the most stable sites of the chemisorbed oxygen are found in tetrahedral sites below the topmost Al atomic plane. Such subsurface oxygen atoms induce a very large (37%) increase in the mean interplanar distance of the topmost layers and thus deteriorate the surface crystalline structure [244].

The chemical composition and the chemical state of the Al and O ions of thin aluminium-oxide films grown by thermal SO of a Al(431) substrate at a partial oxygen pressure of 1.33×10^{-4} Pa in the temperature range 373–773 K were studied using XPS [242]. At low temperature (<573 K) and high oxygen partial pressure, an aluminium deficient (compared with Al₂O₃) amorphous oxide film is formed with a limited thickness (<4 nm). At higher temperatures (>573 K) and low oxygen partial pressure, an Al-enriched, amorphous oxide film is formed initially, which gradually attains the stoichiometric composition of Al₂O₃ and becomes crystalline (γ -Al₂O₃) (~6 nm).

Oxygen transport and oxidation kinetics of Al(110) at elevated temperatures in O₂ has been studied using MEIS [245]. Oxidation results in the formation of a stable stoichiometric Al₂O₃ layer with fairly abrupt interfaces. The time dependence of the film growth follows inverse logarithmic law, in agreement with the Cabrera–Mott oxidation mechanism [246], and the film growth kinetics is independent of the crystallographic orientation on low-index surfaces [243]. The main drawback of this method is that the thickness and crystal structures of these alumina films cannot be easily controlled.

4.3. Surface oxidation of M_xAl alloys (M = Ni, Fe, Cu)

4.3.1. NiAl

Preparation of UT alumina films by oxidation of Ni_xAl alloy single crystals in low oxygen pressure and at high temperature has been intensively investigated [19,20,38,247–253]. The alumina films prepared by this method are long range ordered and their thickness is about 0.5–1 nm [247–249]. The Ni_xAl single crystal alloys mainly investigated are NiAl (all the low index surfaces) and Ni₃Al ((111) and (100) surfaces).

The crystal structure of NiAl is the CsCl structure which forms a simple-cubic lattice with a lattice parameter of $a_0 = 2.88 \text{ \AA}$ [212]. The SO of its surfaces goes along the

following steps: (i) adsorption of oxygen induces segregation of Al atoms to the top of the surface; (ii) the Al atoms react with the adsorbed oxygen at elevated temperatures and a thin, well-ordered alumina film is grown. Precise control of the film thickness and crystal structure is the principal advantage of this synthesis process. The alumina films grown on the Ni_xAl alloys have been partially reviewed previously [20,31,38,254]; in this section, only the important and new points concerning the UT films are summarised.

4.3.1.1. *NiAl(110)*. By far the most extensively studied alumina UT film is the 0.5 nm thick film formed by high-temperature SO of the NiAl(110) surface [247,252,253,255–270]. The NiAl(110) surface consists of alternating rows of Ni and Al atoms and has a rectangular surface symmetry. LEED analysis demonstrates that it possesses a large rippled relaxation, with the Al sites of the top layer being displaced approximately 0.022 nm above the Ni sites [249,250]. Surface phonon dispersion measurements and surface lattice-dynamics studies of NiAl(110) confirm such surface rippling, where first layer Ni atoms are displaced inwards and first Al atoms are displaced outward [251,252]. The structure of the NiAl(110) as well as the Ni_3Al (111) and (100) surfaces has been studied computationally [271–273], finding in general good agreement with the experimental data. The LEED patterns of the UT alumina films indicated the growth of a two-domain overlayer [259,260]. Each domain exhibits rectangular symmetry and is rotated at 24° with respect to the [110] symmetry direction. On the basis of the bulk materials (see above), one would expect that this film involve hexagonal O planes and octahedrally and tetrahedrally coordinated metal atoms with an overall Al_2O_3 stoichiometry [262,274]. Initial STM studies [258,261] in fact suggested that the film is similar to the κ - or γ -phase, in agreement the analysis of truncated-rod XRD spectra [247]. The detailed structure of oxide films grown on the NiAl(110) was finally clarified by combining DF calculations and STM investigations [256] and exhibits a slightly different structure for this film. The film turns out to have a non-stoichiometric $\text{Al}_{10}\text{O}_{13}$ composition and to be formed by alternating layers of Al and O ions with stacking sequence $(\text{Al}_4^{2+}\text{O}_6^{2-}\text{Al}_6^{3+}\text{O}_7^{2-})$, corresponding to interfacial aluminium (Al_i) and oxygen (O_i) ions, and surface aluminium (Al_s) and oxygen (O_s) ions. Four $\text{Al}_{10}\text{O}_{13}$ units are present in each unit cell, that is commensurate with the NiAl(110) substrate along one of its diagonals, but incommensurate in the orthogonal direction. Its structure – see Figure 18(a,b) – is such that different tunneling conditions in the STM measurements allow one to associate different atoms: O_s , Al_s and Al_i , to bright spots, and thus to univocally locate most of them, see Figure 18(c–e). Starting from the outmost layer, one finds a modulated hexagonal lattice of O_s ions with 0.51 nm periodicity. Almost coplanar with this layer, as predicted for the termination of bulk single crystal alumina surfaces [275–278], Al_s ions are also arranged in a nearly hexagonal pattern with an Al–Al distance of 0.303 nm, corresponding to the Al–Al distance in the surface layer of the $(\sqrt{31} \times \sqrt{31})\text{R} \pm 9^\circ$ reduced sapphire(0001) surface observed after high temperature annealing. They are surrounded by three or four O_s ions (that are all three-coordinated) and lie on top of O_i ions (this is also the reason why they can be distinctly imaged by STM in proper conditions), thus occupying tetrahedral or incomplete (truncated) octahedral sites in even number. Interfacial Al_i ions in a reduced oxidation state (Al^{2+}) finally lie at the bottom of the oxide layer, arranged in pentagonal and heptagonal rings that can be seen as reconstructions of the *honeycomb* lattice formed by Al ions typical of $\alpha\text{-Al}_2\text{O}_3$.

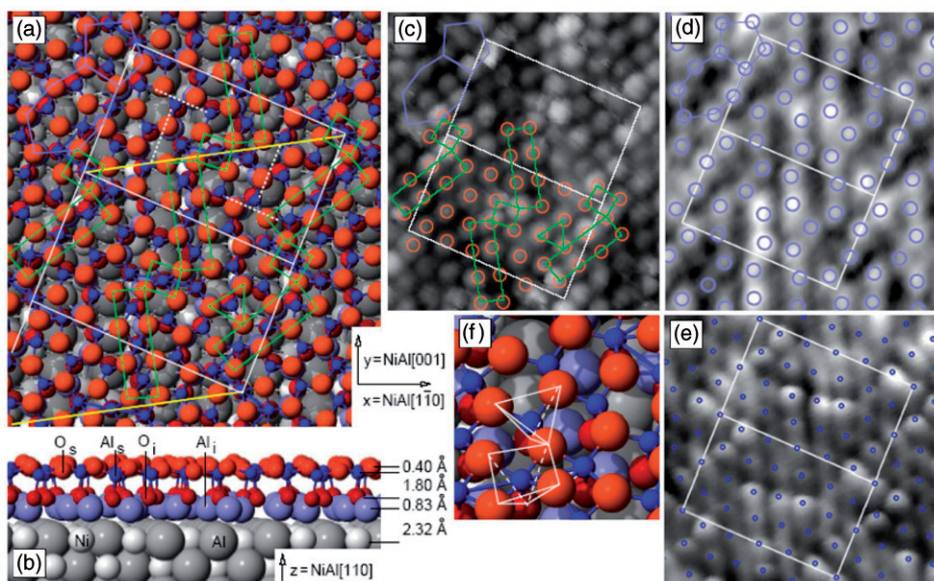


Figure 18. [Colour online] The proposed model of the 0.5 nm thick $\text{Al}_2\text{O}_3/\text{NiAl}(110)$ film, by Kresse et al. (a) Top and (b) side views of the proposed structure, with close up (f) of different Al cation sites. (a) Top and (b) side view of the DF- and STM-based model for the UT aluminium oxide film on $\text{NiAl}(110)$. (c), (d) Experimental STM images of the film at RT and (e) at low temperature. The unit cell is marked by white rectangles. From Reference [256].

As they are reduced and nearly all of them lie underneath O_s ions in the outmost layer, the Al_i ions are imaged as bright spots by STM in proper conditions. The reconstruction in pentagonal and heptagonal rings allow the Al_i ions to achieve three-fold coordination with O_i ions (in bridge positions) and simultaneously avoid Al atoms from the $\text{NiAl}(110)$ substrate (short-range chemical order). Note that the oxide layer is insulating with a wide band-gap. This structure [256] is in good agreement with previous theoretical predictions [262], as well as with photoemission data indicating two alumina oxidation states [263]. The structure has been substantially confirmed by successive investigations [270]. Resolved details of the wavelike morphological features of the film and analysis of the atomic corrugation point to interactions between the film surface and the substrate [268], connected with stress and commensurability [265,266]. The stability of the film has been investigated in Reference [269].

Three main types of defects are present on the surface: oxide step edges resulting from atomic steps in the underlying $\text{NiAl}(110)$ substrate; domain boundaries between the two reflection domains and antiphase domain boundaries that are spaced on average by about 10 nm and separate oxide areas inside a reflection domain (see Figure 19) [253,259]. As the defect structure is important for the growth of the metal clusters, all of these defect sites are preferential nucleation sites resulting in line structures of metal clusters along the step edges and domain boundaries [279]. It can be noted that not only rotation domain boundaries, but also translation domain (antiphase) boundaries exist, i.e. boundaries separating regions whose crystal lattices are displaced relative to each other by

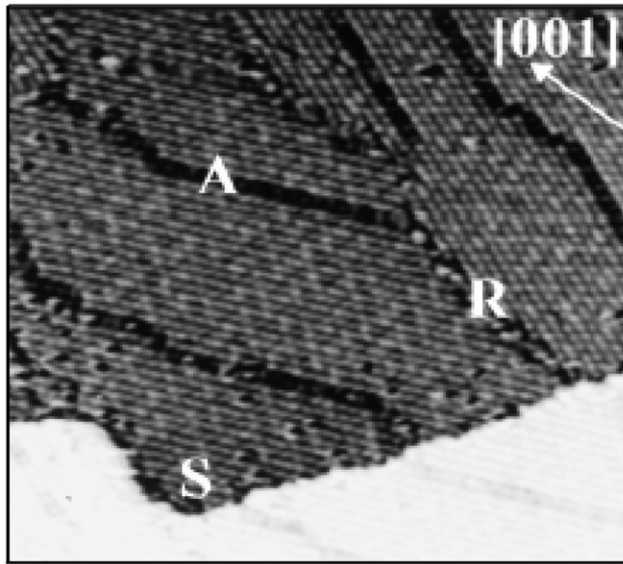


Figure 19. STM image ($500 \times 500 \text{ \AA}^2$) of the aluminium oxide film formed on NiAl(110) by oxidation. A step edge (S), a reflection domain boundary (R), as well as an antiphase domain boundary (A) are indicated. Tunnel current is -0.4 nA , sample bias is -1.3 V . From References [249,259].

a translation that is not a unit-cell vector [258,265]. It has been shown [266] that they do not originate when islands with displaced lattices impinge during growth, but rather that they form spontaneously due to the strain-energy reduction of the dislocations that terminate these planar defects.

Attempts have been made to grow thicker films on the NiAl(110) substrate by direct oxidation at high temperatures [280–285] and oxygen pressure. At higher temperatures, direct oxidation yields thicker films that exhibit complex LEED patterns. A 1.5 nm thick film has been reported from growth at 1070 K [281] and, at a slightly lower temperature (1020 K), a film 1.09 nm thick [282]. No STM or other microscopy data have been reported, so the degree of surface roughness or continuity of these films is not known. Thicker films have also been grown by deposition of Al onto the ordered 0.5 nm $\text{Al}_2\text{O}_3/\text{NiAl}(110)$ films, followed by oxidation at 1070 K [285]. RHEED indicated an ordered film but with the oxide (111) surface tilted with respect to the NiAl(110) surface. A quite different results is obtained when atmospheric pressure SO is considered: in a recent work [286], such a study has been conducted by SO at 870 K producing a well-ordered $\gamma\text{-Al}_2\text{O}_3$ epitaxial layer showing a $R30^\circ$ orientation with respect to the underlying substrate and later following the evolution from $\gamma\text{-Al}_2\text{O}_3$ to $\alpha\text{-Al}_2\text{O}_3$ via *in-situ* grazing incidence XRD (GIXRD) as the temperature was increased to 1200 K.

4.3.1.2. *NiAl(100)*. The (100) layers of NiAl have ABAB ... stacking sequence and the NiAl(100) surface is terminated either by an Al or Ni layer. A preferable Al termination was suggested from LEED I/V studies [249,287], but later 180° -neutral impact collision ion

scattering spectroscopy (NICISS) and high-resolution spot profile analysis of LEED [288] found that the surface structure and composition depends on the cleaning treatment. Long time annealing below 500 K results in a $p(1 \times 1)$ LEED pattern corresponding to a defective Al-terminated surface, whereas, after flashing a 1400 K and rapid cooling down to RT, another $p(1 \times 1)$ phase is found which is nearly perfectly Ni terminated. In the intermediate annealing temperature range about 800 K surface roughening results in an Al terminated missing row surface structure showing a $c(\sqrt{2} \times 3\sqrt{2})R45^\circ$ LEED superstructure [249]. Niehus *et al.* [289,290] studied oxygen adsorption and the initial stages of oxidation of NiAl(100). The growth of well-ordered Al_2O_3 layers was achieved on the $c(\sqrt{2} \times 3\sqrt{2})R45^\circ$ phase. The oxide formation is unaffected by the initial composition (preparation-dependent Al or Ni termination) or reconstruction of the surface [250]. During oxidation, the initial crystallographic structure of the clean surface is completely destroyed, which implies a strong binding of oxygen to the metallic substrate as well as an oxygen-assisted Al segregation at the surface.

The alumina film on NiAl(100) surface grows in stripes perpendicular to each other, corresponding to the $\langle 100 \rangle$ and $\langle 010 \rangle$ directions [289]. High resolution STM images [291] indicate that this oxide surface has double rows of oxygen atoms surrounding single rows of Al^{3+} cations, and is proposed as a θ -phase oxide. Doychak *et al.* [292] have studied the oxidation in air of NiAl(100) by means of TEM. At 1073 (after 10 h) and 1273 (after 0.1 h) the formation of $\theta\text{-Al}_2\text{O}_3$ was found, which is in excellent agreement with the above results. A GIXRD study also confirmed the formation of $\theta\text{-Al}_2\text{O}_3$ layers via oxidation of the NiAl(100) surface at 1220 K. The lattice constants of $\theta\text{-Al}_2\text{O}_3$ explains very well the (2×1) LEED pattern. The lattice mismatch amounts only to 2.5% in one direction ($2a_{\text{NiAl}} = 2.91 \text{ \AA}$, $a_{\theta\text{-Al}_2\text{O}_3} = 5.64 \text{ \AA}$) and even only to 1% ($b_{\text{NiAl}} = 2.89 \text{ \AA}$, $b_{\theta\text{-Al}_2\text{O}_3} = 2.91 \text{ \AA}$) in the other direction [293,294]. A model of the $\theta\text{-Al}_2\text{O}_3/\text{NiAl}(100)$ structure is shown in Figure 20: the (110) plane of the oxygen fcc sub-lattice is perpendicular the NiAl(100) surface and parallel to the NiAl[100] direction. Recently, the films formed by electrochemical oxidation have been characterised using RHEED, AES and STM [295]. These films were found to be significantly smoother than films formed by direct thermal oxidation, principally due to the decomposition of 3D island features during the electrochemical oxidation.

4.3.1.3. *NiAl(111)*. The polar NiAl(111) surface has an open structure consisting of alternating Ni and Al layers. NICISS and STM results [296] indicated that the surface is unreconstructed and Ni-terminated. The STM study showed flat terraces which are separated by double atomic steps. The growth of alumina films on NiAl(111) is rather complex: at temperature lower than 900 K a short-range order $\alpha\text{-Al}_2\text{O}_3$ is grown and can be described as clusters of randomly oriented oxygen fcc lattices with Al cations solely occupying tetrahedral interstices [297]. At 900–1100 K the films show γ -like oxide structure and change to long-range-order $\alpha\text{-Al}_2\text{O}_3$ when the temperature increases above 1100 K. Hexagonal symmetry was found at LEED patterns [298] with lattice constant of the real space unit cell of 3.04 \AA for $\gamma\text{-Al}_2\text{O}_3$, which is very close to those of alumina films on NiAl(110) surface. The γ - and $\theta\text{-Al}_2\text{O}_3$ have virtually the same structure in view of bond angle and bond lengths [299]. In both cases the Al cations occupy both tetrahedral and octahedral vacancies in the fcc oxygen sub-lattice.

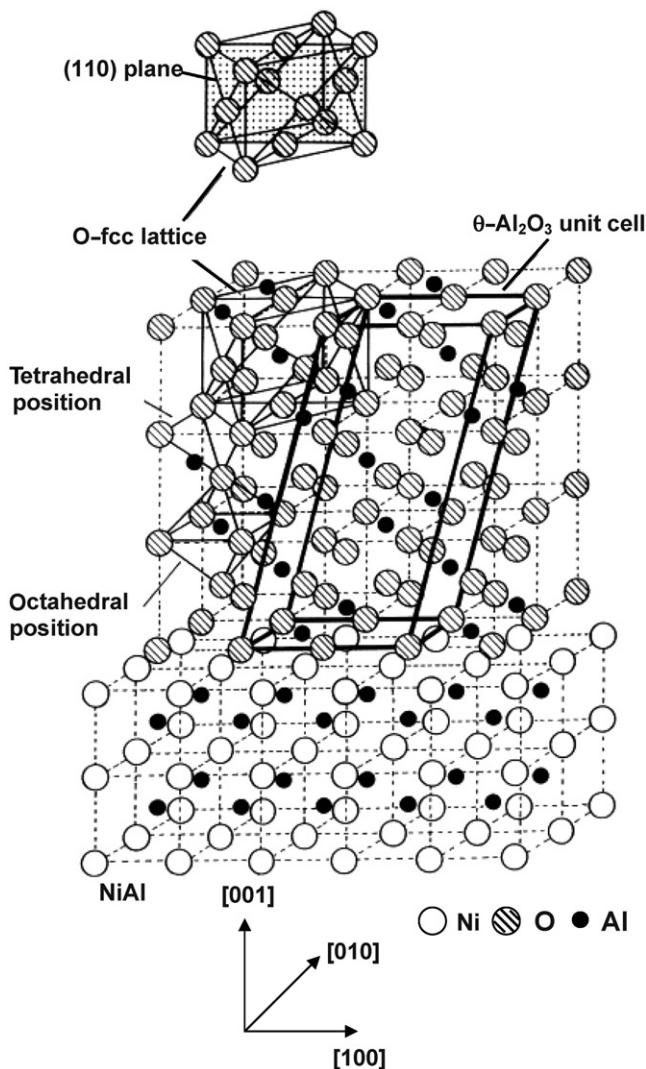


Figure 20. Structural model for the θ - $\text{Al}_2\text{O}_3/\text{NiAl}(100)$ system; it illustrates the relationship between the oxygen fcc sub-lattice and the $\text{NiAl}(100)$ bcc structure. From Reference [31].

In conclusion, the oxidation of the (100), (110) and (111) surfaces of NiAl at elevated temperatures in low oxygen pressure leads to the formation of thin, crystalline films of alumina on top of the sample.

4.3.2. Ni_3Al

Ni_3Al is a cubic-ordered intermetallic compound crystallising in the Cu_3Au structure, which has a fcc unit cell with a lattice constant of 3.56 Å. The three Ni atoms occupy the face centers and Al the cube corners. In a slightly aluminium-rich or stoichiometric Ni_3Al

alloy, the outmost surface layer should have the ideal 3Ni:1Al stoichiometry. It was reported that due to the preferential sputtering of Al atoms, ion sputtering yields a Ni-rich Ni₃Al(111) surface [300]. If the sample is annealed at temperature higher than 1023 K, Al segregates to the surface, although an Al excess on the surface is not stable, and upon cooling Al diffuses back into the bulk until the stoichiometric bulk-like composition is recovered. The structure of the Ni₃Al(111) and (100) surfaces has been studied computationally [271–273], finding in general good agreement with the experimental data. The oxidation of (111), (110) and (100) surfaces of Ni₃Al was studied by several authors [301–309].

4.3.2.1. *Ni₃Al(111)*. The alumina film grown on Ni₃Al(111) [274,310–322] has been classified as γ -like [311,316] and displays hexagonal symmetry in LEED and STM images. Its unit cell size and orientation is ($\sqrt{67} \times \sqrt{67}$)R12.2° with respect to the 505 pm cell of an ordered Ni₃Al(111) surface [312]. In STM images, a ‘dot’ structure with one bright spot per unit cell can be observed at a sample voltage of about 2.0 V, while a *honeycomb-like* network structure appears at a sample voltage of about 3.2 V (see Figure 21) coexisting with a *stripe* phase [313] and sometimes another ($\sqrt{67} \times \sqrt{67}$)R17° phase. The structure of the oxide films has been clarified by a combined DF and STM study [310], and presents several analogies with that of the AlO_x/NiAl(110) film [256]: (a) it is composed of alternating layers of aluminium and oxygen ions with stacking sequence Al_i–O_i–Al_s–O_s, with the top-most two layers almost coplanar; (b) all O_s ions are three-coordinated to Al_s ions, with the latter lying in tetrahedral or (truncated) octahedral sites with O_i ions in eclipsed positions underneath them; (c) the Al_i ions are arranged in a reconstructed *honeycomb* lattice, so as to avoid Al atoms from the Ni₃Al(111) substrate (short-range chemical order, see Figure 4 for the arrangement of the Ni₃Al(111) surface, analogous to that of the Pt₃Ti alloy). The main differences are in the three-fold axes positions, in which there is an O_i ion in three-fold coordination to Al_i ions instead of the usual two-fold (bridge) coordination, and in the fact that the Al_i ions are now arranged in pentagonal and distorted hexagonal (not heptagonal) rings, except at the three-fold axis position, in which they form a perfect triangle, and at the six-fold axis position, in which they form a perfect hexagon. An important feature of this structure is that the C₆-axis position corresponds to a hole that crosses the oxide film down to an Al atom from the Ni₃Al(111) substrate. In analogy with some titania UT films considered in Section 3.3.4, this feature makes of the AlO_x/Ni₃Al(111) film an excellent template for the deposition of metal NPs [303,310,323].

4.3.2.2. *Ni₃Al(110)*. Al₂O₃/Ni₃Al(110) has been reported to resemble the κ -phase [324,325]. The topography of this film is substantially different from the film grown on the (111) surface. STM images revealed rows along the (110) direction with a 1 nm distance [325]. LEED patterns of both the initial chemisorbed oxygen layer [326] and the 0.7 nm thick oxide film [327] revealed substantial diffuse scattering, indicative of an incommensurate oxide/metal interface. Importantly, the STM image and LEED data agree closely with first-principles DF structural calculations for a fully relaxed κ -phase three-layer film [325]. The calculated structure, shown in Figure 22, displays a 2 × 1 unit cell characteristic of the κ -like phase, while the 1 nm distance between

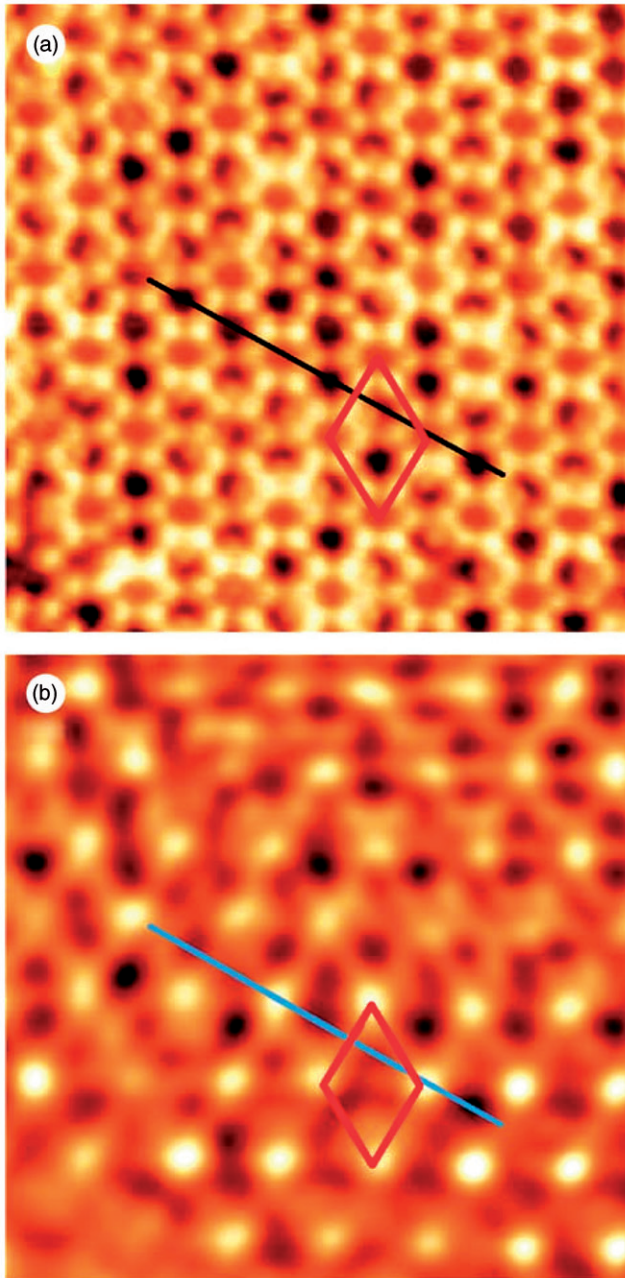


Figure 21. [Colour online] STM images of the alumina film on Ni₃Al(111) measured at 23 K and different bias voltages; (a) *honeycomb-like* network structure at $U_{\text{bias}} = 3.2$ V and $I_{\text{T}} = 122$ pA, and (b) the dot structure at $U_{\text{bias}} = 2.0$ V and $I_{\text{T}} = 105$ pA. The unit cell of the dot structure is drawn in red. Size: 27.8×27.8 nm². From Reference [312].

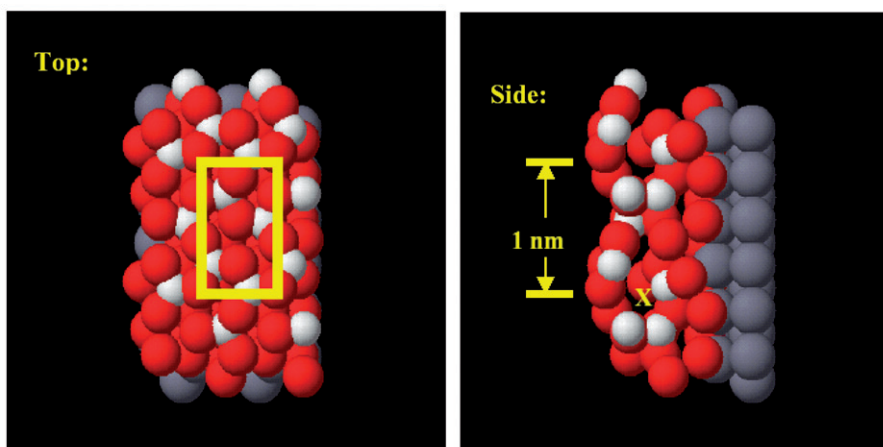


Figure 22. [Colour online] First-principles DF results for the structure of a fully relaxed κ -phase alumina film. The theoretically predicted structure is in excellent agreement with experiments, exhibiting a 10 \AA repeat distance and unit cell which matches the LEED results, indicating that the actual film is indeed κ phase. The calculations also predict the presence of interstitial vacancies, which may store atomic hydrogen. From Reference [325].

double rows of oxygen anions coordinated to Al cations is in excellent agreement with the STM results.

4.3.2.3. *Ni₃Al(100)*. The oxidation of the (111) and (100) surfaces of Ni_3Al was studied by XPS, LEED, STM and LEIS [272,311]. Despite the different surface orientations no significant difference in the LEIS and XPS data were found, while two different structural phases were found on the oxidation of $\text{Ni}_3\text{Al}(100)$ at 800 and 1100 K, respectively [328]. These alumina films have hexagonal surface meshes, with unit vectors lengths in the range from 2.9 to 3.1 Å , and grow on the (111) plane parallel to the substrate surface plane. This distance is approximately twice the value of the O^{2-} ionic radius (1.4 Å). Therefore, one can conclude that the observed unit meshes always correspond to compact hexagonal planes of oxygen ions.

4.3.3. *FeAl*

FeAl is another ordered alloy of the CsCl-type with a lattice parameter $a = 2.9090 \text{ Å}$ [329]. Bulk phase diagram [330] shows that at around 898 K there is a transition from the single CsCl phase to a two phase region, where CsCl and FeAl_2 structures coexist. The segregation and ordering behaviour of (100), (110), (111), (210) and (310) phases of FeAl surfaces have been investigated by means of AES and LEED [331]. For all the five surfaces, sequential annealing after sputtering leads to segregation of Al on top of the surface layer. For intermediate annealing temperatures several ordered superstructures are found, which can partly be attributed to metastable Fe_3Al films developing at the surfaces.

The SO of the (100), (110) and (111) surfaces of FeAl was investigated by LEED and XPS [332]. In general, the films, 0.5–0.8 nm thick, resemble the transitional phase oxides

grown on Ni aluminide surfaces, including the formation of an interfacial Al layer in a lower ionic state than in the bulk oxide. SO at RT leads to the formation of an amorphous oxide film on top of an Al-depleted interlayer. At low oxygen pressure, annealing FeAl(100) at 980 K lead to the formation of a $c(6 \times 6)$ superstructure. At an oxidation temperature of 1130 K, additionally, an $a(2 \times 1)$ overlayer is observed. Oxidation of the FeAl(111) surface at 980 K also leads to an ordered oxide overlayer. The unit cell is hexagonal and is described by $(6.4 \times 6.4)R30^\circ$. The oxidation of FeAl(110) surface is very complex. Exposure to approximately 1000 L at 1130 K leads to a well-ordered oxide film. An identical diffraction pattern was observed on the oxide surface and was assigned by the matrix:

$$\begin{pmatrix} 3.37 & -1 \\ 2.53 & 4 \end{pmatrix}$$

The oxide UT film grown on FeAl(110) has been further studied using high resolution STM [333]. The atomically resolved images are in good agreement with theoretical calculations for ordered, UT alumina films regarding the mixing of interfacial and oxide wave functions to produce states within the bulk band gap [274], and stripes and *zigzag-like* features are observed in the STM images due to equal Al^{3+} occupancy of tetrahedral and octahedral sites induced by the extremely thin nature of the film [262].

The formation mechanism of UT alumina films on the FeAl surface at high temperatures and low oxygen pressures is similar to that on NiAl alloy. But in this method temperature is the important factor that influences the surface structure of alumina films. The film growth can be divided into two regions of different kinetics: in the first region, the oxygen-uptake rate varies significantly with surface orientation, the growth kinetics can be described by a power law with the same exponent, around $2/3$, for the (100) and (110) surfaces and ~ 1 for the (111) surface; for higher oxides film thickness all surfaces exhibit very similar kinetics which are much slower than in the low-exposure regime. Recently, the electronic structure of alumina film grown on FeAl(110) has been studied by angle-resolved photoemission spectroscopy [334]. The oxide valence states do not show dispersion as a function of the perpendicular component of the electron wave vector; however, they show a two-dimensional electronic structure parallel to the plane of the thin film due to the limited thickness of the oxide thin films. The appearance of a peak in the anticipated band gap of the bulk oxide film suggests a unique electronic structure of the two-dimensional oxide films.

4.3.4. CuAl

Recently, the SO of Cu-9%Al(111) single crystal has been studied [335–339]. Cu-9%Al(111) has an α phase (fcc) [340] and Al atoms are randomly substituted with Cu atoms in the alloy [341]. Similar to other Al alloys, when the Cu-9%Al(111) single crystal is heated up at higher temperature, Al atoms will segregate at the surface [339,342]. The UT alumina films obtained by SO at around 950 K in oxygen atmosphere were investigated by LEED, STM, RHEED, XPS and AES [337–339]. Long range well-ordered flat γ - Al_2O_3 films were found with $(7/\sqrt{3} \times 7\sqrt{3})R30^\circ$ structure. It was also reported that the alumina on the Cu–Al alloy crystal does not show stress-induced domain boundaries

and grows in large defect-free domains, being then a promising candidate for metal–insulator–metal structures.

Finally, we mention that, among the many aluminium-containing alloys, the oxidation of those exhibiting quasi-crystal [343] arrangements in their bulk phases [344–346] may seem interesting in view of the search for novel metal-supported oxide nanostructures. Indeed, this has been considered in the literature [347–351]. However, no clear structural patterns have so far emerged, and in the best characterised case [351] a multidomain structure was evidenced that bears some resemblance to alumina grown on NiAl(110).

4.4. Ultrathin alumina films on other metal surfaces

Epitaxial α -Al₂O₃(0001) films have also been prepared on different metal surfaces including Pt(111), Re(0001), Ru(0001), Ta(110), Fe(110), Nb(110) and Mo(110) [352–359] by both the RD and PO methods. This procedure yields Al₂O₃ thin films which have structural and electronic properties close to crystalline bulk Al₂O₃ but their surface structures may differ for different metal substrates due to the lattice mismatch between oxide films and metal substrates. For example, the in-plane lattice mismatches of Pt(111), Re(0001) and Ru(0001) with the oxygen sublattice of α -Al₂O₃(0001) are >0.79%, >0.43% and <1.75%, respectively [352–355]. Their chemical composition greatly depends on the preparation conditions (e.g. oxygen pressure and annealing temperature). The main disadvantage of this growth procedure is the fact that the deposition of Al does not occur on the pure metal surface but on the partially oxidised or completely oxidised metal surface. This considerably changes the thermodynamics at the Al₂O₃/metal interface and affects the structural properties of the alumina film. The PO method could avoid this problem, but the final crystal structure of Al₂O₃ is not optimised [20,31]. The unit cell of UT alumina film (0.3 nm) on Re(0001) has a lattice constant which is ~12% larger than that of the Re(0001) substrate, corresponding to a (9 × 9) overlayer coincidence lattice, with eight O²⁻–O²⁻ lattice spacings in the overlayer fitting onto nine lattice spacings on the Re(0001) substrate [354]. The thick alumina films (1.47 nm) on Re(0001) surface have a hexagonal lattice structure with a lattice constant of ~2.8 Å. This oxide is equivalent to that expected from crystalline α - or γ -Al₂O₃.

When Al-oxide films are deposited at 300 K onto the Ru(0001) substrate, no ordered LEED pattern is observed from the film with thickness >0.5 nm, even after annealing the films at 1170 K. For thicker films ~2.5 nm deposited at 1170 K, a diffuse hexagonal LEED pattern was found. This indicated that alumina films grow with long range order on the Ru(0001) substrate only when the films are thick. The lattice spacing of the film is close to the lattice constant of the Ru(0001) surface (2.7 Å).

Thin α -Al₂O₃ films were also prepared on Ta(110) despite the fact that there is no simple epitaxial relationship between the two surface leading to a rotated Kurdjumov-Sachs orientational relationship [356]. In the α -Al₂O₃/Ta(110) system, a considerable in-plane expansion in the close-packed oxygen layer (3.05 Å compared with 2.77 Å) was observed in the surface of bulk α -Al₂O₃(0001), indicating the presence of significant strain.

Step-by step PO of thin Al layers at RT leads to the formation of amorphous alumina on Fe(110) surface, while a subsequent annealing at 550 K of the amorphous films results

in the formation of a well-ordered $\text{Al}_2\text{O}_3(0001)$ layer [357]. A polycrystalline Al_2O_3 film was formed on a Nb(110) surface even annealed at 1200 K [358,359]

5. Conclusions and perspectives

In this work the literature data on titania and alumina UT oxide films grown on metals and metal alloy surfaces have been reviewed. Our aim was to compare the different preparation procedures and to clarify how they can influence the final product. We have also tried to define the current status of structural information accumulated on these systems, putting particular emphasis on the structural novelty of interface-stabilised phases with respect to bulk ones.

The two systems here considered represent two prototypical examples of rather different behaviours: alumina is a non-reducible oxide, whereas titania is a reducible oxide which can switch among several oxidation states. The latter system thus possesses a greater number of degrees of freedom and the possibility to span over a larger variety of structural and chemical situations, in the bulk as well as in UT films. Indeed, the richness of different structural situations found for the TiO_x UT films is comparable to what has been found on correlated systems, e.g. VO_x UT films [22] where vanadium spans over an even larger set of possible oxidation states. Other well-traceable chemical differences between Al and Ti are: (i) their affinity toward oxygen, estimated by comparing the standard enthalpy of formation of corundum-like M_2O_3 solids from gas phase species, that is 2300 kJ mol^{-1} for Al_2O_3 and 2470 kJ mol^{-1} for Ti_2O_3 , respectively, or the metal-oxygen bond strength in diatomic molecules, that is 511 kJ mol^{-1} for AlO and $672.4 \text{ kJ mol}^{-1}$ for TiO, respectively [360]; (ii) the ionicity of their bonds, as Ti oxides are in general more covalent than Al oxides. Despite these differences, one finds unexpected similarities. For example, Al is also capable to produce structural defects, connected with the possibility of occupying both octahedral and tetrahedral sites and in general the tendency to produce disordered configurations. This in practice results in a rich variety of different phases when UT alumina films are examined, many of which still await structural characterisation. In this respect it can be noted that the high degree of structural order observed for UT alumina films grown on the NiAl(100) [253] and $\text{Ni}_3\text{Al}(111)$ [311] alloys might be associated with the presence of Al atoms in the bulk alloy that direct the growth of the Al ions at the oxide/support interface. Moreover, from the chemical point of view, Al ions in contact with the metal support can exhibit unusual (lower) oxidation states [256], thus strengthening their similarity to Ti. The net result is thus that some similarities are actually observed between alumina and titania for well-characterised UT systems, especially in the single or double ML regime, as discussed in Sections 3.3.4.2, 4.3.1.2 and 4.3.2.1. This might be of wider significance, as a certain degree of metallisation could be a general feature of interfacial oxide MLs (metal proximity effect).

The realisation of such a wealth of structural potentialities is determined by both thermodynamic and kinetic factors. In general terms, a thermodynamic description of the growth of an UT MO_x oxide film on a metal (M') substrate should take into account the surface free energies of the metal substrate, the oxide/metal interface and the oxide surface [361], together with some basic energetic quantities such as the strength of $\text{M}-\text{O}$ and $\text{M}'-\text{O}$ bonds, the mixing energy for the formation of the $\text{M}-\text{M}'$ alloy and the interplay between polarity and lattice mismatch between the metal support and the overgrowing oxide [362].

These thermodynamic quantities will likely affect kinetic parameters too. For example, the different affinity of M and M' towards oxygen is particularly important during a RD in an oxygen background pressure. The incoming M atoms may hit either a bare M' surface or an oxygen chemisorption phase, and this will direct the formation of the film-substrate interface layer, an effect that has been recently employed to produce stoichiometric SiO_x UT films on Mo(112) [363]. Analogously, the fact that both Al and Ti can form surface and bulk alloys with many of the substrates adopted for growing UT oxide films, and thus the possibility of thermally activated interdiffusion of M into M' substrates [41] needs to be considered. Clearly, these are simply preliminary considerations, where more rigorous models should also include the detailed kinetics of film growth and the involved lattice transformations. As a whole, the main message emerging from this review is indeed that the often unprecedented structural properties and chemical composition of oxide UT films greatly depend on the preparation processes, annealing temperatures, oxygen pressures and substrates. For example, the panorama of the literature data on the preparation procedures tells us that, while the titania UT films can be easily prepared by Ti deposition (either PO or RD) on a different substrate, alumina UT films can be better obtained as epitaxially ordered layers by SO of alloy surfaces at high temperatures and in low oxygen pressures, an observation whose deeper reason still needs to be fully clarified.

In the strive for clarifying these issues, theory and simulations understandably play an increasingly important, often fundamental, role. Despite the limitations of current approaches, in fact, the possibility of performing computational 'gedanken experiment' and thus to disentangle, via in-depth analyses, the origin of the various basic interactions in these complex multifunctional systems, together with the often sufficiently accurate prediction of the topology of local minima and saddle points in the energy hypersurface, renders theoretical simulations (nowadays first-principles, but based on empirical potentials in a likely near future) an invaluable tool in the process of characterising and predicting novel structures and properties.

In conclusion, we remark that the two systems reported here are good examples where both the preparative skill and the characterisation capabilities at the nanoscale of surface scientists can be tested. Actually, in studying these UT oxide films much has been learned in the field of basic SS. The next challenge is associated with our capability to use such systems as models for understanding even more complex problems, exploiting the fact that some of these UT films are extremely well characterised and can thus be used as models where the role of defects, stoichiometry, under-coordination and morphology on the final material properties can be studied.

Among the most interesting aspects, the role of UT oxide films as model supports for heterogeneous catalysis has been recognised since the early stage of their developments, as proven by the number of excellent reviews where such aspects have been fully developed [23–25,32,33]. In this connection we like to stress once more that, when an ordered array of defects (e.g. steps, misfit dislocations, different stacking and vacancies) is obtained, the resulting UT films can act as templates to direct preferential nucleation for metal NPs growth. The work in this field has been recently reviewed [364,365]. When compared with metal-based templates [366], which are usually stable only in UHV conditions, oxide-based UT templates seem more promising because some of them present an intrinsic higher chemical stability that may open the way to real applications.

Finally, we note that until now the electronic and electrical properties of UT oxide films have not been fully investigated, neither in terms of basic science nor with the perspective of applications. It is easy to foresee that more efforts will be put in this field in a near future, also because of the ever increasing importance of nano-electronics.

Glossary

| | |
|-------------|--|
| AES | Auger electron spectroscopy |
| AO | Atomic oxygen |
| bcc | Body centred cubic |
| BE | Binding energy |
| CMOS | Complementary metal–oxide–semiconductor |
| D | Dimension |
| DF | Density-functional |
| DF-GO | Density-functional global optimisation |
| DOS | Density of states |
| DRS | Direct recoils spectroscopy |
| E_f | Fermi level |
| EELS | Electron energy loss spectroscopy |
| ESD | Electron stimulated desorption |
| fcc | Face centred cubic |
| FT-RAIRS | Fourier transform-reflectance–absorption infrared spectroscopy |
| GIXRD | Grazing incidence XRD |
| GGA | Generalised gradient approximation |
| GO | Global optimisation |
| hcp | Hexagonal close packed |
| HREELS | High resolution electron energy loss spectroscopy |
| HRTEM | High resolution transmission electron microscopy |
| IRAS | Infrared reflection absorption spectroscopy |
| ISS | Ion-scattering spectroscopy |
| L | Langmuir |
| LDOS | Local density of states |
| LEED | Low energy electron diffraction |
| LEEM | Low energy electron microscopy |
| LEIS | Low energy ion scattering |
| M | Metal |
| MEIS | Medium energy ion scattering |
| MEM | Mirror electron microscopy |
| ML | Monolayer |
| MLE | Monolayer equivalent |
| MO_x | Metal oxide with a generic stoichiometry |
| μ -LEED | Micro-LEED |
| NICISS | Neutral impact collision ion scattering spectroscopy |
| NPs | Nanoparticles |
| PO | Post-oxidation |
| P_{O_2} | Oxygen pressure |

| | |
|-------|---|
| PSD | Photo-stimulated desorption |
| RHEED | Reflection high energy electron diffraction |
| RD | Reactive deposition |
| RT | Room temperature |
| SMSI | Strong metal support interaction |
| SO | Surface oxidation |
| SS | Surface science |
| STM | Scanning tunnelling microscopy |
| STS | Scanning tunnelling spectroscopy |
| SXPS | Soft X-ray photoelectron spectroscopy |
| T | Temperature |
| TDS | Thermal desorption spectroscopy |
| TEM | Transmission electron microscopy |
| TMOs | Transition metal oxides |
| UHV | Ultra-high-vacuum |
| UPS | Ultraviolet photoelectron spectroscopy |
| UT | Ultrathin |
| VB | Valence-band |
| XAS | X-ray absorption spectroscopy |
| XAFS | X-ray absorption fine structure |
| XANES | X-ray absorption near-edge structure |
| xc | Exchange-correlation |
| XPD | X-ray photoelectron diffraction |
| XPS | X-ray photoemission spectroscopy |
| XRD | X-ray diffraction |

Acknowledgements

QW would like to thank the Alexander von Humboldt foundation for financial support. AF acknowledges financial support from the SEPON project within the ERC Advanced Grants. Much of the work done in the field by GG and AF has been funded by the European Community through two STRP projects: GSOMEN and NanoChemSens (VI FRAMEWORK PROGRAMME), by the Italian Ministry of Instruction, University and Research (MIUR) through the fund PRIN-2005, project title: 'Novel electronic and chemical properties of metal oxides by doping and nanostructuring' and by the University of Padova, through the grant CPDA071781.

References

- [1] A. Baiker, *Chem. Rev.* **99**, 453 (1999).
- [2] G. C. Bond, *Chem. Soc. Rev.* **20**, 441 (1991).
- [3] N. L. Wu, S. Y. Wang, and I. A. Rusakova, *Science* **285**, 1375 (1999).
- [4] K. Rajeshwar, N. R. de Tacconi, and C. R. Chenthamarakshan, *Chem. Mater.* **13**, 2765 (2001).
- [5] F. M. Al-Kharafi and W. A. Badawy, *Corrosion* **54**, 377 (1998).
- [6] A. S. Hamdy, *Surf. Coat. Technol.* **200**, 3786 (2006).
- [7] A. P. Alivisatos, K. P. Johnsson, X. G. Peng, T. E. Wilson, C. J. Loweth, M. P. Bruchez, and P. G. Schultz, *Nature* **382**, 609 (1996).
- [8] N. Nakagawa, H. Y. Hwang, and D. A. Muller, *Nature Mater.* **5**, 204 (2006).
- [9] M. Bibes and A. Barthelemy, *IEEE Trans. Electron Devices* **54**, 1003 (2007).

- [10] V. E. Henrich and P. A. Cox, *The Surface Science of Metal Oxides* (University Press, Cambridge, 1994).
- [11] C. Noguera, *Physics and Chemistry of Oxide Surfaces* (University Press, Cambridge, 1996).
- [12] H.-J. Freund, *Angew. Chem. Int. Ed.* **36**, 452 (1997).
- [13] G. Renaud, *Surf. Sci. Rep.* **32**, 5 (1998).
- [14] H.-J. Freund, *Faraday Disc.* **114**, 1 (1999).
- [15] D. W. Goodman, *Chem. Rev.* **95**, 523 (1995).
- [16] C. R. Henry, *Surf. Sci. Rep.* **31**, 231 (1998).
- [17] R. Imbihl, R. J. Behm, and R. Schlogl, *Phys. Chem. Chem. Phys.* **9**, 3459 (2007).
- [18] G. A. Somorjai, R. L. York, D. Butcher, and J. Y. Park, *Phys. Chem. Chem. Phys.* **9**, 3500 (2007).
- [19] M. Bäumer and H.-J. Freund, *Prog. Surf. Sci.* **61**, 127 (1999).
- [20] S. A. Chambers, *Surf. Sci. Rep.* **39**, 105 (2000).
- [21] R. M. Lambert and G. Pacchioni, *Chemisorption and Reactivity on Supported Clusters and Thin Films*, (NATO ASI Series, Series E: Applied Sciences, Kluwer, 1997) Vol. 331.
- [22] S. Surnev, M. G. Ramsey, and F. P. Netzer, *Prog. Surf. Sci.* **73**, 117 (2003).
- [23] M. S. Chen and D. W. Goodman, *J. Phys.: Condens. Matter* **20**, 264013 (2008).
- [24] H.-J. Freund and G. Pacchioni, *Chem. Soc. Rev.* **37**, 2224 (2008).
- [25] J. Goniakowski, F. Finocchi, and C. Noguera, *Rep. Prog. Phys.* **71**, 016501 (2008).
- [26] H.-J. Freund, *Surf. Sci.* **601**, 1438 (2007).
- [27] S. Schintke and W.-D. Schneider, *J. Phys.: Condens. Matter* **16**, R49 (2004).
- [28] D. K. Fork, J. M. Phillips, R. Ramesh and R. W. Wolf, *Epitaxial Oxide Thin Films and Heterostructures*, Material Research Society Symposium Proceedings, Vol. 341, 1994.
- [29] J. S. Speck, D. K. Fork, R. W. Wolf and T. Shiosaki, *Epitaxial Oxide Thin Films II*, Material Research Society Symposium Proceedings, Vol. 401, 1995.
- [30] G. Granozzi, H.-J. Freund and S. Chambers, editors, *Thin Solid Films*, E-MRS Spring Conference Proceedings, Vol. 400 (1–2), 2001.
- [31] R. Franchy, *Surf. Sci. Rep.* **38**, 195 (2000).
- [32] J. Schoiswohl, M. Sock, Q. Chen, G. Thornton, G. Kresse, M. G. Ramsey, S. Surnev, and F. P. Netzer, *Top. Catal.* **46**, 137 (2007).
- [33] J. Schoiswohl, S. Surnev, and F. P. Netzer, *Top. Catal.* **36**, 91 (2005).
- [34] J. Schoiswohl, S. Surnev, F. P. Netzer, and G. Kresse, *J. Phys.: Condens. Matter* **18**, R1 (2006).
- [35] M. Trueba and S. P. Trasatti, *Eur. J. Inorg. Chem.* **17**, 3393 (2005).
- [36] X. Chen and S. S. Mao, *Chem. Rev.* **107**, 2891 (2007).
- [37] U. Diebold, *Surf. Sci. Rep.* **48**, 53 (2003).
- [38] J. A. Kelber, *Surf. Sci. Rep.* **62**, 271 (2007).
- [39] G. Granozzi and M. Sambì, *Adv. Mater.* **8**, 315 (1996).
- [40] E. Bauer, in *Science of Microscopy 3*, edited by P. W. Hawkes and J. C. Spence (Springer, Berlin, 2007), Vol. 1.
- [41] S. Agnoli, T. O. Menteş, M. A. Niño, A. Locatelli, and G. Granozzi, *Phys. Chem. Chem. Phys.* **11**, 3727 (2009).
- [42] M. Sambì, R. Sensolo, G. A. Rizzi, M. Petukhov, and G. Granozzi, *Surf. Sci.* **537**, 36 (2003).
- [43] T. Orzali, S. Agnoli, M. Sambì, and G. Granozzi, *Surf. Sci.* **569**, 105 (2004).
- [44] C. S. Fadley, *Prog. Surf. Sci.* **16**, 275 (1984).
- [45] C. Freysoldt, P. Rinke, and M. Scheffler, *Phys. Rev. Lett.* **99**, 086101 (2007).
- [46] W. Kohn, *Rev. Mod. Phys.* **71**, 1253 (1999).
- [47] K. Burke, J. P. Perdew, and M. Ernzerhof, *J. Chem. Phys.* **109**, 3760 (1998).
- [48] A. D. Becke, *J. Chem. Phys.* **98**, 1372 (1993).
- [49] V. I. Anisimov, J. Zaanen, and O. K. Andersen, *Phys. Rev. B* **44**, 943 (1991).
- [50] V. I. Anisimov, I. V. Solov'yev, M. A. Korotin, M. T. Czyzyk, and G. A. Sawatzky, *Phys. Rev. B* **48**, 16929 (1993).

- [51] A. I. Liechtenstein, V. I. Anisimov, and J. Zaanen, *Phys. Rev. B* **52**, R5467 (1994).
- [52] M. Cococcioni and S. de Gironcoli, *Phys. Rev. B* **71**, 035105 (2005).
- [53] E. Apra and A. Fortunelli, *J. Mol. Struct. (Theochem)* **501–502**, 251 (2000).
- [54] S. Casassa, A. M. Ferrari, M. Busso, and C. Pisani, *J. Phys. Chem. B* **106**, 12978 (2002).
- [55] Y. Wang and D. J. Doren, *D.J. Solid State Commun.* **136**, 186 (2005).
- [56] E. Finazzi, C. Di Valentin, G. Pacchioni, and A. Selloni, *J. Chem. Phys.* **129**, 154113 (2008).
- [57] L. Bengtsson, *Phys. Rev. B* **59**, 12301 (1999).
- [58] L. Yu, V. Ranjan, W. Lu, J. Bernholc, and M. B. Nardelli, *Phys. Rev. B* **77**, 245102 (2008).
- [59] P. Giannozzi, *Quantum ESPRESSO* <http://www.quantum-espresso.org/>
- [60] R. Car and M. Parrinello, *Phys. Rev. Lett.* **55**, 2471 (1985).
- [61] K.-M. Ho, A. A. Shvartsburg, B. Pan, Z.-Y. Lu, C.-Z. Wang, J. G. Wacker, J. L. Fye, and M. F. Jarrold, *Nature* **392**, 582 (1998).
- [62] E. Apra, R. Ferrando, and A. Fortunelli, *Phys. Rev. B* **73**, 205414 (2006).
- [63] M. Sierka, J. Dobler, J. Sauer, G. Santambrogio, M. Brummer, L. Woste, E. Janssens, G. Meijer, and K. R. Asmis, *Angew. Chem. Int. Ed.* **46**, 3372 (2007).
- [64] G. Barcaro, E. Apra, and A. Fortunelli, *Chem. Eur. J.* **13**, 6408 (2007).
- [65] M. Sierka, T. K. Todorova, S. Kaya, D. Stacchiola, J. Weissenrieder, J. Lu, H. Gao, S. Shaikhutdinov, H.-J. Freund, and J. Sauer, *Chem. Phys. Lett.* **424**, 115 (2006).
- [66] V. Rosato, M. Guillopé, and B. Legrand, *Phil. Mag. A* **59**, 321 (1989).
- [67] W. Vervisch, C. Mottet, and J. Goniakowski, *Phys. Rev. B* **65**, 245411 (2002).
- [68] S. Olivier, R. Conte, and A. Fortunelli, *Phys. Rev. B* **77**, 054104 (2008).
- [69] R. Ferrando, G. Rossi, F. Nita, G. Barcaro, and A. Fortunelli, *ACS Nano* **2**, 1849 (2008).
- [70] R. Ferrando, A. Fortunelli, and R. L. Johnston, *Phys. Chem. Chem. Phys.* **10**, 640 (2008).
- [71] B. G. Dick Jr and A. W. Overhauser, *Phys. Rev.* **120**, 90 (1958).
- [72] G. V. Lewis and C. R. A. Catlow, *J. Phys. C: Solid State Phys.* **18**, 1149 (1985).
- [73] T. S. Bush, J. D. Gale, R. A. Catlow, and P. D. Battle, *J. Mater. Chem.* **4**, 831 (1994).
- [74] A. K. Rappé and W. A. Goddard III, *J. Phys. Chem.* **95**, 3358 (1991).
- [75] N. C. Pyper, *J. Chem. Phys.* **114**, 4390 (2001).
- [76] A. J. Rowley, P. Jemmer, M. Wilson, and P. A. Madden, *J. Chem. Phys.* **108**, 10209 (1998).
- [77] V. Swamy, J. D. Gale, and L. S. Dubrovinsky, *J. Phys. Chem. Solids* **62**, 887 (2001).
- [78] A. Hallil, R. Tétot, F. Berthier, I. Braems, and J. Creuze, *Phys. Rev. B* **73**, 165406 (2006).
- [79] N. A. Benedek, A. L. S. Chua, C. Elsässer, A. P. Sutton, and M. W. Finnis, *Phys. Rev. B* **78**, 064110 (2008).
- [80] S. K. R. S. Sankaranarayanan and S. Ramanathan, *Phys. Rev. B* **78**, 085420 (2008).
- [81] J. Tersoff and D. R. Hamann, *Phys. Rev. Lett.* **50**, 1998 (1983).
- [82] K. Reuter and M. Scheffler, *Phys. Rev. B* **65**, 035406 (2002).
- [83] J. Schnadt, A. Michaelides, J. Knudsen, R. T. Vang, K. Reuter, E. Lægsgaard, M. Scheffler, and F. Besenbacher, *Phys. Rev. Lett.* **96**, 146101 (2006).
- [84] G. Barcaro, S. Agnoli, F. Sedona, G. A. Rizzi, A. Fortunelli, and G. Granozzi, *J. Phys. Chem. C* **113**, 5721 (2009).
- [85] S. Agnoli, M. Sambì, G. Granozzi, J. Schoiswohl, S. Surnev, F. P. Netzer, M. Ferrero, A. M. Ferrari, and C. Pisani, *J. Phys. Chem. B* **109**, 17197 (2005).
- [86] C.-G. Wu, C.-C. Chao, and F.-T. Kuo, *Catal. Today* **97**, 103 (2004).
- [87] D. W. Flaherty, Z. Dohnalek, A. Dohnalkova, B. W. Arey, D. E. McCready, N. Ponnusamy, C. B. Mullins, and B. D. Kay, *J. Phys. Chem. C* **111**, 4765 (2007).
- [88] I. N. Remediakis, N. Lopez, and J. K. Nørskov, *Angew. Chem. Int. Ed.* **44**, 1824 (2005).
- [89] M. Sanchez, R. Guirado, and M. E. Rincon, *J. Mater. Sci.: Mater. Electron.* **18**, 1131 (2007).
- [90] Y. S. Mok, J.-O. Jo, and C. Woo, *J. Adv. Oxid. Technol.* **10**, 439 (2007).
- [91] H.-Y. Zheng, H.-X. Qian, and W. Zhou, *Appl. Surf. Sci.* **254**, 2174 (2008).
- [92] A. Pillonnet, J. Mugnier, V. Le Bihan, C. Leluyer, G. Ledoux, C. Dujardin, B. Masenelli, D. Nicolas, and P. Melinon, *J. Lumin.* **119**, 560 (2006).

- [93] R. Kishore, S. N. Singh, and B. K. Das, *Renewable Energy* **12**, 131 (1997).
- [94] W. X. Que, A. Uddin, and X. Hu, *J. Power Sources* **159**, 353 (2006).
- [95] G. V. Samsonov, *The Oxide Handbook*, 2nd ed. (IFI/Plenum Press, New York, 1982).
- [96] J. F. Baumard, D. Panis, and A. M. Anthony, *J. Solid State Chem.* **20**, 43 (1977).
- [97] C. Picard and P. Gerdanian, *J. Solid State Chem.* **14**, 66 (1975).
- [98] L. A. Bursill and B. G. Hyde, *Prog. Solid State Chem.* **7**, 177 (1972).
- [99] M. Bowker, *Curr. Opin. Solid State Mater. Sci.* **10**, 153 (2006).
- [100] M. K. Nowotny, L. R. Sheppard, T. Bak, and J. Nowotny, *J. Phys. Chem. C* **112**, 5275 (2008).
- [101] M. V. Ganduglia-Pirovano, A. Hofmann, and J. Sauer, *Surf. Sci. Rep.* **62**, 219 (2007).
- [102] S. P. Denker, *J. Appl. Phys.* **37**, 142 (1966).
- [103] J. Murray and H. A. Wriedt, *Bull. Alloy Phase Diagrams* **8**, 148 (1987).
- [104] A. I. Gusev, A. A. Rempel, and A. J. Magerl, *Disorder and Order in Strongly Non-stoichiometric Compounds: Transition Metal Carbides, Nitrides and Oxides* (Springer, Berlin, 2001).
- [105] M. D. Banus, T. B. Reed, and A. J. Strauss, *Phys. Rev. B: Solid State* **5**, 2775 (1972).
- [106] A. A. Valeeva, A. A. Rempel, and A. I. Gusev, *Inorg. Mater.* **37**, 603 (2001).
- [107] A. A. Valeeva, A. A. Rempel, W. Sprengel, and H.-E. Schaefer, *Phys. Chem. Chem. Phys.* **5**, 2304 (2003).
- [108] A. A. Valeeva, A. A. Rempel, and A. I. Gusev, *JETP Lett.* **73**, 702 (2001).
- [109] A. A. Valeeva, A. A. Rempel, and A. I. Gusev, *Russ. J. Phys. Chem.* **76**, 1251 (2002).
- [110] M. Catti, G. Sandrone, and R. Dovesi, *Phys. Rev. B* **55**, 16122 (1997).
- [111] H. Akatsugawa and E. Iguchi, *Phys. Rev. B* **56**, 12931 (1997).
- [112] J. Ashkenazi, M. G. Vincent, K. Yvon, and J. M. Honig, *J. Phys. C: Solid State Phys.* **14**, 353 (1981).
- [113] A. Tanaka, *Jap. J. Phys. Soc.* **73**, 152 (2004).
- [114] V. Eyert, U. Schwingenschlögl, and U. Eckern, *Europhys. Lett.* **70**, 782 (2005).
- [115] A. T. Paxton and L. Thien-Nga, *Phys. Rev. B* **57**, 1579 (1998).
- [116] M. Casarin, C. Maccato, and A. Vittadini, *J. Phys. Chem. B* **106**, 795 (2002).
- [117] H. Zhang and J. F. Banfield, *J. Phys. Chem. B* **104**, 3481 (2000).
- [118] J. Muscat, V. Swamy, and N. M. Harrison, *Phys. Rev. B* **65**, 224112 (2002).
- [119] M. Ramamoorthy, D. Vanderbilt, and R. D. King-Smith, *Phys. Rev. B* **49**, 16721 (1994).
- [120] M. Lazzeri, A. Vittadini, and A. Selloni, *Phys. Rev. B* **63**, 155409 (2001).
- [121] X.-Q. Gong and A. Selloni, *Phys. Rev. B* **76**, 235307 (2007).
- [122] T. Sasaki, M. Watanabe, H. Hashizume, H. Yamada, and H. Nakazawa, *J. Am. Chem. Soc.* **118**, 8329 (1996).
- [123] I. E. Grey, C. Li, I. C. Madsen, and J. A. Watts, *J. Solid State Chem.* **66**, 7 (1987).
- [124] T. Sasaki, Y. Ebina, Y. Kitami, M. Watanabe, and T. Oikawa, *J. Phys. Chem. B* **105**, 6116 (2001).
- [125] T. Sasaki and M. Watanabe, *J. Phys. Chem. B* **101**, 10159 (1997).
- [126] K. Fukuda, I. Nakai, C. Oishi, M. Nomura, M. Harada, Y. Ebina, and T. Sasaki, *J. Phys. Chem. B* **108**, 13088 (2004).
- [127] W. Li, C. Liu, Y. Zhou, Y. Bai, X. Feng, Z. Yang, L. Lu, X. Lu, and K.-Y. Chan, *J. Phys. Chem. C* **112**, 20539 (2008).
- [128] R. Marchand, L. Brohan, and M. Tournoux, *Mater. Res. Bull.* **15**, 112 (1980).
- [129] J. B. Bignolas and M. Bujor, *Surf. Sci.* **108**, L453 (1981).
- [130] A. Azoulay, N. Shamir, E. Fromm, and M. H. Mintz, *Surf. Sci.* **370**, 1 (1997).
- [131] C. Oviedo, *J. Phys.: Condens. Matter* **5**, A153 (1993).
- [132] G. Lu, S. L. Bernasek, and J. Schwartz, *Surf. Sci.* **458**, 80 (2000).
- [133] I. Vaquila, M. C. G. Passeggi Jr, and J. Ferron, *Appl. Surf. Sci.* **93**, 247 (1996).
- [134] I. Vaquila, M. C. G. Passeggi Jr, and J. Ferron, *Surf. Sci.* **292**, L795 (1993).
- [135] D. M. Hanson, R. Stockbauer, and T. E. Madey, *Phys. Rev. B* **24**, 5513 (1981).

- [136] E. Bertel, R. Stockbauer, and T. E. Madey, *Surf. Sci.* **141**, 355 (1984).
- [137] Y. Takakuwa, S. Ishidzuka, A. Yoshigoe, Y. Teraoka, Y. Mizuno, H. Tonda, and T. Homma, *Nucl. Instrum. Methods Phys. Res. B* **2000**, 376 (2003).
- [138] Y. Takakuwa, S. Ishidzuka, A. Yoshigoe, Y. Teraoka, Y. Yamauchi, Y. Mizuno, H. Tonda, and T. Homma, *Appl. Surf. Sci.* **216**, 395 (2003).
- [139] P. H. McBreen and M. Polak, *Surf. Sci.* **179**, 483 (1987).
- [140] A. Petri, A. Neumann, and J. Küppers, *J. Vac. Sci. Technol. A* **8**, 2576 (1990).
- [141] U. Bardi, *Rep. Prog. Phys.* **57**, 939 (1994).
- [142] Y. Baer, F. Heden, J. Hedman, M. Klasson, C. Nordling, and K. Siegbahn, *Solid State Commun.* **8**, 517 (1970).
- [143] D. E. Eastmann, *Solid State Commun.* **10**, 933 (1972).
- [144] W. Chen, L. Severin, M. Göthelid, M. Hammar, S. Cameron, and J. Paul, *Phys. Rev. B* **50**, 5620 (1994).
- [145] G. W. Fernando, R. E. Watson, and M. Weinert, *Phys. Rev. B* **45**, 8233 (1992).
- [146] S. Ringler, E. Janin, M. Boutonnet-Kizling, and M. Göthelid, *Appl. Surf. Sci.* **162–163**, 190 (2000).
- [147] U. Bardi and P. N. Ross, *J. Vac. Sci. Technol. A* **2**, 1461 (1984).
- [148] J. Paul, S. D. Cameron, D. J. Dwyer, and F. M. Hoffmann, *Surf. Sci.* **177**, 121 (1986).
- [149] W. Chen, S. Cameron, M. Göthelid, M. Hammer, and J. Paul, *J. Phys. Chem.* **99**, 12892 (1995).
- [150] T. Matsumoto, M. Batzill, S. Hsieh, and B. E. Koel, *Surf. Sci.* **572**, 127 (2004).
- [151] I. Kurzina, V. Shevlyuga, A. Atrei, B. Cortigiani, G. Rovida, and U. Bardi, *Surf. Rev. Lett.* **10**, 861 (2003).
- [152] S. Hsieh, G. F. Liu, and B. E. Koel, *J. Vac. Sci. Technol. A* **26**, 1336 (2008).
- [153] A. Atrei, U. Bardi, and G. Rovida, *Surf. Sci.* **391**, 216 (1997).
- [154] W. S. Oh, C. Xu, D. Y. Kim, and D. W. Goodman, *J. Vac. Sci. Technol. A* **15**, 1710 (1997).
- [155] Q. Guo, W. S. Oh, and D. W. Goodman, *Surf. Sci.* **437**, 49 (1999).
- [156] X. Lai, Q. Guo, B. K. Min, and D. W. Goodman, *Surf. Sci.* **487**, 1 (2001).
- [157] M.-S. Chen, A. K. Santra, and D. W. Goodman, *Phys. Rev. B* **69**, 155404 (2004).
- [158] M. S. Chen and D. W. Goodman, *Science* **306**, 252 (2004).
- [159] M. S. Chen, W. T. Wallace, D. Kumar, Z. Yan, K. K. Gath, Y. Cai, Y. Kuroda, and D. W. Goodman, *Surf. Sci.* **581**, L115 (2005).
- [160] D. Kumar, M. S. Chen, and D. W. Goodman, *Thin Solid Films* **515**, 1475 (2006).
- [161] Y. Zhang, L. Giordano, and G. Pacchioni, *J. Phys. Chem. C* **111**, 7437 (2007).
- [162] Z. Chang and G. Thornton, *Surf. Sci.* **462**, 68 (2000).
- [163] T. V. Ashworth and G. Thornton, *Thin Solid Films* **400**, 43 (2001).
- [164] T. V. Ashworth, C. A. Muryn, and G. Thornton, *Nanotechnology* **16**, 3041 (2005).
- [165] A. C. Papageorgiou, G. Cabailh, Q. Chen, A. Resta, E. Lundgren, J. N. Andersen, and G. Thornton, *J. Phys. Chem. C* **111**, 7704 (2007).
- [166] T. Orzali, M. Casarin, G. Granozzi, M. Sambì, and A. Vittadini, *Phys. Rev. Lett.* **97**, 156101 (2006).
- [167] M. Gratzel, *Nature* **409**, 575 (2001).
- [168] D. Cummins, G. Boschloo, M. Ryan, D. Corr, S. N. Rao, and D. Fitzmaurice, *J. Phys. Chem. B* **104**, 11449 (2000).
- [169] A. C. Papageorgiou, C. L. Pang, Q. Chen, and G. Thornton, *ACS Nano* **1**, 409 (2007).
- [170] T. Maeda, Y. Kobayashi, and K. Kishi, *Surf. Sci.* **436**, 249 (1999).
- [171] M. C. G. Passeggi Jr, L. I. Vergara, S. M. Mendoza, and J. Ferrón, *Surf. Sci.* **507–510**, 825 (2002).
- [172] P. Finetti, M. Caffio, B. Cortigiani, A. Atrei, and G. Rovida, *Surf. Sci.* **602**, 1101 (2008).
- [173] M. Caffio, G. Rovida, and A. Atrei, *Surf. Sci.* **601**, 528 (2007).
- [174] D. R. Jennison, O. Dulub, W. Hebenstreit, and U. Diebold, *Surf. Sci.* **492**, L677 (2001).
- [175] O. Carp, C. L. Huisman, and A. Reller, *Prog. Solid State Chem.* **32**, 33 (2004).

- [176] S. J. Tauster, S. C. Fung, and J. Garten, *J. Am. Chem. Soc.* **100**, 170 (1978).
- [177] O. Dulub, W. Hebenstreit, and U. Diebold, *Phys. Rev. Lett.* **84**, 3646 (2000).
- [178] S. Hsieh, D. Beck, T. Matsumoto, and B. E. Koel, *Thin Solid Films* **466**, 123 (2004).
- [179] T. Matsumoto, M. Batzill, S. Hsieh, and B. E. Koel, *Surf. Sci.* **572**, 146 (2004).
- [180] A. B. Boffa, H. C. Galloway, P. W. Jacobs, J. J. Benitez, J. D. Batteas, M. Salmeron, A. T. Bell, and G. A. Samorjai, *Surf. Sci.* **326**, 80 (1995).
- [181] F. Sedona, G. A. Rizzi, S. Agnoli, F. X. Llabres i Xamena, A. Papageorgiou, D. Ostermann, M. Sambì, P. Finetti, K. Schierbaum, and G. Granozzi, *J. Phys. Chem. B* **109**, 24411 (2005).
- [182] F. Sedona, Ph. D. thesis, University of Padova, 2005.
- [183] P. Finetti, F. Sedona, G. A. Rizzi, U. Mick, F. Sutara, M. Svec, V. Matolin, K. Schierbaum, and G. Granozzi, *J. Phys. Chem. C* **111**, 869 (2007).
- [184] F. Sedona, S. Agnoli, and G. Granozzi, *J. Phys. Chem. B* **110**, 15359 (2006).
- [185] G. Barcaro, F. Sedona, A. Fortunelli, and G. Granozzi, *J. Phys. Chem. C* **111**, 6095 (2007).
- [186] F. Sedona, G. Granozzi, G. Barcaro, and A. Fortunelli, *Phys. Rev. B* **77**, 115417 (2008).
- [187] Y. Zhang, L. Giordano, G. Pacchioni, A. Vittadini, F. Sedona, P. Finetti, and G. Granozzi, *Surf. Sci.* **601**, 3488 (2007).
- [188] R. A. Bennett, C. L. Pang, N. Perkins, R. D. Smith, P. Morrall, R. I. Kvon, and M. Bowker, *J. Phys. Chem. B* **106**, 4688 (2002).
- [189] M. Bowker, *Chem. Soc. Rev.* **36**, 1656 (2007).
- [190] S. Agnoli, T. Orzali, M. Sambì, A. Vittadini, M. Casarin, and G. Granozzi, *J. Phys. Chem. C* **112**, 20038 (2008).
- [191] G. Kresse, S. Surnev, M. G. Ramsey, and F. P. Netzer, *Surf. Sci.* **492**, 329 (2001).
- [192] F. Sedona, S. Agnoli, M. Casarin, M. Sambì, A. Vittadini, and G. Granozzi, submitted.
- [193] F. Sedona, M. Eusebio, G. A. Granozzi, D. Ostermann, and K. Schierbaum, *Phys. Chem. Chem. Phys.* **7**, 697 (2005).
- [194] J. Chen, J. Kubota, A. Wada, J. N. Kondo, and K. Donen, *J. Phys. Chem. C* **112**, 12477 (2008).
- [195] J. Chen, J. Kubota, A. Wada, J. N. Kondo, and K. Donen, *J. Am. Chem. Soc.* **131**, 4580 (2009).
- [196] A. Männig, Z. Zhao, D. Rosenthal, K. Christmann, H. Hoster, H. Rauscher, and R. J. Behm, *Surf. Sci.* **576**, 29 (2005).
- [197] S. Winiarz, W. Polewska, and R. Czajka, *Mater. Lett.* **61**, 4818 (2007).
- [198] Z. Song, J. Hrbek, and R. Osgood, *Nanoletters* **5**, 1327 (2005).
- [199] D. V. Potapenko, J. Hrbek, and R. M. Osgood, *ACS Nano* **2**, 1353 (2008).
- [200] J. Biener, E. Farfan-Arribas, M. Biener, C. M. Friend, and R. J. Madix, *J. Chem. Phys.* **123**, 094705 (2005).
- [201] J.-D. Grunwaldt and A. Baiker, *J. Phys. Chem. B* **103**, 1002 (1999).
- [202] S. Winiarz, W. Polewska, and R. Czajka, *Mater. Lett.* **61**, 4818 (2007).
- [203] N. D. McCavish and R. A. Bennett, *Surf. Sci.* **546**, 47 (2003).
- [204] R. A. Bennett and N. D. McCavish, *Topics Catal.* **36**, 11 (2005).
- [205] R. A. Bennett, J. S. Mulley, M. A. Newton, and M. Surman, *J. Chem. Phys.* **127**, 084707 (2007).
- [206] E. T. Arakawa and M. W. Williams, *J. Phys. Chem. Solids* **29**, 735 (1968).
- [207] K. Wefer and C. Misra, *Alcoa Technical Paper No. 19* (Alcoa Labs. 1972).
- [208] R. S. Zhou and R. L. Snyder, *Acta Crystallogr. Sect. B: Struct. Sci.* **47**, 617 (1991).
- [209] I. Levin and D. Brandon, *J. Am. Ceram. Soc.* **81**, 1995 (1998).
- [210] C. K. Lee, E. Cho, H. S. Lee, K. S. Seol, and S. Han, *Phys. Rev. B* **76**, 245110 (2007).
- [211] L. Pauling and S. B. Hendriks, *J. Am. Chem. Soc.* **47**, 781 (1925).
- [212] R. W. G. Wyckoff, *Crystal Structures*, 2nd ed. (Wiley, New York, 1964).
- [213] M. L. Kronberg, *Acta Metall.* **5**, 507 (1957).
- [214] W. E. Lee and K. P. D. Lagerlof, *J. Electron Microsc. Tech.* **2**, 247 (1985).

- [215] I. Tanaka and H. Adachi, *Phys. Rev. B* **54**, 4604 (1996).
- [216] J. C. Boettger, *Phys. Rev. B* **55**, 750 (1997).
- [217] K. T. Thomson, R. M. Wentzcovitch, and M. S. T. Bukowinski, *Science* **274**, 1880 (1996).
- [218] S. D. Kenny, D. Nguyen-Manh, H. Fujitani, and A. P. Sutton, *Phil. Mag. Lett.* **78**, 469 (1998).
- [219] R. Ahuja, J. M. Osorio-Guillen, J. S. de Almeida, B. Holm, W. Y. Ching, and B. Johansson, *J. Phys.: Condens. Matter* **16**, 2891 (2004).
- [220] P. Liu and J. Skogsmo, *Acta Crystallogr. Sect. B* **47**, 425 (1991).
- [221] M. Halvarsson, Ph. D. thesis, Chalmers University of Technology, 1994.
- [222] B. Ollivier, R. Retoux, P. Lacorre, D. Massiot, and G. Ferey, *J. Mater. Chem.* **7**, 1049 (1997).
- [223] Y. Yourdshahyan, U. Engberg, L. Bengtsson, B. I. Lundqvist, and B. Hammer, *Phys. Rev. B* **55**, 8721 (1997).
- [224] Y. Yourdshahyan, C. Ruberto, M. Halvarsson, L. Bengtsson, V. Langer, and B. I. Lundqvist, *J. Am. Ceram. Soc.* **82**, 1365 (1999).
- [225] R. Vali and S. M. Hosseini, *Comput. Mater. Sci.* **29**, 138 (2004).
- [226] S. D. Mo, Y. N. Xu, and W. Y. Ching, *J. Am. Ceram. Soc.* **80**, 1193 (1997).
- [227] E. Husson and Y. Repelin, *Eur. J. Solid State Inorg. Chem.* **33**, 1223 (1996).
- [228] S. J. Wilson and J. D. C. McConnell, *J. Solid State Chem.* **34**, 315 (1980).
- [229] S.-H. Cai, S. N. Rashkeev, S. T. Pantelides, and K. Sohlberg, *Phys. Rev. Lett.* **89**, 235501 (2002).
- [230] S.-H. Cai, S. N. Rashkeev, S. T. Pantelides, and K. Sohlberg, *Phys. Rev. B* **67**, 224104 (2003).
- [231] A. P. Borosy, B. Silvi, M. Allavena, and P. Nortier, *J. Phys. Chem.* **98**, 13189 (1994).
- [232] S. D. Mo and W. Y. Ching, *Phys. Rev. B* **57**, 15219 (1998).
- [233] M. Wilson, M. Exner, Y.-M. Huang, and M. W. Finnis, *Phys. Rev. B* **54**, 15683 (1996).
- [234] G. Paglia, A. L. Rohl, C. E. Buckley, and J. D. Gale, *Phys. Rev. B* **71**, 224115 (2005).
- [235] G. Paglia, E. S. Boin, and S. J. L. Billinge, *Chem. Mater.* **18**, 3242 (2006).
- [236] F. Maglia, S. Gennari, and V. Buscaglia, *J. Am. Ceram. Soc.* **91**, 283 (2008).
- [237] E. Menendez-Proupin and G. Gutierrez, *Phys. Rev. B* **72**, 035116 (2005).
- [238] W. Y. Ching, L. Z. Ouyang, P. Rulis, and H. Z. Yao, *Phys. Rev. B* **78**, 014106 (2008).
- [239] L. Smrcok, V. Langer, and J. Krestan, *Acta Crystall. Sect. C* **62**, 183 (2006).
- [240] P. L. J. Gunter, J. W. Niemantsverdriet, F. H. Ribeiro, and G. A. Somorjai, *Catal. Rev. Sci. Eng.* **39**, 77 (1997).
- [241] A. Kiejna and B. I. Lundqvist, *Surf. Sci.* **540**, 1 (2002).
- [242] L. P. H. Jeurgens, W. G. Sloof, F. D. Tichelaar, and E. J. Mittemeijer, *Surf. Sci.* **506**, 313 (2002).
- [243] A. Hasnaoui, O. Politano, J. M. Salazar, G. Aral, P. K. Kalia, A. Nakano, and P. Vashishta, *Surf. Sci.* **579**, 47 (2005).
- [244] A. Kiejna and B. I. Lundqvist, *Surf. Sci.* **504**, 1 (2002).
- [245] D. Starodub, T. Gustafsson, and E. Garfunkel, *Surf. Sci.* **552**, 199 (2004).
- [246] N. Cabrera and N. F. Mott, *Rep. Progr. Phys.* **12**, 163 (1948).
- [247] A. Stierle, F. Renner, R. Streitel, H. Dosch, W. Drube, and B. C. Cowie, *Science* **303**, 1652 (2004).
- [248] A. Stierle, F. Renner, R. Streitel, and H. Dosch, *Phys. Rev. B* **64**, 165413 (2001).
- [249] D. R. Mullins and S. H. Overbury, *Surf. Sci.* **199**, 141 (1988).
- [250] H. L. Davis and J. Noonan, *Phys. Rev. Lett.* **54**, 566 (1985).
- [251] M. Wuttig, W. Hoffmann, E. Preuss, R. Franchy, H. Ibach, Y. Chen, M. L. Xu, and S. Y. Tong, *Phys. Rev. B* **42**, 5443 (1990).
- [252] Y. Chen, M. L. Xu, S. Y. Tong, M. Wuttig, W. Hoffmann, R. Franchy, and H. Ibach, *Phys. Rev. B* **42**, 5451 (1990).
- [253] R. M. Jaegerm, H. Kühlenbeck, H. J. Freund, M. Wuttig, W. Hoffmann, R. Franchy, and H. Ibach, *Surf. Sci.* **259**, 235 (1991).
- [254] Q. Fu and T. Wagner, *Surf. Sci. Rep.* **62**, 431 (2007).

- [255] K. H. Hansen, T. Worren, S. Stempel, E. Laegsgaard, M. Bäumer, H. J. Freund, F. Besenbacher, and I. Stensgaard, *Phys. Rev. Lett.* **83**, 4120 (1999).
- [256] G. Kresse, M. Schmid, E. Napetschnig, M. Shishkin, L. Köhler, and P. Varga, *Science* **308**, 1440 (2005).
- [257] M. Klimenkov, S. Nepijko, H. Kuhlenbeck, and H. J. Freund, *Surf. Sci.* **385**, 66 (1997).
- [258] M. Kulawik, N. Nilus, H. P. Rust, and H. J. Freund, *Phys. Rev. Lett.* **91**, 256101 (2003).
- [259] J. Libuda, F. Winkelmann, M. Bäumer, H. J. Freund, T. Bertrams, H. Neddermeyer, and K. Müller, *Surf. Sci.* **318**, 61 (1994).
- [260] T. Bertrams, A. Brodde, and H. Neddermeyer, *J. Vac. Sci. Technol. B* **12**, 2122 (1994).
- [261] G. Ceballos, Z. Song, J. I. Pascual, H.-P. Rust, H. Conrad, M. Bäumer, and H.-J. Freund, *Chem. Phys. Lett.* **359**, 41 (2002).
- [262] D. R. Jennison and A. Bogicevic, *Surf. Sci.* **464**, 108 (2000).
- [263] J. Libuda, M. Frank, A. Sandell, S. Andersson, P. A. Bruhwiler, M. Battmer, N. Martensson, and H. J. Freund, *Surf. Sci.* **384**, 106 (1997).
- [264] A. Stierle, C. Tieg, H. Dosch, V. Formoso, E. Lundgren, J. N. Andersen, L. Köhler, and G. Kresse, *Surf. Sci.* **529**, L263 (2003).
- [265] M. Schmid, M. Shishkin, G. Kresse, E. Napetschnig, P. Varga, M. Kulawik, N. Nilus, H.-P. Rust, and H.-J. Freund, *Phys. Rev. Lett.* **97**, 046101 (2006).
- [266] K. F. McCarty, J. P. Pierce, and C. B. Carter, *Appl. Phys. Lett.* **88**, 141902 (2006).
- [267] M. Heyde, M. Kulawik, H.-P. Rust, and H.-J. Freund, *Phys. Rev. B* **73**, 125320 (2006).
- [268] G. H. Simon, T. König, M. Nilus, H.-P. Rust, M. Heyde, and H.-J. Freund, *Phys. Rev. B* **78**, 113401 (2008).
- [269] J. P. Pierce, N. C. Bartelt, R. Stumpf, and K. F. McCarty, *Phys. Rev. B* **77**, 195438 (2008).
- [270] T. Nishimura, Y. Hoshino, T. Okazawa, and Y. Kido, *Phys. Rev. B* **77**, 073405 (2008).
- [271] L. Jurczyszyn, A. Krupski, S. Degen, B. Pieczyrak, M. Kralj, C. Becker, and K. Wandelt, *Phys. Rev. B* **76**, 045101 (2007).
- [272] L. Jurczyszyn, A. Rosenhahn, J. Schneider, C. Becker, and K. Wandelt, *Phys. Rev. B* **68**, 115425 (2003).
- [273] E. Vesselli, L. Bianchettin, A. Baraldi, A. Sala, G. Comelli, S. Lizzit, L. Petaccia, and S. de Gironcoli, *J. Phys.: Condens. Matter* **20**, 195223 (2008).
- [274] D. R. Jennison, C. Verdozzi, P. A. Schultz, and M. P. Sears, *Phys. Rev. B* **59**, R15605 (1999).
- [275] X.-G. Wang, A. Chaka, and M. Scheffler, *Phys. Rev. Lett.* **84**, 3650 (2000).
- [276] M. Digne, P. Sautet, P. Raybaud, P. Euzen, and H. Toulhoat, *J. Catal.* **211**, 1 (2002).
- [277] A. Marmier and S. C. Parker, *Phys. Rev. B* **69**, 115409 (2004).
- [278] H. P. Pinto, R. M. Nieminen, and S. D. Elliott, *Phys. Rev. B* **70**, 125402 (2004).
- [279] M. Bäumer, J. Libuda, A. Sandell, H. J. Freund, G. Graw, T. Bertrams, and T. Neddermeyer, *Ber. Bunsen-Ges. Phys. Chem.* **99**, 1381 (1995).
- [280] T. T. Lay, M. Yoshitake, and B. Mebarki, *J. Vac. Sci. Technol. A* **20**, 2027 (2002).
- [281] T. T. Lay, M. Yoshitake, and W. Song, *Appl. Surf. Sci.* **239**, 451 (2005).
- [282] W. Song and M. Yoshitake, *Thin Solid Films* **464**, 52 (2004).
- [283] W. Song and M. Yoshitake, *Appl. Surf. Sci.* **251**, 14 (2005).
- [284] W. Song and M. Yoshitake, *Appl. Surf. Sci.* **241**, 164 (2005).
- [285] Y. Lykhach, V. Moroz, and M. Yoshitake, *Appl. Surf. Sci.* **241**, 250 (2005).
- [286] A. Vlad, A. Stierle, N. Kasper, H. Dosch, and M. Rühle, *J. Mater. Res.* **21**, 3047 (2006).
- [287] H. L. Davis and J. R. Noonan, *Mater. Res. Soc. Symp. Proc.* **83**, 3 (1987).
- [288] R.-P. Blum, D. Ahlbehrendt, and H. Niehus, *Surf. Sci.* **366**, 107 (1996).
- [289] R.-P. Blum, D. Ahlbehrendt, and H. Niehus, *Surf. Sci.* **396**, 176 (1998).
- [290] R.-P. Blum and H. Niehus, *Appl. Phys. A* **66**, S529 (1998).
- [291] V. Maurice, N. Frey, and P. Marcus, *Surf. Sci.* **581**, 88 (2005).
- [292] J. Doychak, J. L. Smialek, and T. E. Mitchel, *Met. Trans. A* **20**, 499 (1989).
- [293] P. Gassmann, R. Franchy, and H. Ibach, *Surf. Sci.* **319**, 95 (1994).

- [294] P. Gassmann, R. Franchy, and H. Ibach, *J. Electron Spectrosc. Relat. Phenom.* **64/65**, 315 (1993).
- [295] M. S. Zei, C. S. Lin, W. H. Wen, C. I. Chiang, and M. F. Luo, *Surf. Sci.* **600**, 1942 (2006).
- [296] H. Niehus, W. Raunau, K. Besocke, R. Spitzl, and G. Comsa, *Surf. Sci.* **225**, L8 (1990).
- [297] R. Manaila, A. Devenyi, and E. Candet, *Thin Solid Films* **122**, 131 (1984).
- [298] B. C. Lippens and J. J. Steggerda, in *Physical and Chemical Aspects of Adsorbents and Catalysts*, edited by B. G. Linsen (Academic Press, New York, 1970).
- [299] H. Saalfel, *Neues Jahrb. Miner. Abh.* **95**, 1 (1960).
- [300] D. Sondericker, F. Jona, and P. M. Marcus, *Phys. Rev. B* **34**, 6770 (1986).
- [301] A. Lehnert, A. Krupski, S. Degen, K. Franke, R. Decker, S. Rusponi, M. Kralj, C. Becker, H. Brune, and K. Wandelt, *Surf. Sci.* **600**, 1804 (2006).
- [302] V. Podgursky, I. Costina, and R. Franchy, *Surf. Sci.* **529**, 419 (2003).
- [303] S. Degen, C. Becker, and K. Wandelt, *Faraday Discuss.* **125**, 343 (2004).
- [304] A. Wiltner, A. Rosenhahn, J. Schneider, C. Becker, P. Pervan, M. Milun, M. Kralj, and K. Wandelt, *Thin Solid Films* **400**, 71 (2001).
- [305] A. M. Venezia and C. M. Loxton, *Surf. Sci.* **194**, 136 (1988).
- [306] A. M. Venezia and C. M. Loxton, *Surf. Interface Anal.* **11**, 287 (1988).
- [307] E. W. A. Young, J. C. Riviere, and L. S. Welch, *Appl. Surf. Sci.* **31**, 370 (1988).
- [308] R. D. Noebe and R. Gibala, *Scr. Met.* **20**, 1635 (1986).
- [309] C. Becker, K. von Bergmann, A. Rosenhahn, J. Schneider, and K. Wandelt, *Surf. Sci.* **486**, L443 (2001).
- [310] M. Schmid, G. Kresse, A. Buchsbaum, E. Napetschnig, S. Gritschneider, M. Reichling, and P. Varga, *Phys. Rev. Lett.* **99**, 196104 (2007).
- [311] U. Bardi, A. Artrei, and G. Rovida, *Surf. Sci.* **268**, 87 (1992).
- [312] S. Degen, A. Krupski, M. Kralj, A. Langner, C. Becker, M. Sokolowski, and K. Wandelt, *Surf. Sci.* **576**, L57 (2005).
- [313] S. Gritschneider, S. Degen, C. Becker, K. Wandelt, and M. Reichling, *Phys. Rev. B* **76**, 014123 (2007).
- [314] S. G. Addepalli, B. Ekstrom, N. P. Magtoto, J.-S. Lin, and J. A. Kelber, *Surf. Sci.* **442**, 385 (1999).
- [315] A. Rosenhahn, J. Schneider, J. Kandler, C. Becker, and K. Wandelt, *Surf. Sci.* **433-435**, 705 (1999).
- [316] C. Becker, J. Kandler, H. Raaf, R. Linke, T. Pelster, M. Dräger, M. Tanemura, and K. Wandelt, *J. Vac. Sci. Technol. A* **16**, 1000 (1998).
- [317] A. Rosenhahn, J. Schneider, C. Becker, and K. Wandelt, *J. Vac. Sci. Technol. A* **18**, 1923 (2000).
- [318] T. Maroutian, S. Degen, C. Becker, K. Wandelt, and R. Berndt, *Phys. Rev. B* **68**, 155414 (2003).
- [319] S. Gritschneider, C. Becker, K. Wandelt, and M. Reichling, *J. Am. Chem. Soc.* **129**, 4925 (2007).
- [320] G. Hamm, C. Barth, C. Becker, K. Wandelt, and C. R. Henry, *Phys. Rev. Lett.* **97**, 126106 (2007).
- [321] S. Le Pevedic, D. Schmaus, and C. Cohen, *Surf. Sci.* **602**, 67 (2008).
- [322] F. Qin, B. Hunt, B. Unal, D. Jing, M. Shen, C. J. Jenks, B. Gleeson, D. J. Sordelet, and P. A. Thiel, *Surf. Sci.* **602**, 1092 (2008).
- [323] G. Hamm, C. Becker, and C. R. Henry, *Nanotechnology* **17**, 1943 (2006).
- [324] F. Qin, N. P. Magtoto, and J. A. Kelber, *Mater. High Temp.* **21**, 193 (2004).
- [325] F. Qin, N. P. Magtoto, J. A. Kelber, and D. R. Jennison, *J. Mol. Catal. A* **228**, 83 (2005).
- [326] G. F. Cotterill, H. Niehus, and D. J. O'Connor, *Surf. Rev. Lett.* **3**, 1355 (1996).
- [327] F. Qin, N. Magtoto, and J. A. Kelber, *Surf. Sci.* **565**, L277 (2004).

- [328] O. Kurnosikov, C. F. J. Flipse, H. J. M. Swagten, B. Koopmans, and W. J. M. de Jonge, *Surf. Sci.* **600**, 4375 (2006).
- [329] Landolt-Bornstein, *New Series IV/5a, Phase Equilibria, Crystallographic and Thermodynamic Data of Binary Alloys* (Springer, Berlin, 1991).
- [330] W. Koster and T. Godecke, *Z. Metallkd* **71**, 765 (1980).
- [331] L. Hammer, H. Graupner, V. Blum, K. Heinz, G. W. Ownby, and D. M. Zehner, *Surf. Sci.* **412/413**, 69 (1998).
- [332] H. Graupner, L. Hammer, K. Heinz, and D. M. Zehner, *Surf. Sci.* **380**, 335 (1997).
- [333] O. Kizikaya, D. A. Hite, D. M. Zehner, and P. T. Sprunger, *Surf. Sci.* **529**, 223 (2003).
- [334] O. Kizikaya, I. C. Senevirathne, and P. T. Sprunger, *J. Appl. Phys.* **101**, 063706 (2007).
- [335] M. Yoshitake, S. Bera, and Y. Yamauchi, *Surf. Interface Anal.* **35**, 824 (2003).
- [336] Y. Yamauchi, M. Yoshitake, and W. Song, *Jpn. J. Appl. Phys.* **42**, 4721 (2003).
- [337] M. Yoshitake, S. Bera, Y. Yamauchi, and W. Song, *J. Vac. Sci. Technol. A* **21**, 1290 (2003).
- [338] S. Nemsak, M. Yoshitake, and K. Masek, *Surf. Sci.* **600**, 4357 (2006).
- [339] E. Napetschnig, M. Schmid, and P. Varga, *Surf. Sci.* **602**, 1750 (2008).
- [340] X. J. Liu, I. Ohnuma, R. Kainuma, and K. Ishida, *J. Alloys Compounds* **264**, 201 (1998).
- [341] P. A. Dowben and A. Miller, *Surface Segregation Phenomena* (CRC Press, Boca Raton, FL, 1990).
- [342] Y. Yu, K. Sagisaka, and D. Fujita, *Surf. Sci.* **603**, 723 (2009).
- [343] D. Shechtman, I. Blech, D. Gratias, and J. W. Cahn, *Phys. Rev. Lett.* **53**, 1951 (1984).
- [344] B. Dubost, J. M. Lang, M. Tanaka, P. Sainfort, and M. Audier, *Nature* **324**, 48 (1986).
- [345] A.-P. Tsai, *Acc. Chem. Res.* **36**, 31 (2003).
- [346] D. A. Shulyatev, *Crystallogr. Rep.* **52**, 938 (2007).
- [347] P. A. Thiel, *Progr. Surf. Sci.* **75**, 191 (2004).
- [348] D. Rouxel and P. Pigeat, *Prog. Surf. Sci.* **81**, 488 (2006).
- [349] I. Wehner and U. Köster, *Oxid. Met.* **54**, 445 (2000).
- [350] H. El Kadiri, R. Molins, Y. Bienvenu, and M. F. Horstemeyer, *Oxid. Met.* **64**, 63 (2005).
- [351] J.-N. Longchamp, S. Burkardt, M. Erbudak, and Y. Weisskopf, *Phys. Rev. B* **76**, 094203 (2007).
- [352] M. L. Hildner, T. J. Minvielle, and R. J. Wilson, *Surf. Sci.* **396**, 16 (1998).
- [353] Y.-T. Wu, H.-S. Tao, E. Garfunkel, T. E. Madey, and N. D. Shinn, *Surf. Sci.* **336**, 123 (1995).
- [354] Y.-T. Wu, E. Garfunkel, and T. E. Madey, *Surf. Sci.* **365**, 337 (1996).
- [355] Y.-T. Wu, E. Garfunkel, and T. E. Madey, *J. Vac. Sci. Technol. A* **14**, 2554 (1996).
- [356] P. J. Chen and D. W. Goodman, *Surf. Sci.* **312**, L767 (1994).
- [357] Y. S. Dedkov and M. Fonin, *Appl. Surf. Sci.* **253**, 3860 (2007).
- [358] C. Dietrich, B. Koslowski, and P. Ziemann, *J. Appl. Phys.* **97**, 083535 (2005).
- [359] C. Dietrich, H.-G. Boyen, and B. Koslowski, *J. Appl. Phys.* **94**, 1478 (2003).
- [360] D.R. Lide, *Handbook of Chemistry and Physics*, 85th ed. (CRC Press, Boca Raton, FL, 2004).
- [361] C. T. Campbell, *Surf. Sci. Rep.* **27**, 1 (1997).
- [362] F. P. Netzer, *Surf. Rev. Lett.* **9**, 1553 (2002).
- [363] D. J. Stacchiola, M. Baron, S. Kaya, J. Weissenrieder, S. Shaikhutdinov, and H.-J. Freund, *Appl. Phys. Lett.* **92**, 011911 (2008).
- [364] Q.-H. Wu, *Current Nanosci.* **5**, 58 (2009).
- [365] C. Becker and K. Wandelt, *Top. Curr. Chem.* **287**, 45 (2009).
- [366] H. Brune, *Surf. Sci. Rep.* **31**, 121 (1998).